A Computer Simulation of Structural Mechanics

— A Mesoscopic Model —

A Dissertation
Presented to the
Department of Physics and Astronomy
Brigham Young University

In Partial Fulfillment
of the Requirements for the Degree
Doctor of Philosophy

by
Eric W. Gardner
December 1995

This dissertation by Eric W. Gardner is accepted in its present form by the Department of Physics and Astronomy of Brigham Young University as satisfying the dissertation requirement for the degree of Doctor of Philosophy.

Manuel Berrondo, Committee Chair

Larry V. Knight, Committee Member

David D. Allred, Committee Member

H. Mark Nelson, Committee Member

Bruce Jay Collings, Statistics Minor

11/27/95
Date

Jean Francois VanHuele, Graduate Coordinator

TABLE OF CONTENTS

LIST OF FIGURES

I. Introduction

Several packages exist for computational analysis and simulation of structures. Most are based on the finite element method, and are powerful as well as flexible. However, there are some cases where a different approach may prove useful. Non-linear response of structures, both static and dynamic, and the constitutive integration problem are two such cases[1].

This thesis will present a different approach, called the mesoscopic model, which is one intermediate between a view of the atoms and the macroscopic continuum limit (hence the name "mesoscopic"). It is inspired by the microscopic composition of crystals[2], using experimental quantities (elastic constants), but is not an atomistic model. A large number of mass points interact with their neighbors through "springs" (Hooke's law forces), or anharmonic interactions depending on the problem[3]. The dynamical equations are then solved by direct integration.

Structures of interest in this dissertation are thin plates which can be configured into shapes useful for optical components such as mirrors. These plates can be curved by depositing a film onto one surface, and, if desired, etching a pattern into the back of the plate to control the curvature[4]. These structures can then be used as substrates for mirrors or other optics.

A. Significance of the Problem

Numerical computations are a useful tool for the design and construction of actual structures. They allow the investigation of design parameters and security factors before investment of time and resources into actual construction.

However, these calculations are only as useful as the models used to create them. Models where linear elasticity is applicable are well understood, but when dealing with nonlinear problems there are not so many well developed models because, in general, linear superposition is not applicable. The typical approach to a nonlinear problem is to modify the differential equations of elasticity by substituting the term corresponding to Hooke's law by a nonlinear term, obtained empirically[5].

The finite element method is a discretization of the partial differential equations of elasticity. Its foundations can be understood from the variational principles of mechanics, and its appeal comes largely from its ability to provide a picture of the discrete structure. The mesoscopic model proposed here will also provide a picture of the structure, and may also employ linear or nonlinear interactions, depending on the problem. The mathematical problem will be solved using direct integration.

B. Motivation

The model proposed here was motivated by the need to model curved surfaces to be used as substrates for multilayer x-ray mirrors. Of particular interest is silicon, which has many attractive qualities for this purpose and is commercially available in wafer form. The surface of a silicon wafer, polished for semiconductor manufacturing, proves to be a useful surface for depositing thin multilayer films that reflect x rays at the Bragg angle. While these silicon substrates are adequate for flat optics, finding curved surfaces (for

figured optics such as spherical, cylindrical, and elliptical mirrors) with a similar quality finish has not been so easy. It has been shown that silicon can be bent significantly by etching grooves in the back surface along the silicon crystal planes, leaving, in the groove, only a very thin silicon piece[6]. The polished surface can then be coated with a stressing film such as silicon nitride or nickel, or the groove filled with a compressing film such as silicon dioxide, either of which will bend the wafer to a concave form. By controlling the film properties and the groove pattern—such as etch depth, width, and relative position—an arbitrary 2- or 3-dimensional shape can be formed. It would be useful to be able to simulate such a process using a suitable computer model. One such model has been created using finite element codes[7,8], and results of that study will be used as a comparison to the mesoscopic model presented here.

C. Mesoscopic Model

Microscopically, the interactions between atoms in a material are a function of their interatomic distances. There is a minimum potential energy corresponding to the equilibrium point. For short distances from equilibrium the potential can be approximated by Hooke's law (harmonic) forces. As the distance from equilibrium increases the general form of the potential must be considered. If we now scale this picture and consider interacting blocks of atoms, the interaction between blocks will be harmonic, but with appropriately rescaled parameters (mass and stiffness constants for harmonic forces). This model has each particle in equilibrium with each of its neighbors, independent of other particles in the vicinity. This is not true of atomistic potentials where the addition of particles to the system creates a potential and equilibrium distance different from that for two particles. This is one of the primary differences between an atomistic model and the mesoscopic model, and will be discussed more in the following pages.

The model consists of a number of mass blocks represented by points (or pseudoparticles) in a lattice. The pseudoparticles interact with their neighbors with potential energies that are a function of distance between the particles, i.e., springs or elastic bars. While not presented here, the mesoscopic model would also extend to include anharmonic terms in the potential energy, allowing for nonlinear behavior in the material, and stochastic and dissipative terms in the equations to model viscoelastic materials.

The equations of motion—a set of ordinary differential equations, one for each pseudoparticle—is easily obtained from the potential energy. These equations are solved numerically to give the deformation of the solid. With boundary conditions to constrain motion of certain points in the lattice the static problem is solved by minimizing the potential energy of the system.

II. Technical Approach

Both Monte Carlo and molecular dynamics techniques have been widely and successfully used for the study of the microscopic structure of materials. However, these studies use a large number of atoms corresponding to a microscopic scale. To investigate elastic response of materials on a macroscopic scale the microscopic approach is far too cumbersome. The continuum limit and equations of elasticity present an attractive alternative, but numerically solving the problems requires discrete elements of space and time. This suggests an approach much like that of molecular dynamics, but points on the lattice become nodes of concentrated mass interacting with neighboring nodes through a potential. The makeup of this mesoscopic lattice is not the atomic lattice, but the concentrated mass points, possibly in a similar configuration as the atomic lattice but on a much larger scale.

A. Simple Cubic Lattice

The simplest parameters for the lattice are investigated first. The geometry for the lattice is simple cubic, and its initial equilibrium shape is chosen to represent the unloaded system. Each lattice node has equal mass, and interacts with its nearest neighbors—first, second, and third—with pair interactions given by Hooke's law. The equilibrium distance is given by the equilibrium position of the lattice nodes, and stiffness constants derived from experimentally obtained properties of the material, such as microscopic elastic constants, or Young's modulus and Poisson's ratio. An appropriate set of constraints is imposed to fulfill proper boundary conditions.

Other more complex parameters can be chosen to model more complex systems. For example, a more complex cubic lattice such as face centered or body centered, diamond or hexagonal structures; node points with different masses; interaction potentials taking on various functional forms; lattice imperfections mimicked by slight displacements in lattice sites or by leaving some sites empty.

The computations for the mesoscopic model begin by creating the lattice in its equilibrium state, then loading the system and beginning calculations, taking finite steps in time. A friction term is included to damp the system until it reaches its new, loaded equilibrium state. It is possible to create the lattice in a state approximating its analytical solution; however, with the current integration and damping scheme it was found that there was no significant improvement in convergence by doing so.

B. Boundary Conditions

The mesoscopic model is distinguished from a molecular dynamics view for the most part in the neighbor-pair equilibrium potential and the resultant boundary conditions. In the molecular dynamics view when two atoms bond there is a particular equilibrium position defined by the minimum of the potential energy between the two atoms. As other atoms are added to the system, as in a solid, the equilibrium distance between two atoms shifts from the position defined by only the pair of atoms to a new position defined by the altered potential arising from the surrounding atoms. At a boundary the surrounding atoms are not in the same configuration as in the bulk, and the potential, and thus the equilibrium position, change as well.

In the mesoscopic model the equilibrium position between two particles is defined by the spring potential (spring constant and equilibrium distance). As more particles are added to the lattice there is no change in the potential between particles. The particles at

the boundary, therefore, have the same pair potentials as those in the bulk so no special conditions at the boundary are required to maintain the equilibrium lattice configuration. This, again, is a result of the distinction between the molecular dynamics view and the mesoscopic model.

III. Mathematical Model

In order to study real materials the force between particles in the mesoscopic model must be related to those of the materials used. This section builds the mathematical framework necessary to relate the elastic characteristics of a material to the mesoscopic spring constants. While the mesoscopic model may take on various types of intraparticle forces, this thesis restricts itself to those following Hooke's law (more simply characterized as springs, with a spring constant and an equilibrium distance). The results of this section will be a relationship between the mesoscopic spring constants and the elastic constants characterizing materials. We will obtain the continuum limit of the equations of motion for our discrete (mesoscopic) model from which we will obtain the desired relationship.

Elastic properties of materials are defined both from the classical theory of elasticity[9], yielding elastic constants, and from macroscopic theory assuming homogeneous material that follows Hooke's law[10], giving Young's modulus and Poisson's ratio. Starting form the continuum limit, we will derive a relationship between the spring constants of the mesoscopic model and the elastic constants from the theory of elasticity. The notation and arguments used here follow very closely the derivation of the continuum theory of elasticity by Attila Askar[11].

The following section is essentially equivalent to the treatise by Askar and is summarized here including enough to maintain congruence and reference throughout the chapter. The complete mathematical treatment is given in Appendix A. The remainder of

the chapter deviates from Askar, the mesoscopic model differing enough from the classical theory to warrant full treatment.

A. Discrete to Continuous

Consider a lattice consisting of repeating cells of quasiparticles. We write the quasiparticle coordinates in terms of a vector, $\vec{x}(l)$, from the coordinate origin to each cell origin (labeled l), and a vector, $\vec{x}(k)$, from the cell origin to the particle k in the cell.

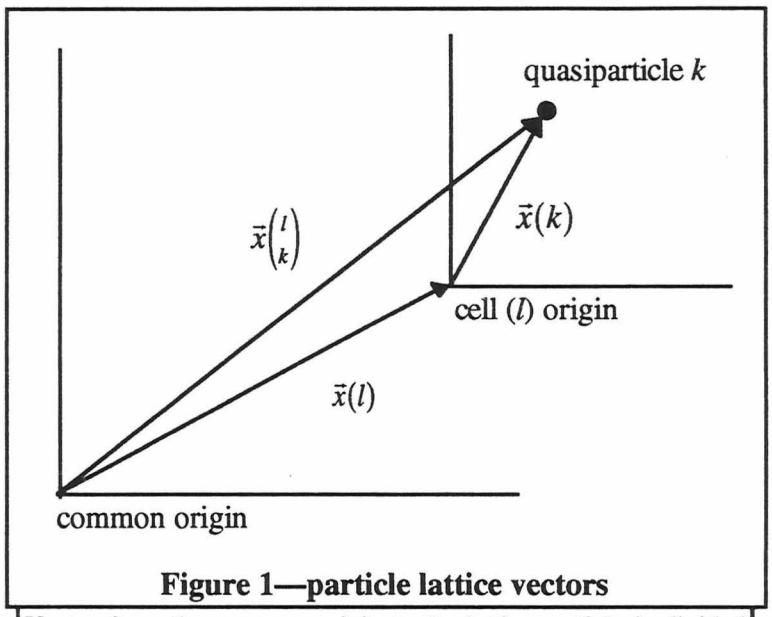

Figure 1—particle lattice vectors

Vector form the common origin to the lattice particle is divided into a vector from the common origin to the lattice cell origin plus a vector from the lattice cell origin to the particle.

1. Notation

Latin letters are used as lattice labels while Greek letters will denote vector components. It is convenient to separate the vectors from the common origin to the quasiparticle into components, as shown in Figure 1,

$$\vec{x}\begin{pmatrix} l \\ k \end{pmatrix} \equiv \vec{x}(l) + \vec{x}(k) \quad . \tag{1}$$

The label l identifies the lattice cell, and k the quasiparticle location within the cell. Because the quasiparticle positions within a cell are the same for each cell, the vector $\vec{x}(k)$ does not carry a lattice label l.

The actual quasiparticle positions are written in lower case ($\vec{x}$). Upper case letters ($\vec{X}$) denote the equilibrium position. The displacement from equilibrium is then written

$$\vec{u}\begin{pmatrix} l \\ k \end{pmatrix} = \vec{x}\begin{pmatrix} l \\ k \end{pmatrix} - \vec{X}\begin{pmatrix} l \\ k \end{pmatrix} \quad . \tag{2}$$

The potential (interaction) energy, V, is a function of the actual positions:

$$V = V\left(\ldots, \vec{x}\begin{pmatrix} l \\ k \end{pmatrix}, \ldots\right) = V\left(\ldots, \vec{X}\begin{pmatrix} l \\ k \end{pmatrix} + \vec{u}\begin{pmatrix} l \\ k \end{pmatrix}, \ldots\right) \quad . \tag{3}$$

2. Taylor Series Expansion

A Taylor series expansion is justified with the assumption

$$\left|\vec{u}\begin{pmatrix} l \\ k \end{pmatrix}\right| << \left|\vec{X}\begin{pmatrix} l \\ k \end{pmatrix}\right| \quad . \tag{4}$$

The potential energy is then approximated by the first non-zero term,

$$U \equiv \frac{1}{2} \sum_{l,k,l',k'} \sum_{\alpha,\beta} u_\alpha \begin{pmatrix} l \\ k \end{pmatrix} u_\beta \begin{pmatrix} l' \\ k' \end{pmatrix} V_{\alpha\beta} \begin{pmatrix} l & l' \\ k & k' \end{pmatrix} \quad , \tag{5}$$

where

$$V_{\alpha\beta}\begin{pmatrix} l & l' \\ k & k' \end{pmatrix} = \left.\frac{\partial^2 V(\vec{x})}{\partial x_\alpha\begin{pmatrix} l \\ k \end{pmatrix}\partial x_\beta\begin{pmatrix} l' \\ k' \end{pmatrix}}\right|_{\vec{x}} \quad . \tag{6}$$

$V_{\alpha\beta}\begin{pmatrix} l & l' \\ k & k' \end{pmatrix}$ is the first non-trivial term and represents the deformation energy. It takes the form of a spring constant in a three-dimensional harmonic oscillator, that is (in one dimension), k in $F = -kx$ and $V = \frac{1}{2}kx^2$. $V_{\alpha\beta}$ allows coupling of energy in the α and β directions. No assumption is made about the form of $V_{\alpha\beta}$. Although it carries indices for the positions l,k and l',k', it is dependent on the whole set of coordinates.

The kinetic energy is simply the sum of each particle's kinetic energy,

$$T = \frac{1}{2}\sum_{l,k}\sum_{\alpha} m_k\left[\dot{u}_\alpha\begin{pmatrix} l \\ k \end{pmatrix}\right]^2 \quad , \tag{7}$$

where

$$\dot{u}_\alpha\begin{pmatrix} l \\ k \end{pmatrix} \equiv \frac{\partial u_\alpha\begin{pmatrix} l \\ k \end{pmatrix}}{\partial t} \quad . \tag{8}$$

Note this form for the kinetic energy allows for different particle masses within a cell.

Now the Lagrangian, $L = T - U$, is written

$$L = \frac{1}{2}\sum_{l,k}\sum_{\alpha}\left\{m_k\left[\dot{u}_\alpha\begin{pmatrix} l \\ k \end{pmatrix}\right]^2 - \sum_{l',k'}\sum_{\beta} u_\alpha\begin{pmatrix} l \\ k \end{pmatrix}u_\beta\begin{pmatrix} l' \\ k' \end{pmatrix}V_{\alpha\beta}\begin{pmatrix} l & l' \\ k & k' \end{pmatrix}\right\} \quad , \tag{9}$$

and the equations of motion obtained from the Lagrangian are

$$m_k \ddot{u}_\alpha \begin{pmatrix} l \\ k \end{pmatrix} = \sum_{l',k'} \sum_{\beta} V_{\alpha\beta} \begin{pmatrix} l & l' \\ k & k' \end{pmatrix} u_\beta \begin{pmatrix} l' \\ k' \end{pmatrix} \quad . \tag{10}$$

3. Invariance Requirements

To this point the potential $V_{\alpha\beta}$ is an arbitrary function. Now, by exploiting some invariance requirements that arise from the form of the potential, such as arbitrariness in numbering the cells, invariance to rigid body motions, etc., some structure can be imposed on the form of $V_{\alpha\beta}$. The results are summarized below.

a) Changing the starting cell—invariance to counting origin. The result is

$$V_{\alpha\beta} = V_{\alpha\beta} \begin{pmatrix} l-l' \\ k \quad k' \end{pmatrix} \quad . \tag{11}$$

b) Changing the direction of counting—invariance to particle interchange. Then

$$V_{\alpha\beta} = V_{\alpha\beta} \begin{pmatrix} |l-l'| \\ k \quad k' \end{pmatrix} \quad . \tag{12}$$

c) Invariance to rigid translation of the lattice, giving

$$\bar{\sum_{l',k'}} V_{\alpha\beta} \begin{pmatrix} l-l' \\ k \quad k' \end{pmatrix} = -V_{\alpha\beta} \begin{pmatrix} 0 \\ k \quad k \end{pmatrix} \quad , \tag{13}$$

where the bar on the summation indicates the exclusion of the term $l',k'=l,k$.

d) Invariance to rigid rotation of the lattice gives

$$\sum_{\alpha,\delta} \sum_{l',k'} V_{\alpha\beta} \begin{pmatrix} l-l' \\ k \quad k' \end{pmatrix} \omega_{\alpha\delta} \left[X_\delta \begin{pmatrix} l' \\ k' \end{pmatrix} - X_\delta \begin{pmatrix} l \\ k \end{pmatrix} \right] = 0 \quad . \tag{14}$$

e) Invariance arising from the definition of $V_{\alpha\beta}$ and symmetry in the order of differentiation yields

$$V_{\alpha\beta}\begin{pmatrix} l & l' \\ k & k' \end{pmatrix} = V_{\beta\alpha}\begin{pmatrix} l' & l \\ k' & k \end{pmatrix} = V_{\alpha\beta}\begin{pmatrix} l' & l \\ k' & k \end{pmatrix} \quad . \tag{15}$$

4. Equations of Motion

With these simplifications on the potential, the equations of motion and the potential energy can be rewritten. If we rewrite equation (10) isolating the $l',k'=l,k$ term, make use of the invariance requirements, and introduce $p = l - l'$, the equations of motion look like this

$$m_k \ddot{u}_\alpha\begin{pmatrix} l \\ k \end{pmatrix} = \sum_{p>0,k'} \sum_{\beta} V_{\alpha\beta}\begin{pmatrix} p & \\ k & k' \end{pmatrix}\left[u_\beta\begin{pmatrix} l-p \\ k' \end{pmatrix} - 2u_\beta\begin{pmatrix} l \\ k \end{pmatrix} + u_\beta\begin{pmatrix} l+p \\ k' \end{pmatrix}\right] \quad . \tag{16}$$

This has the more familiar form of a three-dimensional harmonic oscillator with spring constant $V_{\alpha\beta}\begin{pmatrix} p & \\ k & k' \end{pmatrix}$ between elements k and k' in cells separated by the distance represented by $p = |l - l'|$.

By similar techniques the potential, U, is rewritten to give

$$U = \frac{1}{2} \sum_{l,k,p,k'} \sum_{\alpha,\beta} V_{\alpha\beta}\begin{pmatrix} p & \\ k & k' \end{pmatrix}\left[u_\alpha\begin{pmatrix} l+p \\ k' \end{pmatrix} - u_\alpha\begin{pmatrix} l \\ k \end{pmatrix}\right]\left[u_\beta\begin{pmatrix} l+p \\ k' \end{pmatrix} - u_\beta\begin{pmatrix} l \\ k \end{pmatrix}\right] \quad . \tag{17}$$

5. Continuum Limit

For the continuum limit, consider the equations of motion as described by equation (16). Define $\vec{u}\begin{pmatrix} l \\ k \end{pmatrix} \equiv \vec{u}\left(\vec{x}\begin{pmatrix} l \\ k \end{pmatrix}, t \right)$ and expand $u_\beta\begin{pmatrix} l \pm p \\ k' \end{pmatrix}$ in a Taylor series to give

$$m_k \ddot{u}_\alpha\begin{pmatrix} l \\ k \end{pmatrix} = \sum_{p>0,k'} \sum_{\beta} V_{\alpha\beta}\begin{pmatrix} p & \\ k & k' \end{pmatrix} \sum_{\gamma,\delta} X_\gamma\begin{pmatrix} p & \\ k & k' \end{pmatrix} X_\delta\begin{pmatrix} p & \\ k & k' \end{pmatrix} \frac{\partial^2}{\partial x_\gamma \partial x_\delta} u_\beta\begin{pmatrix} l \\ k \end{pmatrix} \quad . \tag{18}$$

For the energy, start with equation (17), again using a Taylor expansion and keeping only the first non-zero term,

$$U = \frac{1}{2} \sum_{l,k,p,k'} \sum_{\alpha,\beta} V_{\alpha\beta}\begin{pmatrix} p \\ k \quad k' \end{pmatrix} \left[\sum_{\gamma} X_{\gamma}\begin{pmatrix} p \\ k \quad k' \end{pmatrix} \frac{\partial}{\partial x_{\gamma}} u_{\alpha}\begin{pmatrix} l \\ k \end{pmatrix} \right] \left[\sum_{\delta} X_{\delta}\begin{pmatrix} p \\ k \quad k' \end{pmatrix} \frac{\partial}{\partial x_{\delta}} u_{\beta}\begin{pmatrix} l \\ k \end{pmatrix} \right] \quad . \tag{19}$$

Finally, equation (18) is averaged over the cell by summing over k, then dividing by the volume of the cell, v. Use is made of the following substitutions:

$$\begin{aligned} \rho &= \frac{1}{v} \sum_{k} m_k \\ c_{\alpha\gamma\beta\delta} &= \frac{1}{v} \sum_{k,p>0,k'} V_{\alpha\beta}\begin{pmatrix} p \\ k \quad k' \end{pmatrix} X_{\gamma}\begin{pmatrix} p \\ k \quad k' \end{pmatrix} X_{\delta}\begin{pmatrix} p \\ k \quad k' \end{pmatrix} \quad , \end{aligned} \tag{20}$$

giving

$$\rho \frac{\partial^2 u_{\alpha}}{\partial t^2} = \sum_{\beta\gamma\delta} \frac{\partial}{\partial x_{\gamma}} \left(c_{\alpha\gamma\beta\delta} \varepsilon_{\beta\delta} \right) \quad . \tag{21}$$

Similar techniques can be used for the energy, equation (19). In addition, the summation over l is replaced by an integral over the volume, V, and dividing by the cell volume v, to obtain

$$U = \frac{1}{2} \int dV \, c_{\alpha\gamma\beta\delta} \varepsilon_{\alpha\gamma} \varepsilon_{\beta\delta} \quad . \tag{22}$$

B. Pairwise Potential

Thus far the form of the potential has been general. Here we deviate from the elasticity model as presented by Askar. The mesoscopic model is specified now by our mass points and by imposing the following restrictions on the potential energy, U:

a) the potential at each particle is simply the sum of the pairwise interactions due to each of its neighbors, and the total potential is the sum of the pairwise potentials for each quasiparticle,

b) the pairwise potentials given in a) differ depending on their relative positions in the lattice,

c) at equilibrium each pair potential (and thus, force) is zero—this makes quasiparticles at the lattice boundaries no different from those in the bulk, and no other imposition of edge conditions is required for the finite lattice.

From translational and rotational invariance, as already shown, l and l' can only appear through the magnitude of their difference; thus V is a central interaction. Then V can be written

$$V = \frac{1}{2} \sum_{l,k,l',k'} \sum_{i} \hat{V}\left(\left| \vec{x}\begin{pmatrix} l \\ k \end{pmatrix} - \vec{x}\begin{pmatrix} l' \\ k' \end{pmatrix} \right| \right) \quad . \tag{23}$$

where the index i sums over each particle in the lattice. The 1/2 arises because in the summation each pair interaction appears twice.

The first few terms of the Taylor series expansion, equation (6), now look like

$$
\begin{aligned}
V^o &= \frac{1}{2}\sum_{l,k,l',k'}\sum_i \hat{V}_i(r)\Big|_R = \frac{1}{2}\sum_{l,k,l',k'}\hat{V}_i(R) \\
V_\alpha\left(\begin{smallmatrix} l \\ k \end{smallmatrix}\right) &= \frac{\partial}{\partial x_\alpha\left(\begin{smallmatrix} l \\ k \end{smallmatrix}\right)}\sum_{l',k'}\sum_i \hat{V}(r)\Big|_R = \frac{1}{2}\sum_{l',k'}\sum_i \hat{V}'(R)\frac{\overline{X}_\alpha}{R} \\
V_{\alpha\beta}\left(\begin{smallmatrix} p \\ k \end{smallmatrix}\begin{smallmatrix} \\ k' \end{smallmatrix}\right) &= \frac{\partial^2\sum_i \hat{V}_i(r)}{\partial x_\alpha\left(\begin{smallmatrix} l \\ k \end{smallmatrix}\right)\partial x_\beta\left(\begin{smallmatrix} l' \\ k' \end{smallmatrix}\right)}\Big|_R = \sum_i \frac{\partial}{\partial x_\beta\left(\begin{smallmatrix} l' \\ k' \end{smallmatrix}\right)}\left[\hat{V}_i'(R)\frac{x_\alpha}{r}\right]\Big|_R \\
&= \sum_i\left[-\frac{X_\alpha X_\beta}{R^2}\hat{V}_i''(R) + \frac{\hat{V}_i'(R)}{R}\left(\frac{X_\alpha X_\beta}{R^2} - \delta_{\alpha\beta}\right)\right] ,
\end{aligned}
\tag{24}
$$

where we have made use of the following definitions:

$$
\begin{aligned}
r = r\left(\begin{smallmatrix} p \\ k \end{smallmatrix}\begin{smallmatrix} \\ k' \end{smallmatrix}\right) &= \left|\vec{x}\left(\begin{smallmatrix} l \\ k \end{smallmatrix}\right) - \vec{x}\left(\begin{smallmatrix} l' \\ k' \end{smallmatrix}\right)\right| = \left[\sum_\gamma\left(x_\gamma\left(\begin{smallmatrix} l \\ k \end{smallmatrix}\right) - x_\gamma\left(\begin{smallmatrix} l' \\ k' \end{smallmatrix}\right)\right)^2\right]^{\frac{1}{2}} \\
R = R\left(\begin{smallmatrix} p \\ k \end{smallmatrix}\begin{smallmatrix} \\ k' \end{smallmatrix}\right) &= \left|\vec{X}\left(\begin{smallmatrix} l \\ k \end{smallmatrix}\right) - \vec{X}\left(\begin{smallmatrix} l' \\ k' \end{smallmatrix}\right)\right| \\
\frac{\partial r}{\partial x_\alpha} &= \frac{1}{2}\left[\sum_\gamma\left(x_\gamma\left(\begin{smallmatrix} l \\ k \end{smallmatrix}\right) - x_\gamma\left(\begin{smallmatrix} l' \\ k' \end{smallmatrix}\right)\right)^2\right]^{-\frac{1}{2}} 2\left(x_\gamma\left(\begin{smallmatrix} l \\ k \end{smallmatrix}\right) - x_\gamma\left(\begin{smallmatrix} l' \\ k' \end{smallmatrix}\right)\right) = \frac{r_\alpha}{r} ,
\end{aligned}
\tag{25}
$$

and

$$
\hat{V}'(R) = \frac{\partial\hat{V}(r)}{\partial r}\Big|_{r=R} , \quad \hat{V}''(R) = \frac{\partial^2\hat{V}(r)}{\partial r^2}\Big|_{r=R} . \tag{26}
$$

As before, V^o is only a reference potential, and at equilibrium $V_i'(R) = 0$ for all i, so the term $V_\alpha\left(\begin{smallmatrix} l \\ k \end{smallmatrix}\right)$ vanishes, leaving, $V_{\alpha\beta}\left(\begin{smallmatrix} p \\ k \end{smallmatrix}\begin{smallmatrix} \\ k' \end{smallmatrix}\right) = -\frac{X_\alpha X_\beta}{R^2}\sum_i \hat{V}_i'(R)$. For Hooke's law forces, $\hat{V}_i = \frac{1}{2}k_i r_i^2$ so $\hat{V}_i''(R) = k_i$. Finally,

$$V_{\alpha\beta}\left(\begin{smallmatrix} p \\ k \quad k' \end{smallmatrix}\right) = -\frac{X_\alpha X_\beta}{R^2}\sum_i k_i \tag{27}$$

The elasticity coefficient matrix can now be written

$$c_{\alpha\gamma\beta\delta} = \frac{1}{v}\sum_{k,p,k'}\sum_i k_i \frac{X_\alpha X_\gamma X_\beta X_\delta}{R^2} \quad . \tag{28}$$

C. Cubic Monatomic Lattice

Lets look at a simple model, a cubic monatomic lattice. The cell volume, v, is given by a^3, where a is the distance between lattice points. The index k has only one value, leaving only the cell index l. We will look only at the first three nearest neighbor interactions. Those in the first quadrant for a particle at the origin are depicted in Figure 2. For each particle in the bulk, there are 6 first neighbor particles, with spring constant k_1, at $R = a$ and coordinates $(\pm a,0,0)$, $(0,\pm a,0)$, and $(0,0,\pm a)$—along the edge of the cube; 12 second neighbor particles with spring constant k_2, at $R = \sqrt{2}\,a$ and coordinates $(\pm a,\pm a,0)$, $(\pm a,0,\pm a)$, and $(0,\pm a,\pm a)$—across the face of the cube; and 8 third neighbor particles, with spring constant k_3, at $R = \sqrt{3}\,a$ and coordinates $(\pm a,\pm a,\pm a)$—connecting opposite corners of the cube through its center.

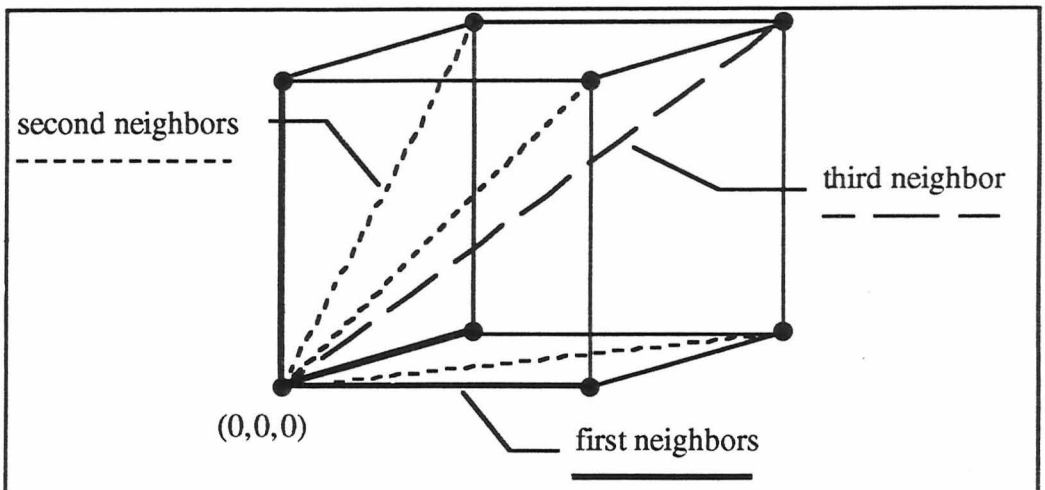

Figure 2—neighbors to a particle at the origin, first quadrant only

For a particle at (0,0,0), shown are its first neighbors at (a,0,0), (0,a,0), and (0,0,a), second neighbors at (a,a,0), (a,0,a), and (0,a,a), and third neighbor at (a,a,a).

Substituting these values into equation (28) yields the desired result:

$$
\begin{aligned}
c_{xxxx} &= c_{yyyy} = c_{zzzz} = a\left[(2)\frac{k_1}{a^2} + (8)\frac{k_2}{2a^2} + (8)\frac{k_3}{3a^2}\right] = \frac{2}{a}\left(k_1 + 2k_2 + \tfrac{4}{3}k_3\right) \\
c_{xxyy} &= c_{xxzz} = c_{yyzz} = a\left[(0)\frac{k_1}{a^2} + (4)\frac{k_2}{2a^2} + (8)\frac{k_3}{3a^2}\right] = \frac{2}{a}\left(k_2 + \tfrac{4}{3}k_3\right) \\
c_{xyxy} &= c_{xzxz} = c_{yzyz} = c_{xxyy} \\
c_{\text{odd}} &= 0
\end{aligned}
\tag{29}
$$

where c_{odd} represents elastic constants in which an index appears an odd number of times.

Traditionally elastic constants have been written with the notation of Voigt[12], reducing the fourth order tensor $c_{\alpha\gamma\beta\delta}$ to an ordinary matrix c_{ij}. We will use that same matrix notation here. The three non-zero components are

$$
\begin{aligned}
c_{11} &= c_{xxxx} = \frac{2}{a}\left(k_1 + 2k_2 + \tfrac{4}{3}k_3\right) \\
c_{12} &= c_{xxyy} = \frac{2}{a}\left(k_2 + \tfrac{4}{3}k_3\right) \\
c_{44} &= c_{xyxy} = c_{12}
\end{aligned}
\tag{30}
$$

D. Mesoscopic spring constants

Equation (30) is the relationship between the experimental quantities (elastic constants) and the spring constants in the model we have been looking for. Having arrived at the relationship, the equations must now be inverted to solve for the spring constants in terms of the elastic constants.

In order to prevent material shear, spring constants between second and/or third neighbors must be included in the mesoscopic model. The simplest approach—given there are only two equations for the three unknown spring constants—is to use only first and second neighbors, making the assumption k_3=0. However, negative values for the k's are often obtained when using this approach with elastic constants from real materials. This necessitates a third constraint which allows calculation of all three spring constants.

The author constructed and compared several relationships for the third constraint. Ideally the constraint would be more than an arbitrary choice and have some physical significance. The method chosen for the calculations performed here, unless otherwise noted, is the following,

$$k_3 = \gamma^{-1} k_2 \ , \tag{31}$$

where γ is a measure of the anisotropy of the material[13], and is defined by $\gamma \equiv \dfrac{2c_{44}}{c_{11} - c_{12}}$.

For an isotropic medium γ= 1. Most single crystals are far from isotropic, typically with

γ values greater than one and as high as 6.5 for potassium. Only tungsten has a value close to unity.

A comparison of the various constraints considered was performed using elastic constants from NaCl. The results were surprisingly similar, but this method more consistently gave positive results for the k_r. For a more complete review of the different methods see Appendix B.

The resulting equations for the $k_i(c_{ij})$ are,

$$\begin{aligned} k_1 &= \frac{a}{2}\left[c_{11} - \frac{4c_{44} + \frac{4}{3}(c_{11} - c_{12})}{2c_{44} + \frac{4}{3}(c_{11} - c_{12})} c_{12}\right] \\ k_2 &= \frac{a}{2}\left[\frac{2c_{12}c_{44}}{2c_{44} + \frac{4}{3}(c_{11} - c_{12})}\right] \\ k_3 &= \frac{a}{2}\left[\frac{c_{12}(c_{11} - c_{12})}{2c_{44} + \frac{4}{3}(c_{11} - c_{12})}\right] \end{aligned} \tag{32}$$

A Hooke's law force has two components, a stiffness constant and an equilibrium distance. The stiffness constants are given by equation (32). In this model the equilibrium distance for each particle-neighbor pair is equal to the distance between them in the equilibrium configuration of the unstressed lattice.

IV. Computations

I wrote the two codes, BEAML and PLATO, to calculate deformation of a lattice of various configurations with the mesoscopic potentials given by equation (32). The codes create a lattice of particles (actually concentrated mass points) representing the configuration of interest, and assign an appropriate potential (a spring constant and equilibrium distance) between each particle's first, second, and third neighbors. Other neighbor-pair potentials are not considered. An iterative technique is employed to numerically solve the equations of motion for the system, calculating change in position of each lattice particle due to each of its neighbor-pair interactions, then repeatedly stepping through the lattice in small time increments until changes in position between steps is small. Figure 3 summarizes the computational method. Both codes solve the equations of motion using the same algorithm. For BEAML stress is introduced to the lattice with a mass placed at the end of the beam. PLATO induces stress on a plate structure by modeling a thin film deposited onto one of its surfaces.

Computational method

- Obtain discrete dynamic equations
- Solve the equations numerically
- Start at unloaded equilibrium
- Load the system
- Allow to oscillate toward new equilibrium position
- Quench motion to reach static condition

Figure 3—computational method

The method is outlined for solving the structural problem.

This chapter presents results of calculations using these two codes. The first section compares deformation of a rectangular beam from the BEAML code and the results given by beam theory. The second section presents results of the PLATO code which calculates a plate stressed by a thin film. The final section presents results of the PLATO code where one surface of the plate has a deposited thin film, and the other has been etched to make a deep ribbed structure.

A. Comparison to Beam Theory

The code BEAML was written to model deformation of a rectangular beam fixed at one end and loaded by a mass at the other end. This code is used to compare the mesoscopic model to the deformation predicted by beam theory, serving the dual purpose of validating both the writing of the code as well as the mesoscopic model itself.

For a rectangular bar with horizontal cross-sectional dimension L_x and vertical dimension L_z, the bar extending from the supported end a distance L_y, and a mass m placed at the extended end, beam theory predicts deflection at a position y along the bar by the equation[14]

$$\Delta z = \frac{2mg}{E}\frac{\left(3L_y y^2 - y^3\right)}{L_z^3 L_x} \quad , \tag{33}$$

where deflection is in the positive z-direction and E is Young's modulus. The only material property considered in this equation is the elastic modulus E, which quantifies the force required to produce unit strain in the material. It is a measure of the material's elasticity.

Equation (33) indicates deflection of the bar at its end ($y = L_y$) is linear with load (mg), and with L_x^{-1}, L_y^3, and L_z^{-3}. The initial comparison of the mesoscopic model to beam theory is to plot BEAML results against these parameters and compare linearity. Results from BEAML are shown in Figure 4 through Figure 7, where Δz is plotted against load, against L_x^{-1}, against L_y^3, and against L_z^{-3}, each varied across a moderate range. Values for those parameters held constant are shown in the plot title (size values are given in number of mass particles in the given direction). Elastic constants are taken from NaCl.

Over the range plotted, the dimensional parameters of the beam are linear with the beam theory parameters, and for load there is a slight negative curvature as load becomes heavier rather than a straight line as beam theory predicts.

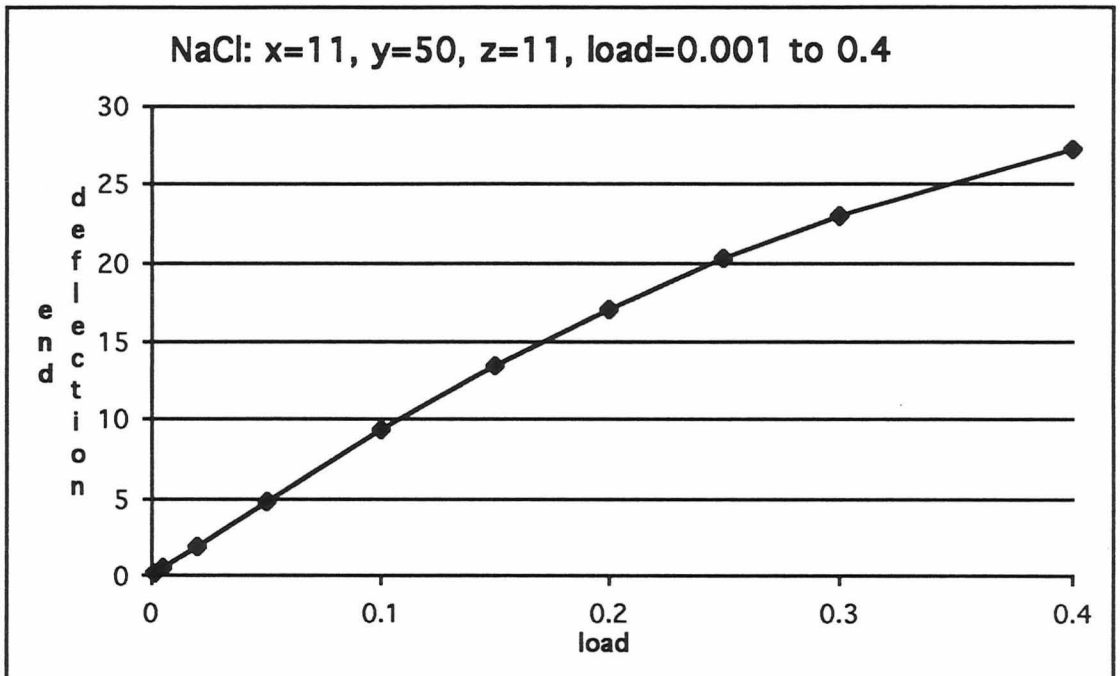

Figure 4—deflection vs. load

Beam theory predicts deflection to be linear with load. BEAML results are linear for light to intermediate loads, with slight negative curvature for heavier loads.

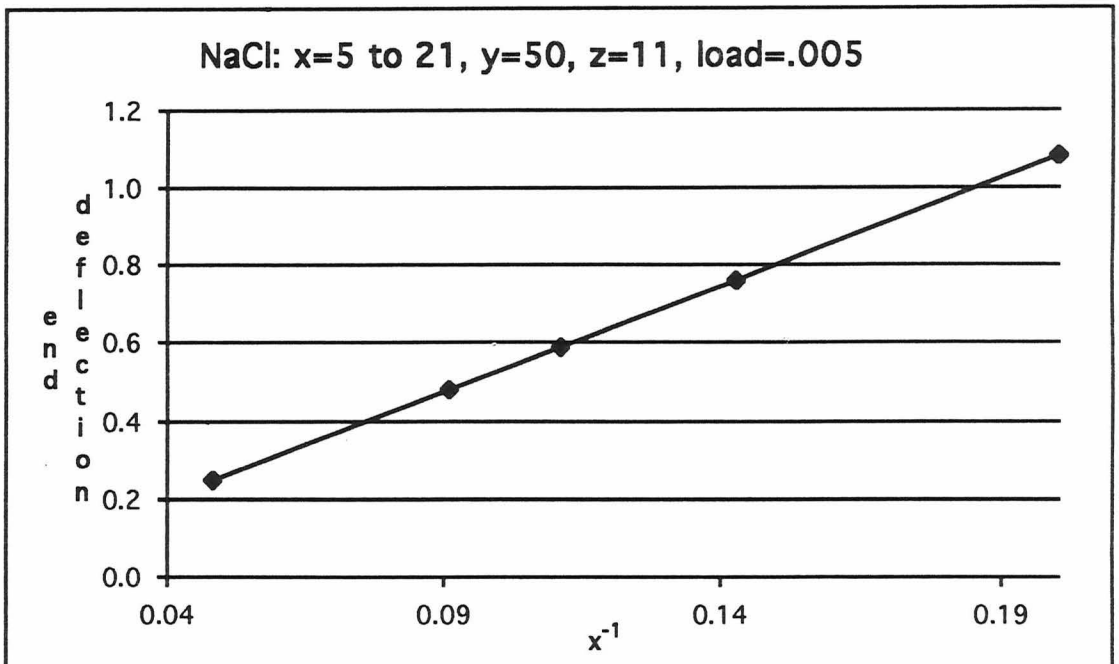

Figure 5—deflection vs. L_x^{-1}

Beam theory predicts deflection to be linear with inverse length in the x-direction. BEAML results are linear for the range of *x*-values tested.

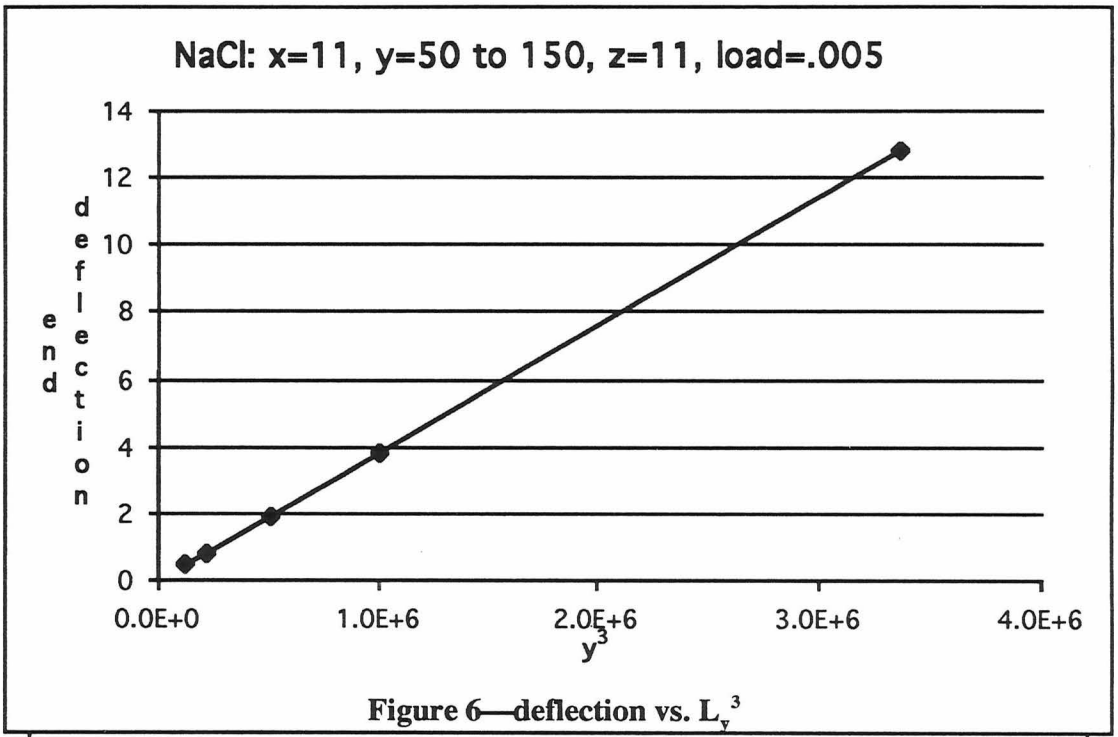

Figure 6—deflection vs. L_y^3

Beam theory predicts deflection to be linear with the cube of length in the y-direction. BEAML results are linear for the range of *y*-values tested.

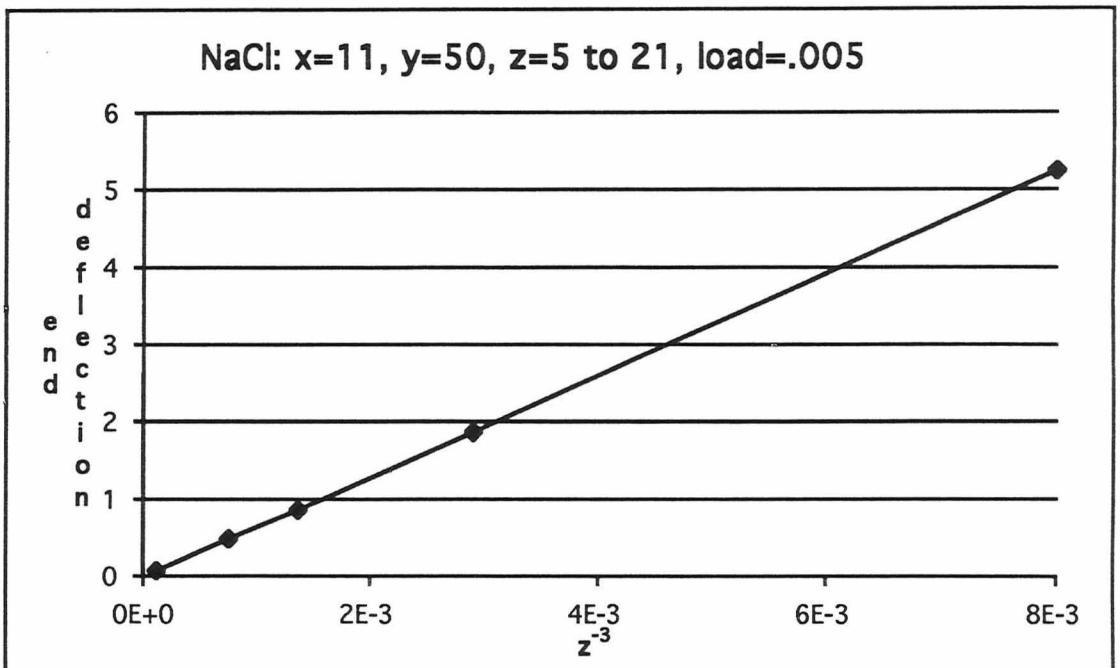

Figure 7—deflection vs. L_z^{-3}

Beam theory predicts deflection to be linear with the inverse cube of length in the z-direction. BEAML results are linear for the range of *z*-values tested.

1. Effective Young's Modulus

The previous section compares the effects of beam theory parameters to those of the mesoscopic model. We now look at the shape of the beam resulting from BEAML compared to the shape from beam theory. Figure 8 plots Δz versus distance, y, along the beam for both models. The beam theory line is simply a calculation from equation (33), while the mesoscopic model line is the result of the calculation of BEAML. Spring constants for the mesoscopic model are obtained from the elastic constants of NaCl. The beam theory parameter E is also from NaCl.

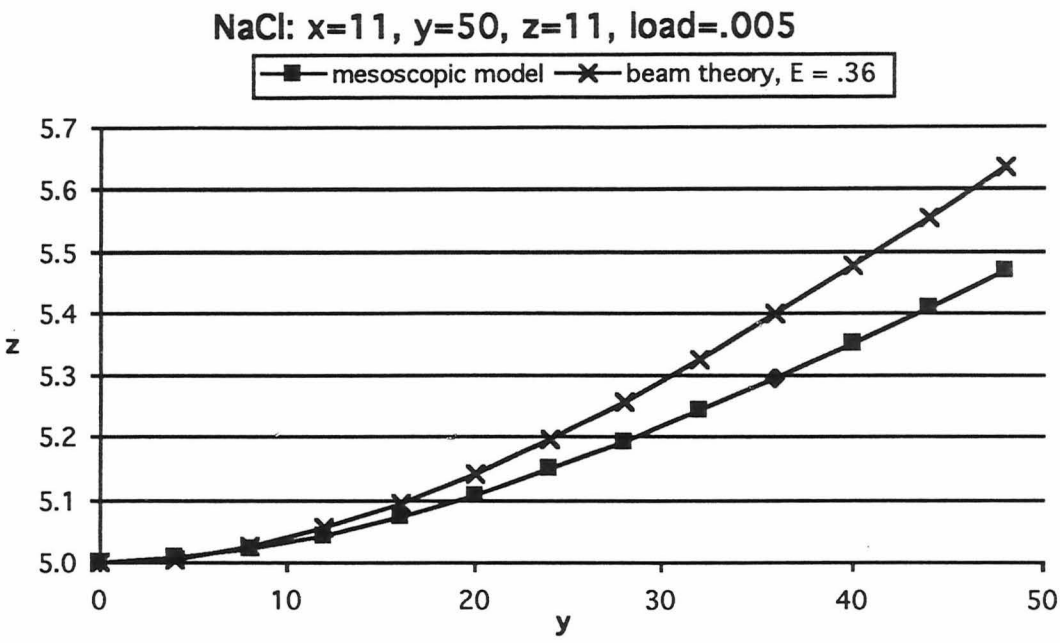

Figure 8—NaCl: y = 50, load = .005

Results of BEAML for NaCl, plotted with *E*.

BEAML predicts a shape that is similar to that of beam theory, but the deflection is not the same for the two models when using Young's modulus for the material. For NaCl the beam theory code predicts greater curvature than does BEAML. However, a value for E *can* be found that will match the beam theory curve to the BEAML curve. This value of E we have called the *effective* Young's modulus (E_{eff}) for the structure being modeled. Several materials and configurations are plotted in Figure 9 through Figure 17 showing results of BEAML along with the beam theory plot using $E = E_{\text{eff}}$ that most closely matches the BEAML line. (In some cases the actual E for the material is also plotted.) In each case the BEAML line and the $E = E_{\text{eff}}$ line are nearly indistinguishable. The beam theory line (using E_{eff}) is slightly more curved in the center than BEAML, but the least squares difference is typically less than 0.005. Also note that E_{eff} depends not only on the material (elastic constants), but on the size of the lattice being modeled as well.

The materials modeled in this comparison are NaCl, NaI, and Si. NaCl and NaI are chosen because of their ionic bonding, which makes the pairwise approximation used in the mesoscopic model valid. Silicon is modeled because of its relevance to the motivation for this research, i.e., curved silicon substrates for multilayer mirrors. For NaCl and NaI the value of E_{eff} is the same for the short beam with different loads, but differs for the longer beam, while silicon is modeled with the same E_{eff} for all four configurations.

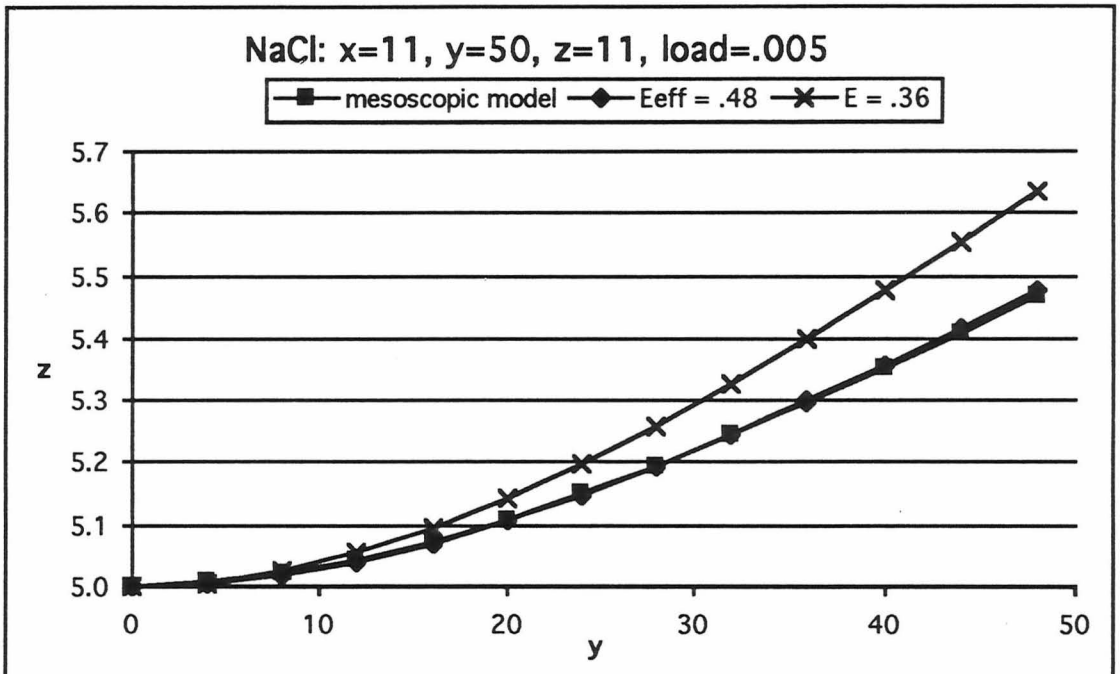

Figure 9—NaCl: y = 50, load = .005

Results of BEAML for NaCl, plotted with E_{eff} and E.

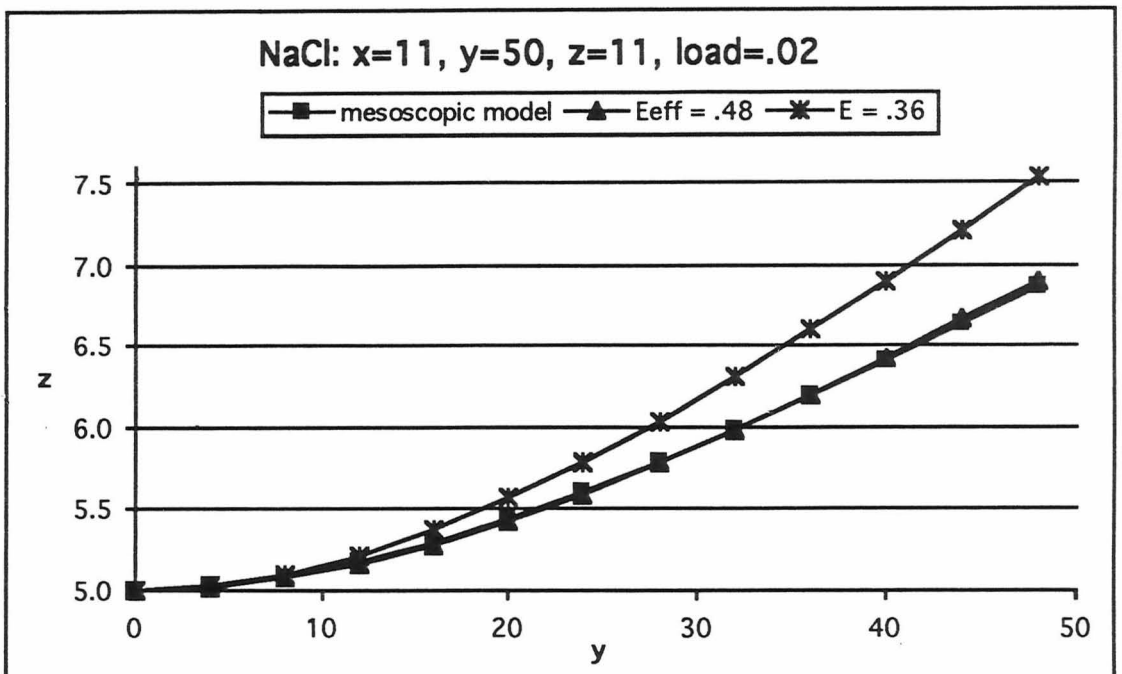

Figure 10—NaCl: y = 50, load = .02

Results of BEAML for NaCl, plotted with E_{eff}.

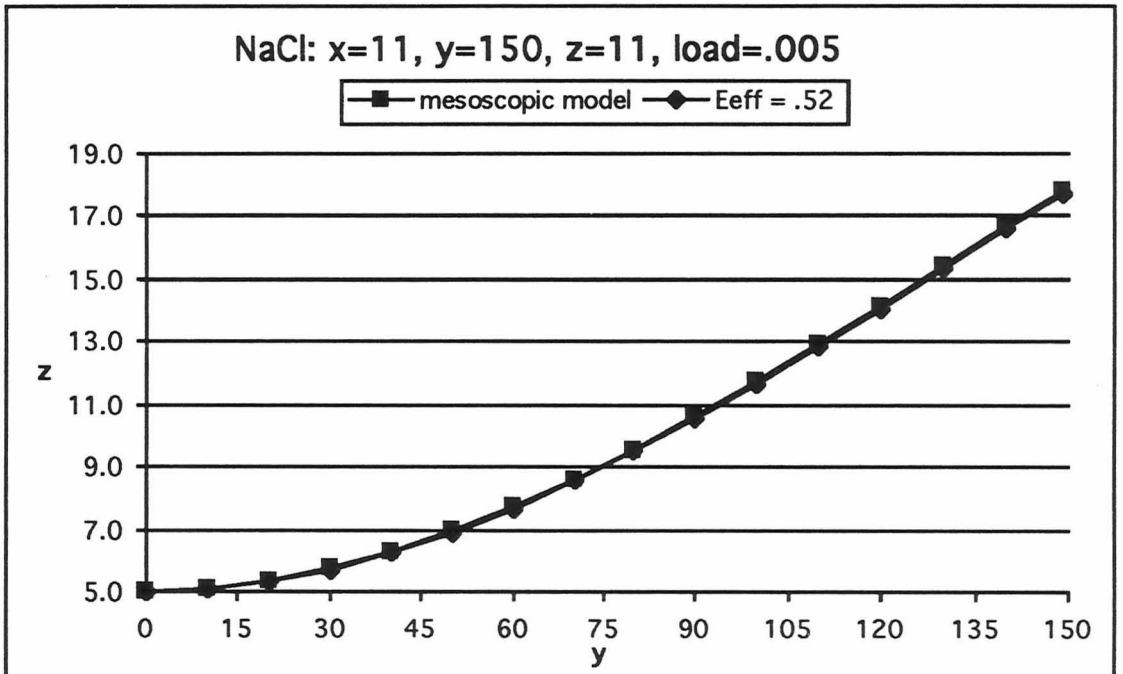

Figure 11—NaCl: y = 150, load = .005

Results of BEAML for NaCl, plotted with E_{eff}.

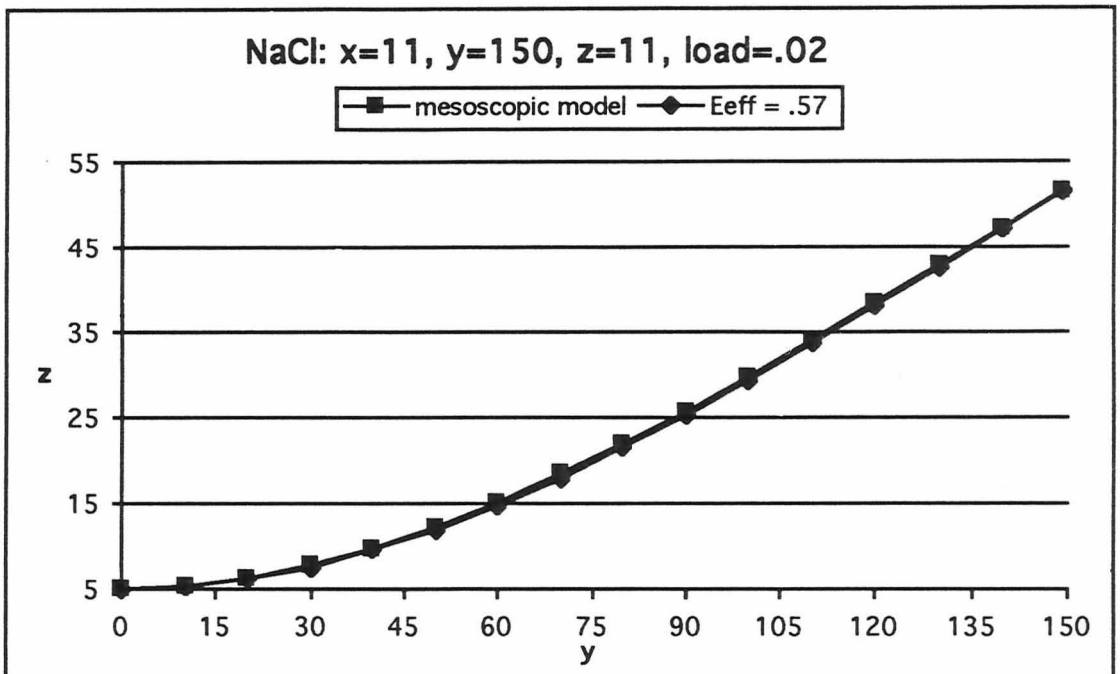

Figure 12—NaCl: y = 150, load = .02

Results of BEAML for NaCl, plotted with E_{eff}.

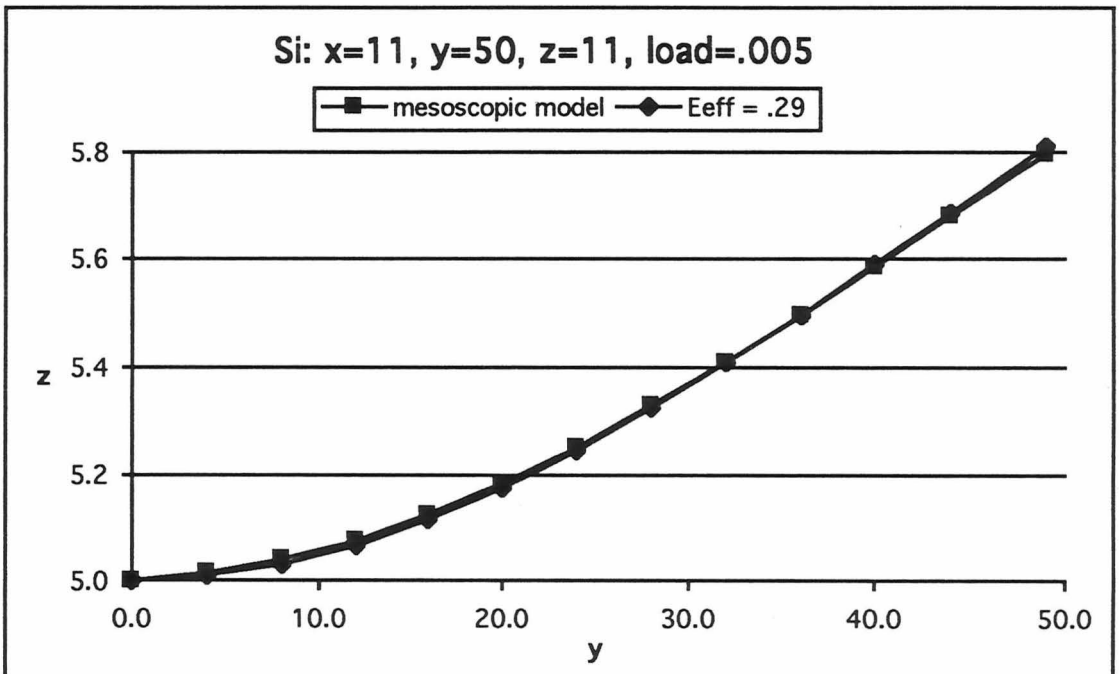

Figure 13—NaI: y = 50, load = .005

Results of BEAML for NaI, plotted with E_{eff}.

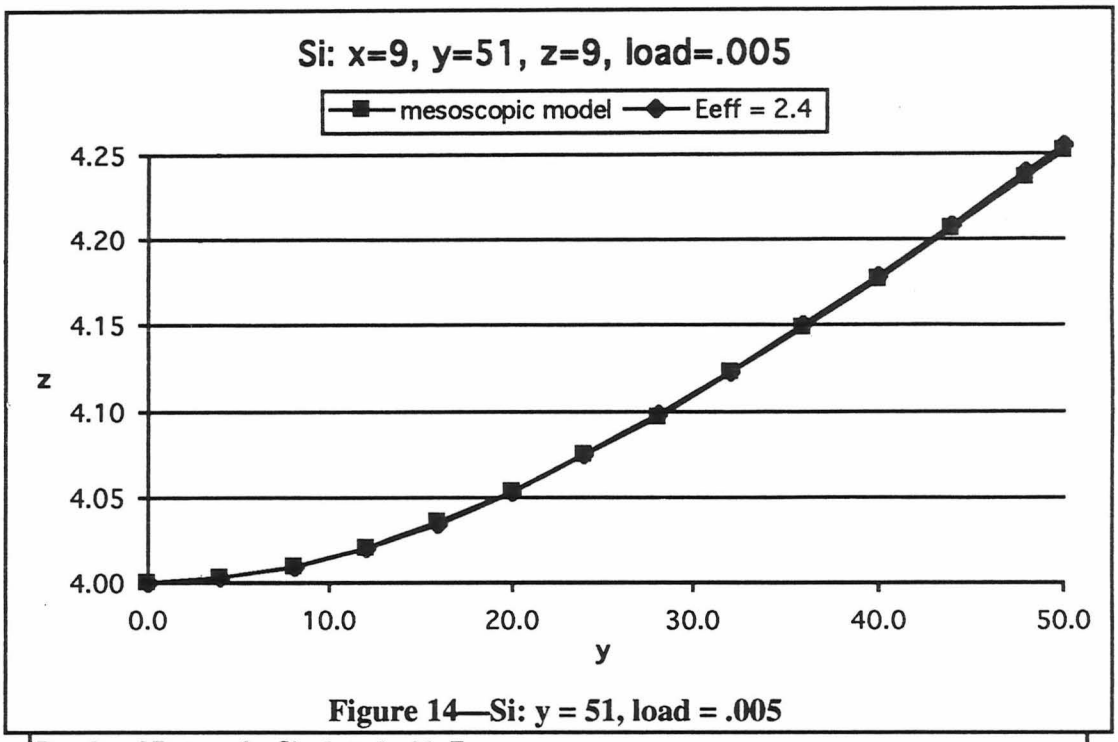

Figure 14—Si: y = 51, load = .005

Results of BEAML for Si, plotted with E_{eff}.

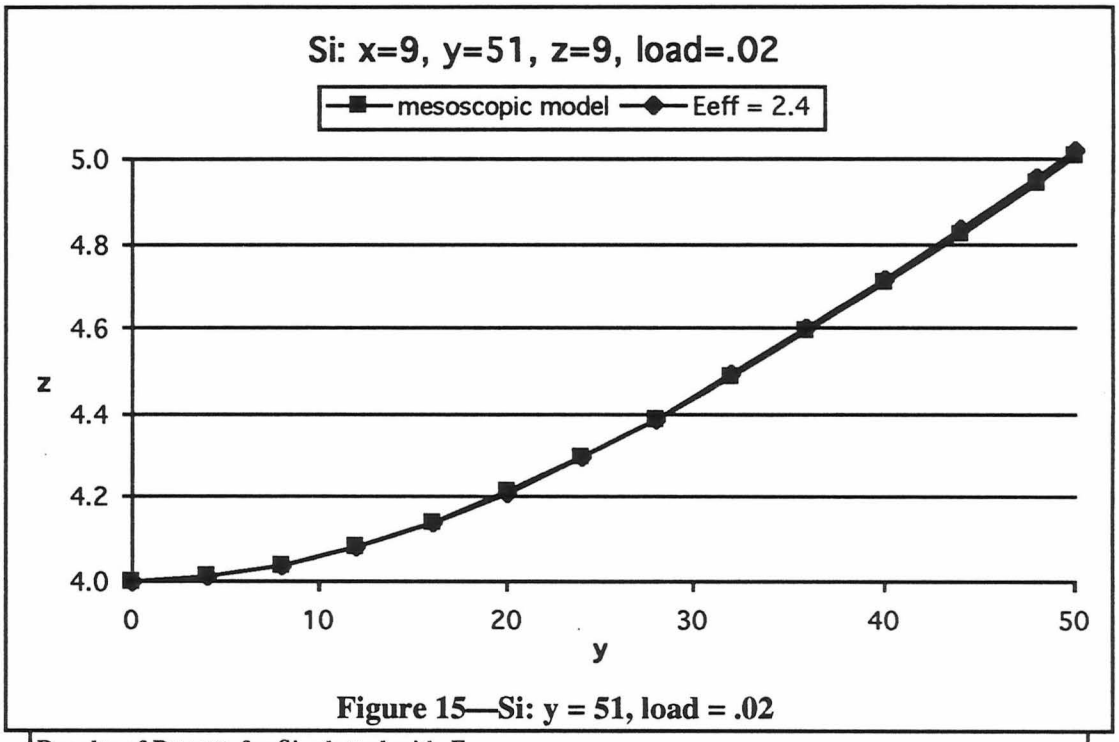

Figure 15—Si: y = 51, load = .02

Results of BEAML for Si, plotted with E_{eff}.

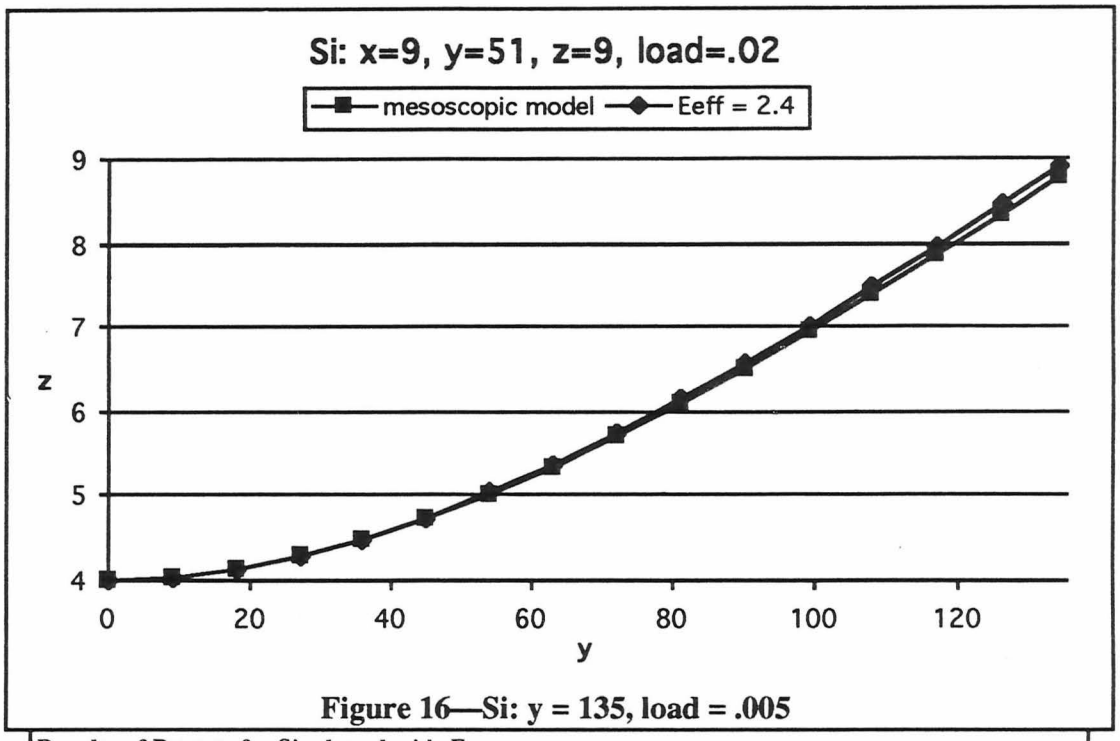

Figure 16—Si: y = 135, load = .005

Results of BEAML for Si, plotted with E_{eff}.

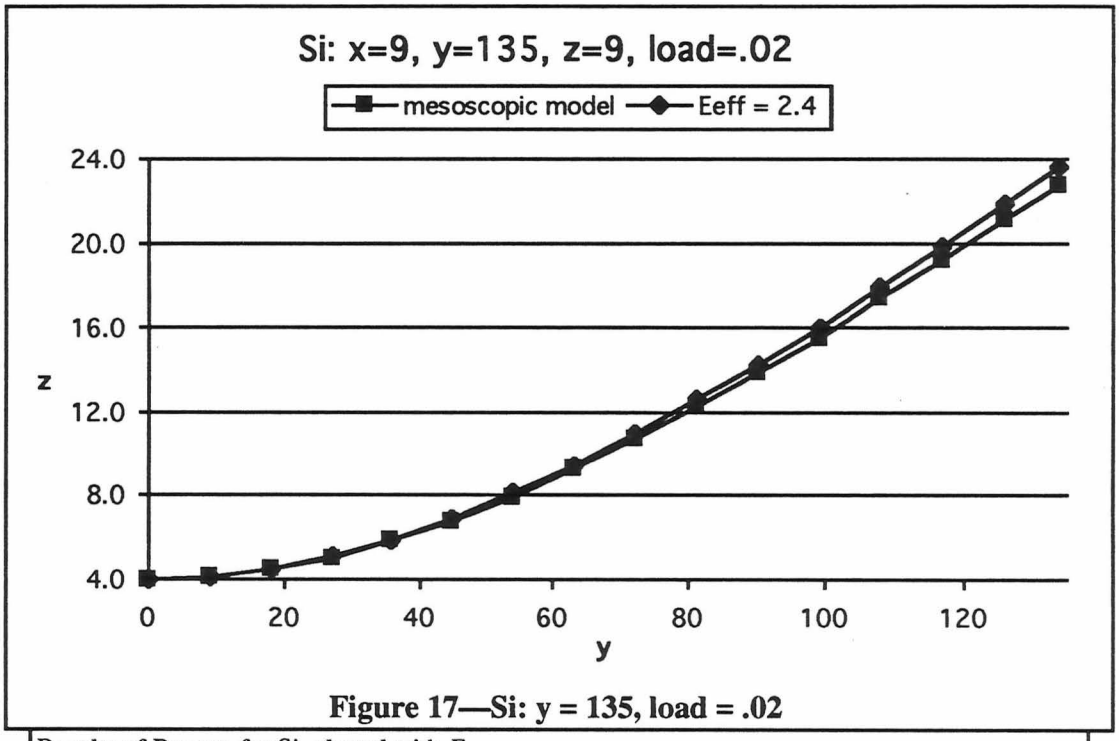

Figure 17—Si: y = 135, load = .02

Results of BEAML for Si, plotted with E_{eff}.

The mismatch of the mesoscopic model with beam theory is not completely unexpected. Young's modulus is a single measure of elasticity, while there are three elastic constants characterizing a cubic material. Each are characteristic of a given material, and are related through the equation (for a cubic crystal) [15],

$$E^{-1} = \frac{c_{11} + c_{12}}{(c_{11} + 2c_{12})(c_{11} - c_{12})} + \left(\frac{1}{c_{44}} - \frac{2}{c_{11} - c_{12}}\right)\left(n_x^2 n_y^2 + n_x^2 n_z^2 + n_y^2 n_z^2\right) \quad . \tag{34}$$

The n_α are the direction cosines. The presence of the direction cosines in this equation makes Young's modulus not unique, depending now on direction. Beam theory considers only a single value, assuming a homogeneous material. Appendix C gives experimental values of Young's modulus, elastic constants, the effective Young's modulus, and this calculated value of Young's modulus for various materials along two directions, one along the edge of the cube, the other from corner to corner through its center. Typically, the experimental values of Young's modulus fall between these two calculated values.

There are several other equations relating E to the c_{ij} [16,17,18] depending on assumptions about the microscopic structure of the material. However, for very few materials does the experimental value of Young's modulus match these calculated values, suggesting the link between these two models is not exact. One explanation for this is the loss of information when trying to model several pieces of information (the three elastic constants in the cubic case) with one number (Young's modulus). It is then not surprising that the mesoscopic model, which has more than one independent parameter, does not match beam theory exactly, and that different geometries may have different values for E_{eff} even though they have the same material properties.

The introduction of E_{eff} has served primarily two purposes. One, to show the results are comparable to beam theory, though not an exact match, and two, to serve as a

reference for comparison. It may be a valuable tool to aid in understanding a new model or for comparing different materials, but its usefulness beyond that is limited.

B. Plate with Thin Film

As indicated earlier, the motivation for this project is modeling of curved silicon substrates. Very thin silicon can be curved by depositing a thin film on one surface of the substrate surfaces and allowing the structure to come to equilibrium. To control the curvature the thickness of the film and/or the substrate can be modified, or ribs can be etched into the back surface of the silicon to obtain various curvature profiles. This section models an unetched silicon substrate (plate) with a nickel film deposited on one surface. The next section will look at ribbed structures.

The PLATO code uses this new method for stressing the structure. Rather than loading a beam with a mass at one end, stress is introduced to the structure by changing the equilibrium conditions of some of the springs in the lattice. This allows modeling of a plate with one set of spring constants and equilibrium positions, as well as a thin film on a surface of the plate with its own set of spring constants and equilibrium positions. The plate by itself is in equilibrium, as is the film by itself. Stress is introduced to the system when the plate and film are joined by spring conditions that are different from their rest configuration.

For example, if we let the equilibrium distance represent the thermal expansion coefficients we can set $X_{film}^{equil} = \frac{\alpha_{plate}}{\alpha_{film}} X_{plate}^{equil}$. Recall in the BEAML model the equilibrium distance is not a parameter characteristic of the material, and it can be set arbitrarily. In this model we use the equilibrium distance to model the difference in (or ratio of) thermal expansion coefficients between the plate and film materials. In the PLATO code the

equilibrium distance in the film is set as suggested above, and the equilibrium distance and spring constants at the interface are set equal to the average of the plate and the film constants. That is, for X_{film}^{equil} defined above, the equilibrium distance is calculated as $X_{interface}^{equil} = \frac{\frac{\alpha_{plate}}{\alpha_{film}} + 1}{2} X_{plate}^{equil}$. This introduces a stress at the plate-film interface because the springs there are not in equilibrium.

This model can be thought of as, for example, the deposition of a thin film onto a substrate at an elevated temperature, allowing the structure to cool to room temperature and equilibrium to be re-established. The film contracts more than the substrate (depending on the ratio of thermal expansion coefficients) and the result is a new configuration for the structure.

PLATO was run for several configurations of a silicon plate with a nickel film. The boundary conditions at the fixed edge (labeled 'wall') are used such that the model represents one half of a plate structure, the full plate assuming symmetric results when mirrored through the plane defined by the 'wall.' A drawing of the plate—showing the film surface, the wall, and the other lines through the plate that are plotted in following figures—is shown in Figure 18.

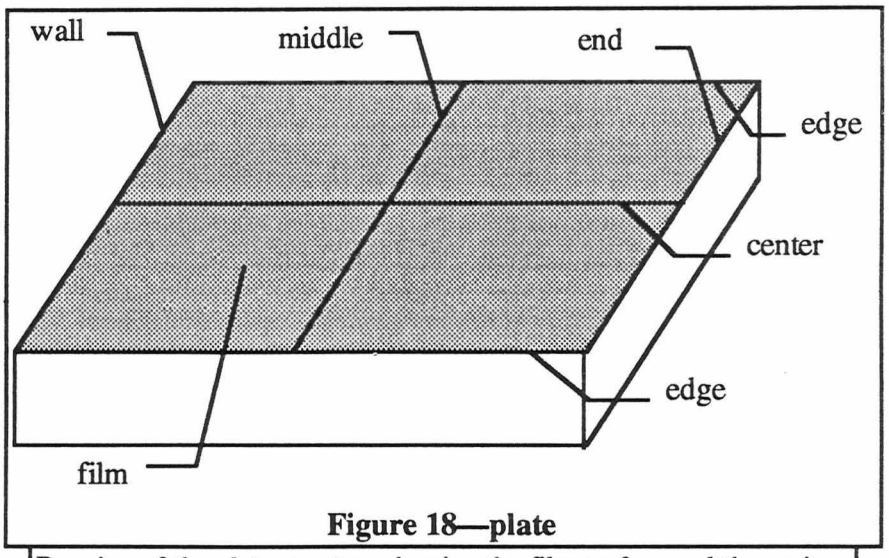

Figure 18—plate

Drawing of the plate structure showing the film surface and the various lines that are plotted in the results. The line labeled 'wall' is on the bound surface. The lines labeled 'edge' and 'end' are free.

PLATO results of a lattice size 37 x 37 x 5 (X x Y x Z) mass points are shown in Figure 19 and Figure 20. Figure 19 shows the lines perpendicular to the wall, and Figure 20 the lines parallel to the wall. The plate is four mass points thick, and the film is a single mass point thick. The ratio (called 'Aratio' in the figure) $\frac{\alpha_{plate}}{\alpha_{film}} = 0.90$. The curve for the back edge is the same as the front edge and is not shown. The curves for the perpendicular and for the parallel show, respectively, very nearly the same curvature. In the rest of this section only the center line (also labeled 'perpendicular') and the wall line (also labeled 'parallel') results will be given.

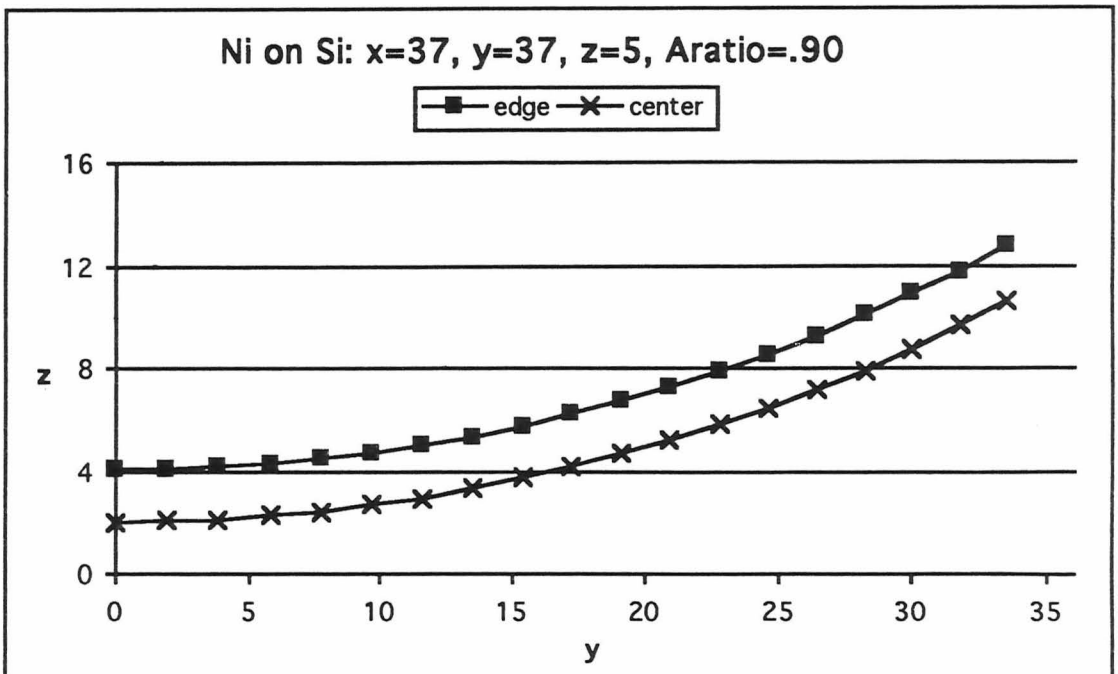

Figure 19—Ni on Si, 37x37x5, Aratio=.9 (perpendicular)

The edge and center lines of the Ni on Si structure described in the title. Curvature of the two lines are nearly the same, equal to about 74 (1.5%).

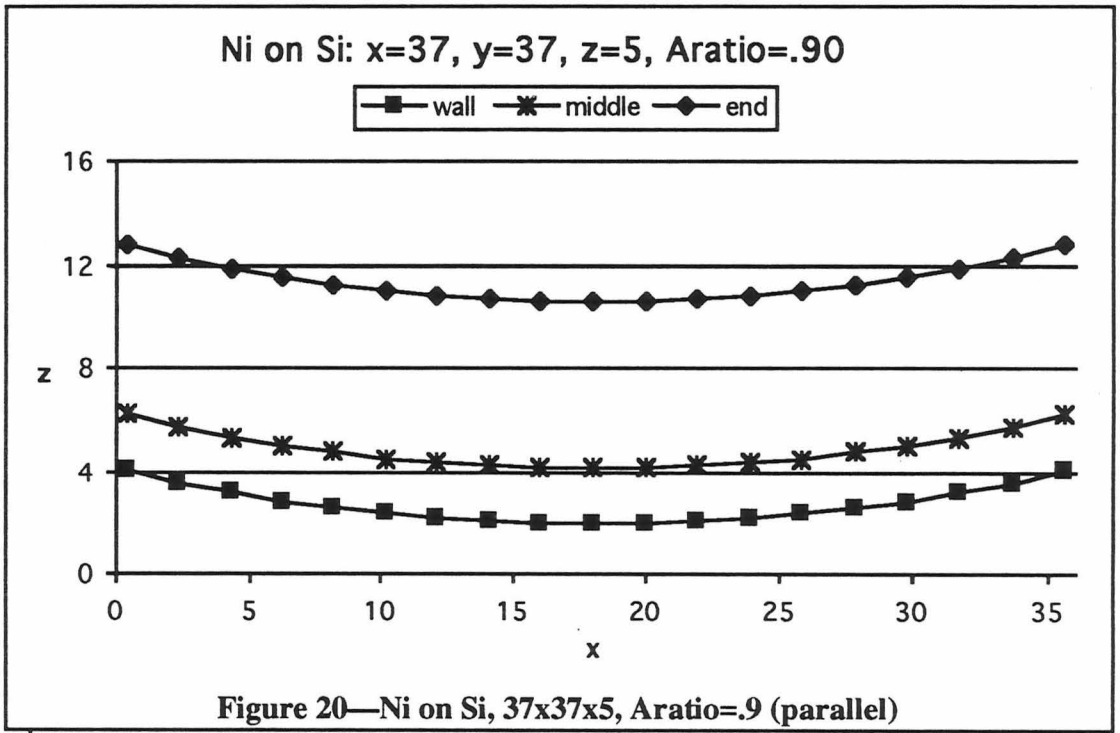

Figure 20—Ni on Si, 37x37x5, Aratio=.9 (parallel)

The wall, middle, and end lines of the Ni on Si structure described in the title. Curvature of the three lines are nearly the same, equal to 85 (9.5%).

Various points along the center and wall lines have been fit to a quadratic curve and to the special quadratic forms, parabolic and circular, as shown in Figure 21 and Figure 22. Radius of curvature changes as distance from the center increases, but it follows more closely the circular shape. Radius of curvature given in this section and the rest of this chapter are the values from near the midpoint between the center of the curve and the edge of the plate. The total range from highest to lowest curvature along the lines (ignoring the outer edge points) is also given in parentheses following the value of the curvature, as a percent of the midpoint value. Radius of curvature of the center line is 74 (1.5%) range, while the wall line is 85 (9.5%).

center		x^2 = az^2 + bz		x^2 = 2Rz - z^2	x^2 = 2pz
y	z	a	b	R	p
0.00	2.00	..	..	..	..
1.99	2.03	-25.86	150.88	75.11	75.10
3.97	2.11	-1.15	148.24	74.11	74.06
5.96	2.24	-0.42	148.07	74.10	73.98
7.94	2.43	-0.48	148.09	74.16	73.94
9.91	2.66	-0.69	148.23	74.22	73.89
11.87	2.96	-0.80	148.33	74.26	73.79
13.83	3.30	-0.92	148.50	74.30	73.65
15.77	3.69	-1.02	148.67	74.32	73.47
17.71	4.14	-1.12	148.87	74.31	73.24
19.62	4.64	-1.20	149.09	74.28	72.96
21.53	5.19	-1.29	149.39	74.23	72.63
23.41	5.79	-1.38	149.73	74.14	72.24
25.27	6.45	-1.48	150.18	74.01	71.79
27.12	7.16	-1.58	150.65	73.84	71.26
28.94	7.92	-1.65	151.12	73.62	70.66
30.73	8.75	-1.75	151.73	73.35	69.98
32.50	9.63	-1.90	152.93	73.02	69.21
34.26	10.59	..	..	72.59	68.29

Figure 21—Ni on Si curvature, 37x37x5, Aratio=.9 (perpendicular)

Curvature along various points along the center line. Shown are the actual data points, a fit to a general quadratic, a parabolic, and a circular surface.

wall		x^2 = az^2 + bz		x^2 = 2Rz - z^2	x^2 = 2pz
x	z	a	b	R	p
0.40	4.02	-8.63	170.60	77.58	76.57
2.35	3.56	-9.26	171.58	79.35	78.57
4.29	3.17	-10.55	173.09	80.96	80.37
6.24	2.84	-12.16	174.44	82.52	82.10
8.19	2.58	-13.45	175.18	84.01	83.72
10.14	2.36	-15.02	175.75	85.34	85.15
12.10	2.20	-15.31	175.81	86.47	86.37
14.07	2.09	-19.07	176.14	87.27	87.23
16.03	2.02	..	..	87.87	87.86
18.00	2.00	..	..	..	..
19.97	2.02	..	..	87.87	87.86
21.93	2.09	-19.07	176.14	87.27	87.23
23.90	2.20	-15.31	175.81	86.47	86.37
25.86	2.36	-15.02	175.75	85.34	85.15
27.81	2.58	-13.45	175.18	84.01	83.72
29.76	2.84	-12.16	174.44	82.52	82.10
31.71	3.17	-10.55	173.09	80.96	80.37
33.65	3.56	-9.26	171.58	79.35	78.57
35.60	4.02	-8.63	170.60	77.58	76.57

Figure 22—Ni on Si curvature, 37x37x5, Aratio=.9 (parallel)

Curvature along various points along the wall line. Shown are the actual data points, a fit to a general quadratic, a parabolic, and a circular surface.

Figure 23 and Figure 24 show the same structure with the ratio $\frac{\alpha_{plate}}{\alpha_{film}} = 0.99$. Curvature decreases to 636 (0.5%) perpendicular to the wall, and to 626 (0.1%) parallel to the wall.

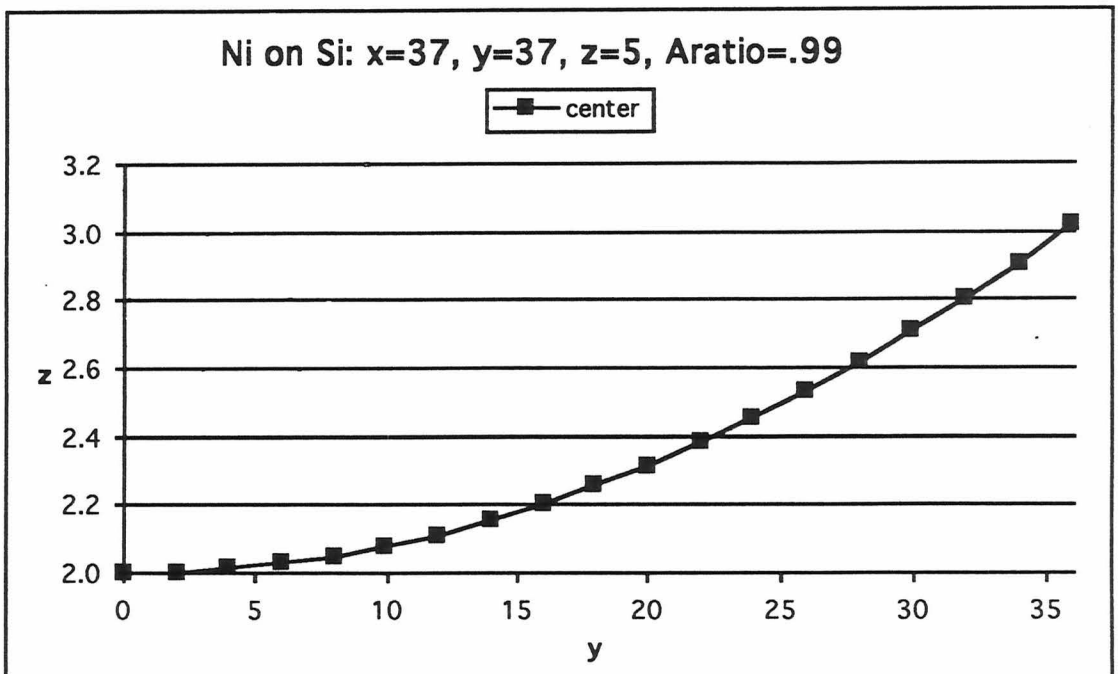

Figure 23—Ni on Si, 37x37x5, Aratio=.99 (perpendicular)

The center line of the Ni on Si structure described in the title. Curvature is 636 (0.5%).

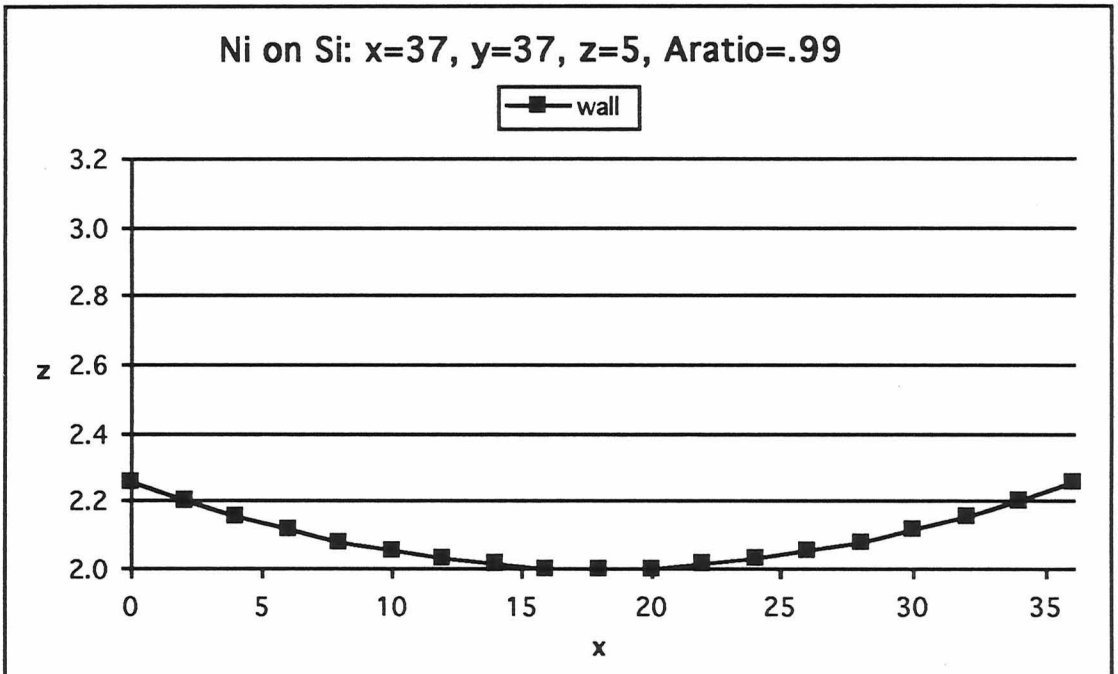

Figure 24—Ni on Si, 37x37x5, Aratio=.99 (parallel)

The wall line of the Ni on Si structure described in the title. Curvature is 626 (0.1%).

To model a thicker film, the same structure from the previous calculations was modeled with a film thickness equal to three mass points, making the overall structure thickness equal to seven (four in the bulk Si plus three in the Ni film). Figure 25 and Figure 26 show the results of this calculation for $\frac{\alpha_{plate}}{\alpha_{film}} = 0.90$. Curvature increases from 74 (1.5%) perpendicular and 85 (9.5%) parallel for the single layer film to 52 (2%) and 61 (10%), respectively, for the thicker film.

Figure 27 and Figure 28 are the same configuration for $\frac{\alpha_{plate}}{\alpha_{film}} = 0.99$. Here curvatures increase from 636 (0.5%) perpendicular and 626 (0.1%) parallel for the single layer film to 481 (2%) and 481 (0.1%), respectively, for the thicker film.

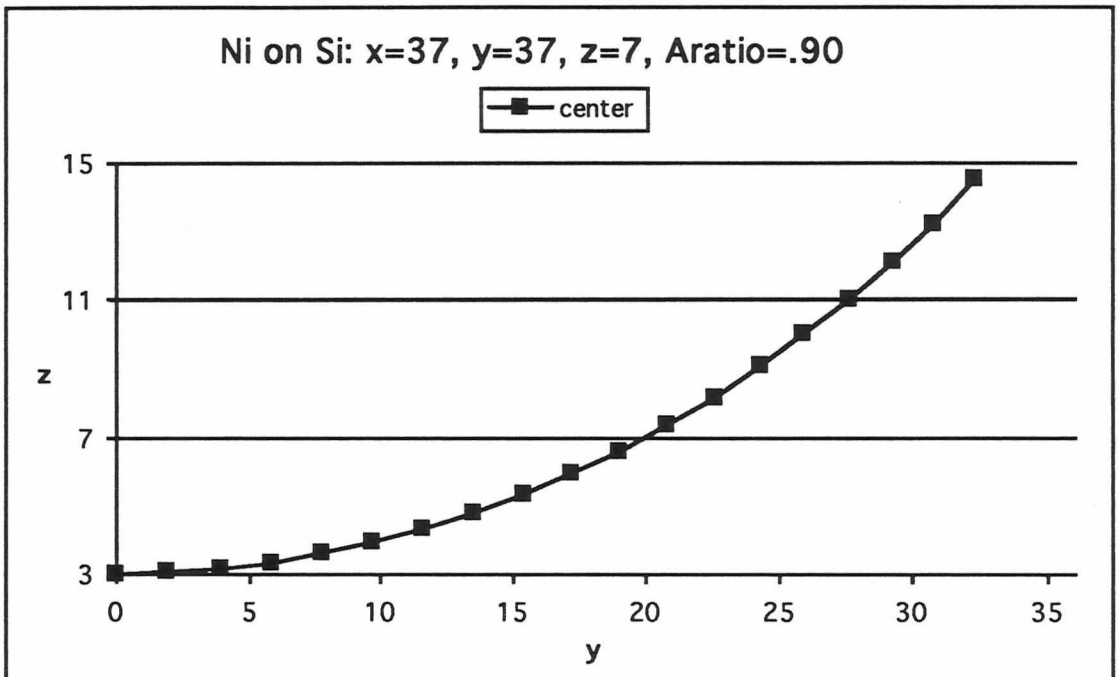

Figure 25—Ni on Si, 37x37x7, Aratio=.90 (perpendicular)

The center line of the Ni on Si structure described in the title. Curvature is 52 (2%).

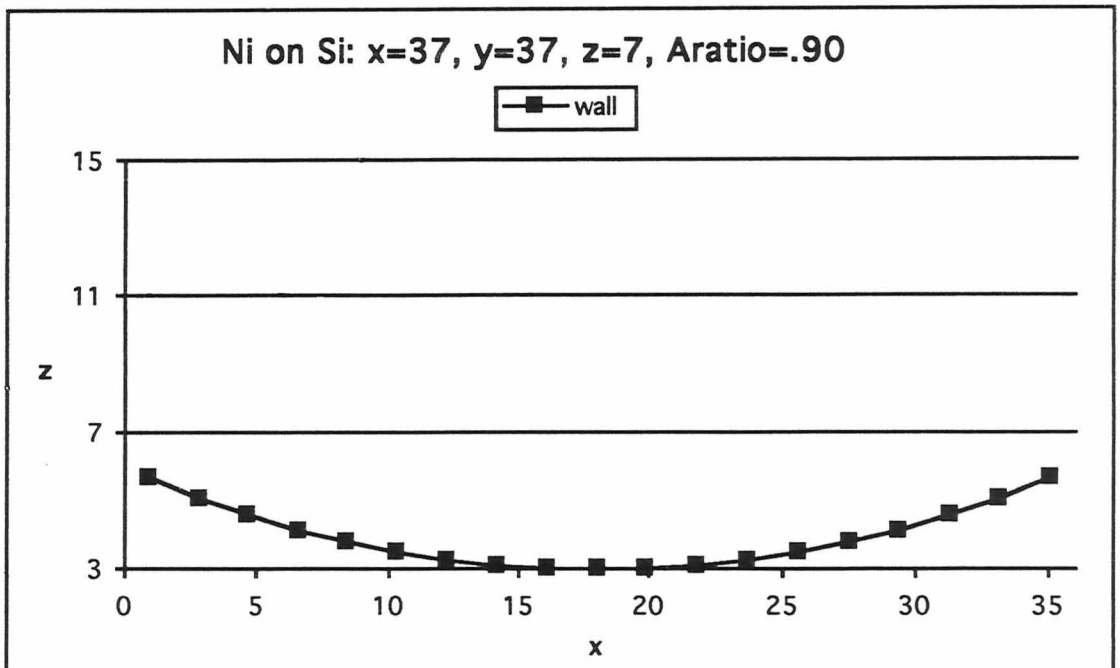

Figure 26—Ni on Si, 37x37x7, Aratio=.90 (parallel)

The wall line of the Ni on Si structure described in the title. Curvature is 61 (10%).

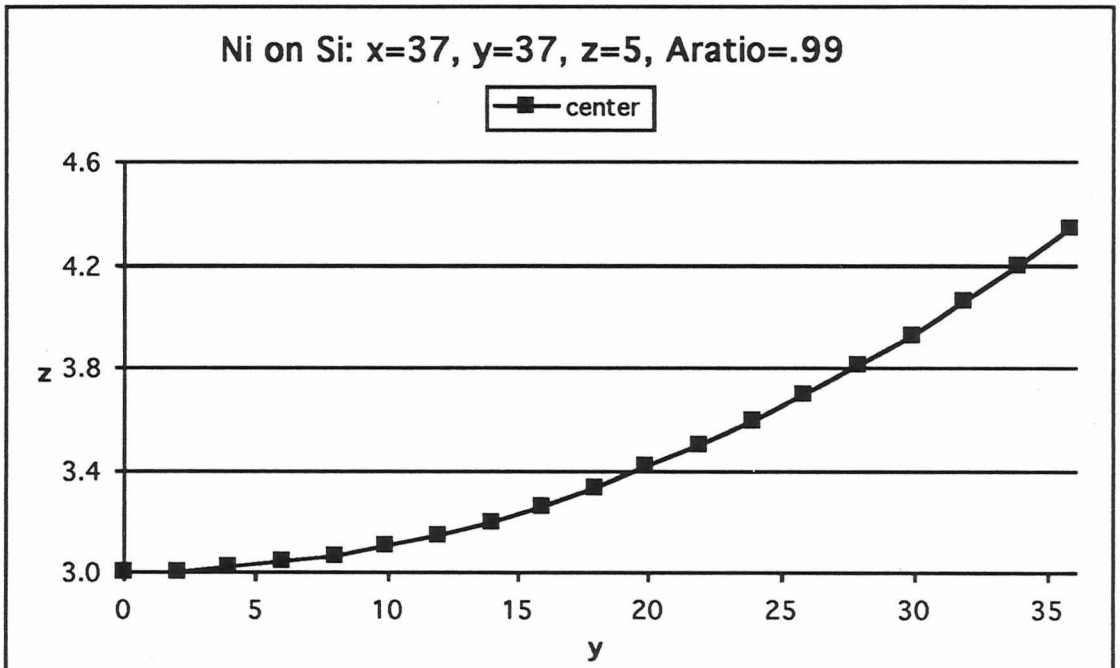

Figure 27—Ni on Si, 37x37x7, Aratio=.99 (perpendicular)

The center line of the Ni on Si structure described in the title. Curvature is 481 (2%).

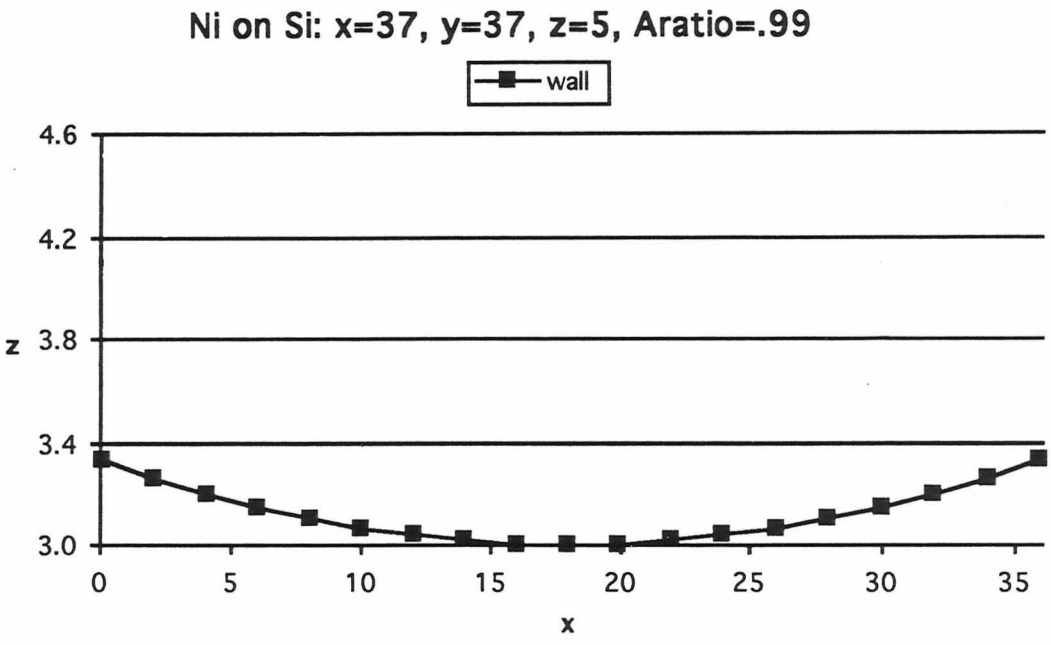

Figure 28—Ni on Si, 37x37x7, Aratio=.99 (parallel)

The wall line of the Ni on Si structure described in the title. Curvature is about 481 (0.1%).

Finally, PLATO is run with mass points 37 x 19 x 5 in size. The y-direction extends out from the bound wall 18 units, the other half of the structure is assumed to be symmetric, mirrored through the xz-plane. The model thus represents a square plate of size 36 x 36 x 4 units. Figure 29 plots the center and wall lines on the same graph for easier comparison of the two lines. As expected, the plots look nearly identical. Figure 30 is a table of curvatures along various points of the two curves showing the slight differences between them.

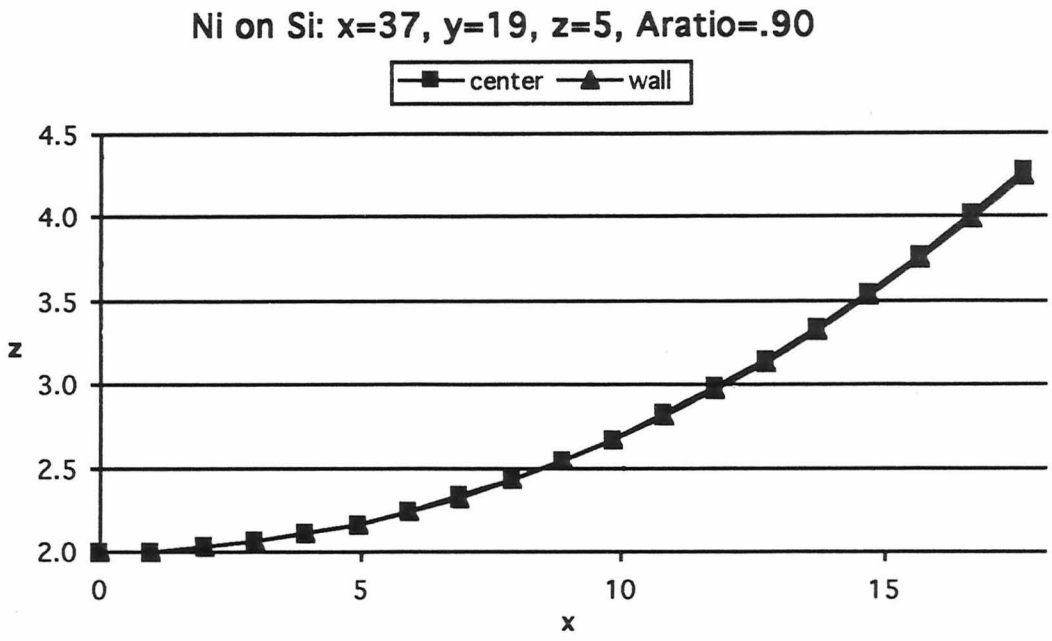

Figure 29—Ni on Si, 37x19x5, Aratio=.90

The wall line of the Ni on Si structure described in the title. This structure models a square plate when mirrored through the xz-plane. Curvature is 72 (5%) for each line.

center		x^2 = az^2 + bz		x^2 = 2Rz - z^2	x^2 = 2pz
y	z	a	b	R	p
0.00	0.00	..	..	..	..
1.98	0.03	-42.72	151.41	75.16	75.15
3.95	0.11	-8.16	147.73	73.49	73.43
5.92	0.24	-5.56	147.11	73.01	72.89
7.89	0.43	-5.01	146.87	72.57	72.36
9.85	0.68	-4.81	146.73	72.08	71.74
11.79	0.98	-4.54	146.48	71.50	71.01
13.73	1.34	-4.46	146.37	70.86	70.19
15.67	1.77	-4.84	147.04	70.11	69.23
17.61	2.28	..	..	69.14	68.00

Figure 30—Ni on Si curvature, 37x19x5, Aratio=.90 (perpendicular)

Curvature along various points along the perpendicular line. Shown are the actual data points, a fit to a general quadratic, a parabolic, and a circular surface.

wall		x^2 = az^2 + bz		x^2 = 2Rz - z^2	x^2 = 2pz
y	z	a	b	R	p
0.00	0.00	..	..	..	..
1.98	0.03	-3.50	148.68	74.30	74.29
3.95	0.11	-4.84	148.82	74.21	74.15
5.92	0.24	-5.20	148.90	73.95	73.83
7.89	0.42	-4.90	148.78	73.56	73.35
9.85	0.67	-4.89	148.76	73.09	72.75
11.80	0.97	-4.55	148.44	72.50	72.02
13.74	1.33	-4.39	148.22	71.87	71.20
15.68	1.75	-4.59	148.58	71.15	70.28
17.61	2.24	..	..	70.26	69.14

Figure 31—Ni on Si curvature, 37x19x5, Aratio=.90 (parallel)

Curvature along various points along the parallel line. Shown are the actual data points, a fit to a general quadratic, a parabolic, and a circular surface.

Figure 32 summarizes the results of the Plato runs in this section.

X-Y-Z	zfilm	Aratio	parallel curvature	perpendicular curvature
37-37-5	1	0.90	85 (9.5%)	74 (1.5%)
37-37-5	1	0.99	626 (0.1%)	636 (0.5%)
37-37-7	3	0.90	61 (10%)	52 (2%)
37-37-7	3	0.99	481 (2%)	481 (0.1%)
37-19-5	1	0.90	73 (5%)	72 (5%)

Figure 32—summary, Ni on Si

Curvature (range in %) near the center of the lines of the Si plates. Curvature is nearly equal in each direction for each structure, particularly the last one which models a square plate.

This section has shown that the mesoscopic model can effectively model a film of a certain thickness and thermal expansion coefficient deposited on a bulk material. Some calibration would have to be performed to make this model useful in real world

applications, but, as expected, curvature increases with increasing thickness and with decreasing ratio $\frac{\alpha_{plate}}{\alpha_{film}}$.

The plates in this model each show positive curvature in both the parallel and perpendicular directions. This is not completely consistent with experimental work performed by Yingua Shi in 1990[19]. His work showed positive curvature in one direction, with very slight curvature—radius on the order of tens of meters—in the opposite direction, yielding a cylindrical surface. The large curvature always occurred along the same crystal axis of the silicon substrate. The curvature measurements along a line in the nearly flat direction gave sometimes both positive and negative values, but always very large, in the tens to hundreds of meters range. This curvature pattern could be due to the anisotropic nature of silicon where elasticity is not the same in each direction. The variation from positive to negative curvature could be due to measurement error, or to nonuniformities in the silicon substrate or film. These conditions are not accounted for in the mesoscopic model presented here. However, with some modification to spring constants or the types of neighbor-particle interactions, the model may be able to reproduce those experimental results. See the chapter on further research for more discussion.

C. Ribbed Plate with Thin Film

A plate with a thin film on one surface can be bent to particular curvatures, but beyond certain values shape is difficult to alter without other types of control. Etching ribs of a specified pattern into the back of the silicon substrate could possibly shape the figure into cylindrical or two or three dimensional parabolic, or spherical shapes that may be useful for multilayer x-ray mirrors. A KOH solution will etch silicon preferentially along certain crystal planes with very high selectivity under the right conditions[20], up to

600:1 along the <110> crystal plane relative to <111>. With a simple mask very steep walled ribs can be etched into the back of silicon cut on the <110> plane, leaving the silicon very thin in the groove and very thick in the rib. With appropriate rib spacing and patterning it is conceivable that many shapes useful for optics could be precisely produced. This section models silicon with periodic ribs etched into the back surface, with a nickel film deposited on the front.

A cross section of the first ribbed structure analyzed is shown in Figure 33. The ribbed structures are specified by thickness z, rib height *zrib*, the film thickness *zfilm*, rib width *yrib*, rib pitch *ypitch*, and number of periods of ypitch, *yper*, and the width of the structure x. The structure attempts to model a full plate by calculating only one half of the structure with boundary conditions such that the other half would be mirrored through the xz-plane. A half rib is always placed at the beginning of the structure, making it symmetric when mirrored across the xz-plane.

The mesoscopic springs are connected the same way as the plate springs—first neighbors, second neighbors, and third neighbors. The inside corners of the ribs also maintain the same neighbor relationships and are therefore not sharp corners. (The figure shows only the mass points, not the springs, making the corners look sharp.) While no first neighbor relationships exist outside of the lattice on an inside corner, second and third neighbors do. For example, the lattice points adjacent to the inside corner have a second neighbor relationship, so a spring extends in to the groove across the corner point. In a similar way third neighbor springs also extend into the groove. These potentials make the inside corners somewhat rounded rather than sharp as appears in the figure. This turns out to be some advantage when modeling silicon, which actually leaves a "V" in the bottom of the etched groove (due to the silicon crystal structure), rather than squared corners.

Results of this section are consistent with the work of Jun Liu's finite element analysis of similar structures[21]. Mr. Liu reports curvatures perpendicular to the ribs (in the plane shown in Figure 33) between 10 and 15 cm., and curvatures parallel to a rib between 70 and 85 cm. Some calibration would have to be performed to attempt to match his results. However, because of heavy computer time requirements of finite element calculations, his analysis split the 3-dimensional plate into two 2-dimensional pieces. One of his pieces is a rib extending parallel to the wall, the other a thin slice of periodic ribs parallel to the center line. The PLATO code models it here in one 3-dimensional piece.

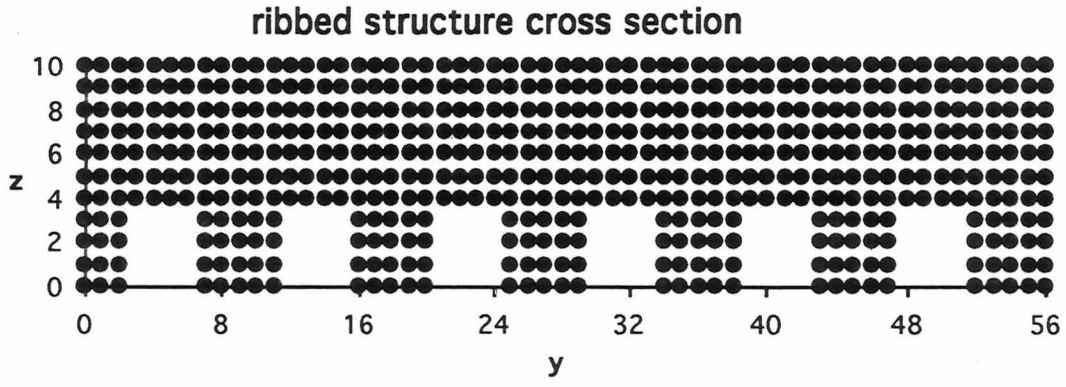

Figure 33—ribbed structure

The ribbed structure is specified by thickness z=11, rib height zrib=5, rib width yrib=5, rib pitch ypitch=9, and number of periods of ypitch, yper=5. (A half rib is always placed at the beginning of the structure, making it symmetric when it is mirrored through the xz-plane.) The width of the structure, x, is not shown in this cross section, and the film thickness, zfilm, is not specified.

Figure 34 and Figure 35 show resultant shape of the ribbed structure of Figure 33, with $\frac{\alpha_{plate}}{\alpha_{film}} = 0.90$.

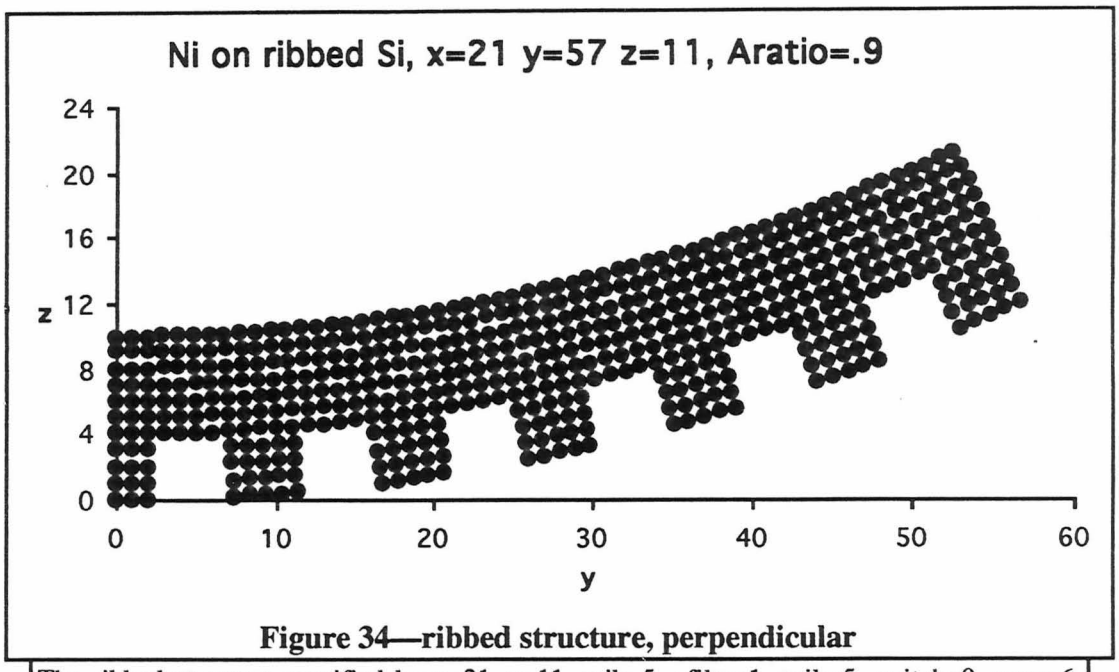

Figure 34—ribbed structure, perpendicular

The ribbed structure specified by x=21, z=11, zrib=5, zfilm=1, yrib=5, ypitch=9, yper=6. Curvature is 130 (1.5%).

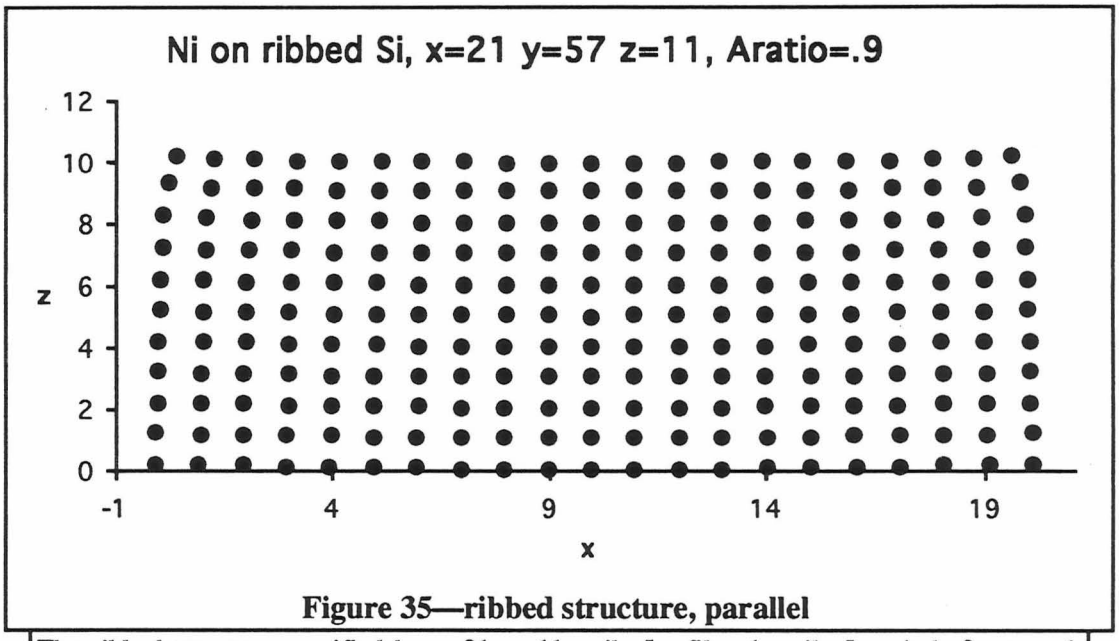

Figure 35—ribbed structure, parallel

The ribbed structure specified by x=21, z=11, zrib=5, zfilm=1, yrib=5, ypitch=9, yper=6. Curvature is 296 (5%).

To examine curvature perpendicular to the ribs (the center line) as a function of lattice size parallel to the ribs (the wall line) a structure was run similar to the previous, with

x=37. Figure 36 and Figure 37 show the results of this calculation. The curvature increases slightly, perpendicular from 130 (1.5%) to 125 (0.3%), and parallel from 296 (5%) to 275 (1.5%).

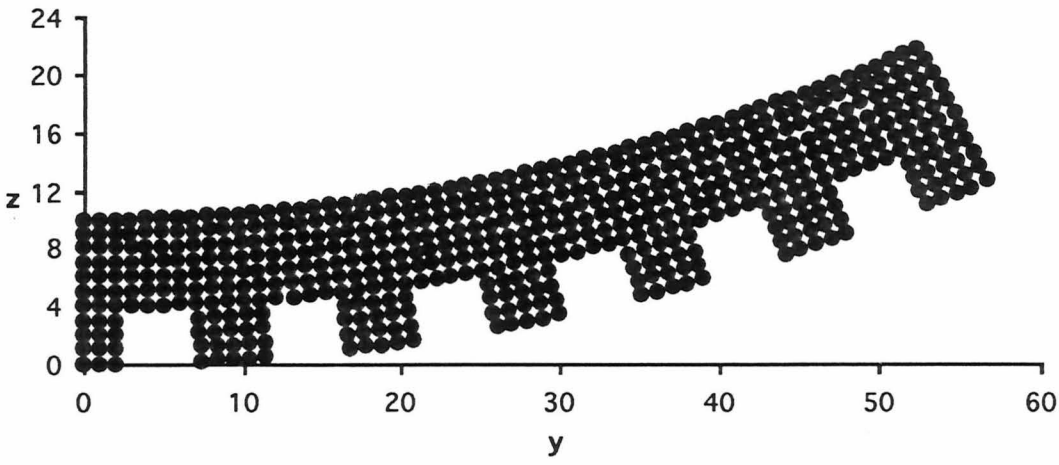

Figure 36—ribbed structure, perpendicular

The ribbed structure specified by x=37, z=11, zrib=5, zfilm=1, yrib=5, ypitch=9, yper=6. Curvature is 125 (0.3%).

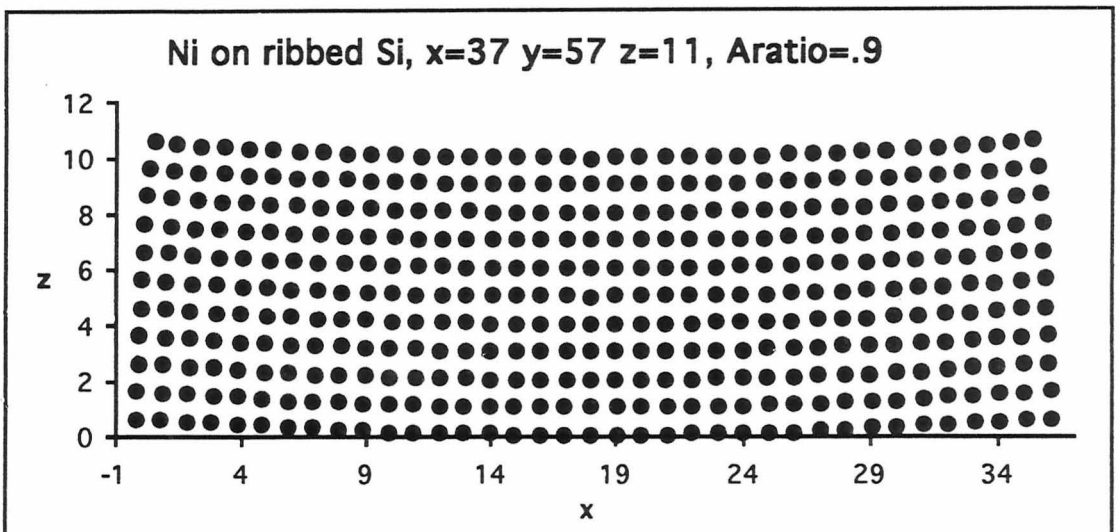

Figure 37—ribbed structure, parallel

The ribbed structure specified by x=37, z=11, zrib=5, zfilm=1, yrib=5, ypitch=9, yper=6. Curvature is 275 (1.5%).

When the number of rib periods is increased from 6 to 10, making the structure 37 x 94 x 11, there was very little change in curvature, perpendicular from 125 (0.3%) to 125 (0.6%), and parallel from 275 (1.5%) to 274 (1.5%). The perpendicular cross section is shown in Figure 38.

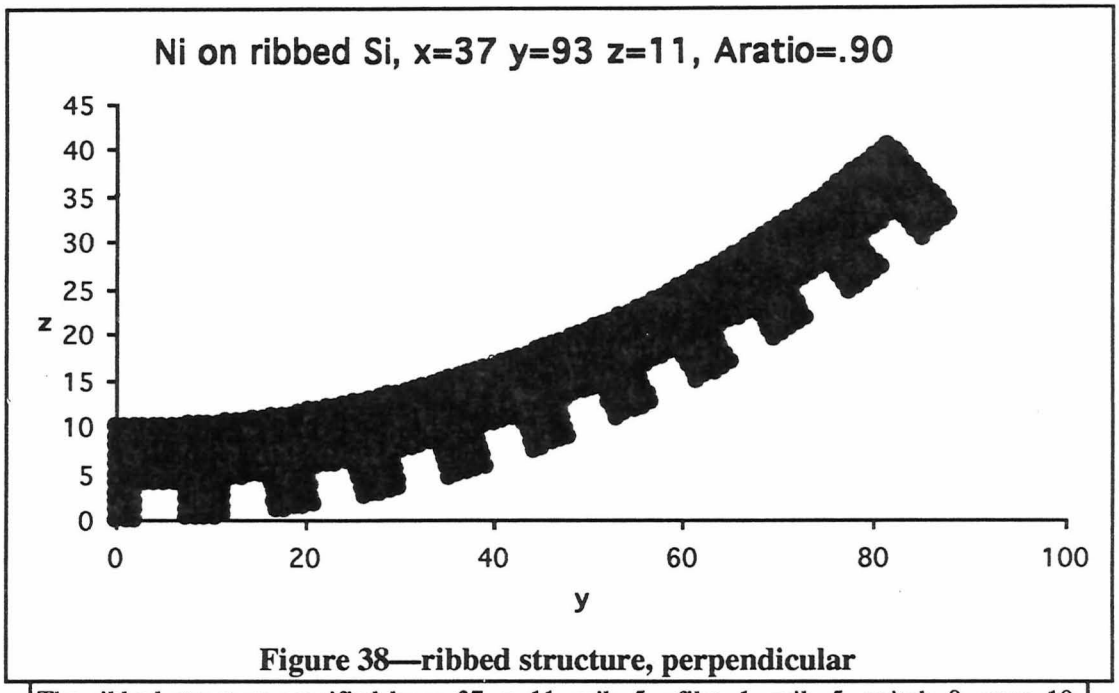

Figure 38—ribbed structure, perpendicular

The ribbed structure specified by x=37, z=11, zrib=5, zfilm=1, yrib=5, ypitch=9, yper=10. Curvature is 125 (0.6%).

These same three calculations are repeated for similar sized plates but with deeper ribs and thinner bulk material: *z*=9, *zrib*=7, *zfilm*=1. Curvature increases from the previous structure, but there is little change with the x- and y-direction size changes. Figure 39 shows a cross section through the ribs of the basic structure. The perpendicular results of these calculations are shown in Figure 40 through Figure 42, and the section is summarized in Figure 43.

The range of curvature in the perpendicular direction for this second structure is different from the first. The first structures have a range of curvatures that vary smoothly from high to low as one measures from one edge to the other. The range in curvature from these second structures is due for the most part to variations from point to point along the curve, like a large scale nonuniform surface.

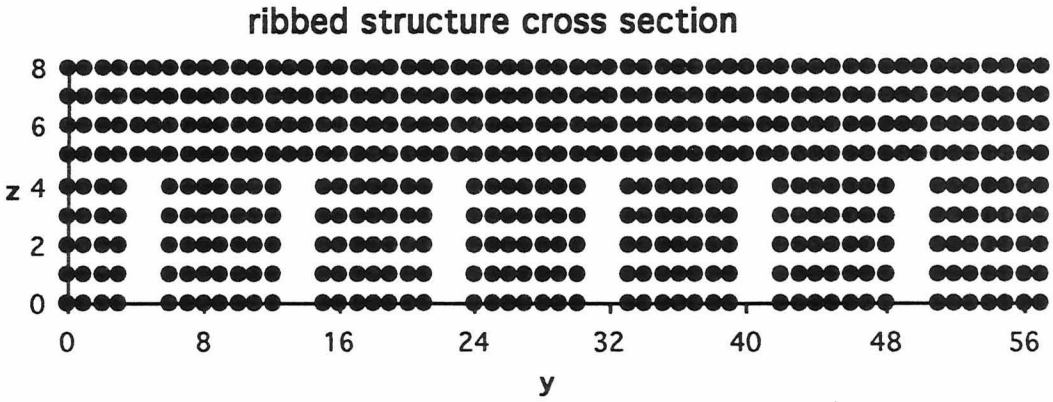

Figure 39—ribbed structure

This ribbed structure is specified by z=9, zrib=6, yrib=7, ypitch=9, yper=6, x and zfilm are not specified.

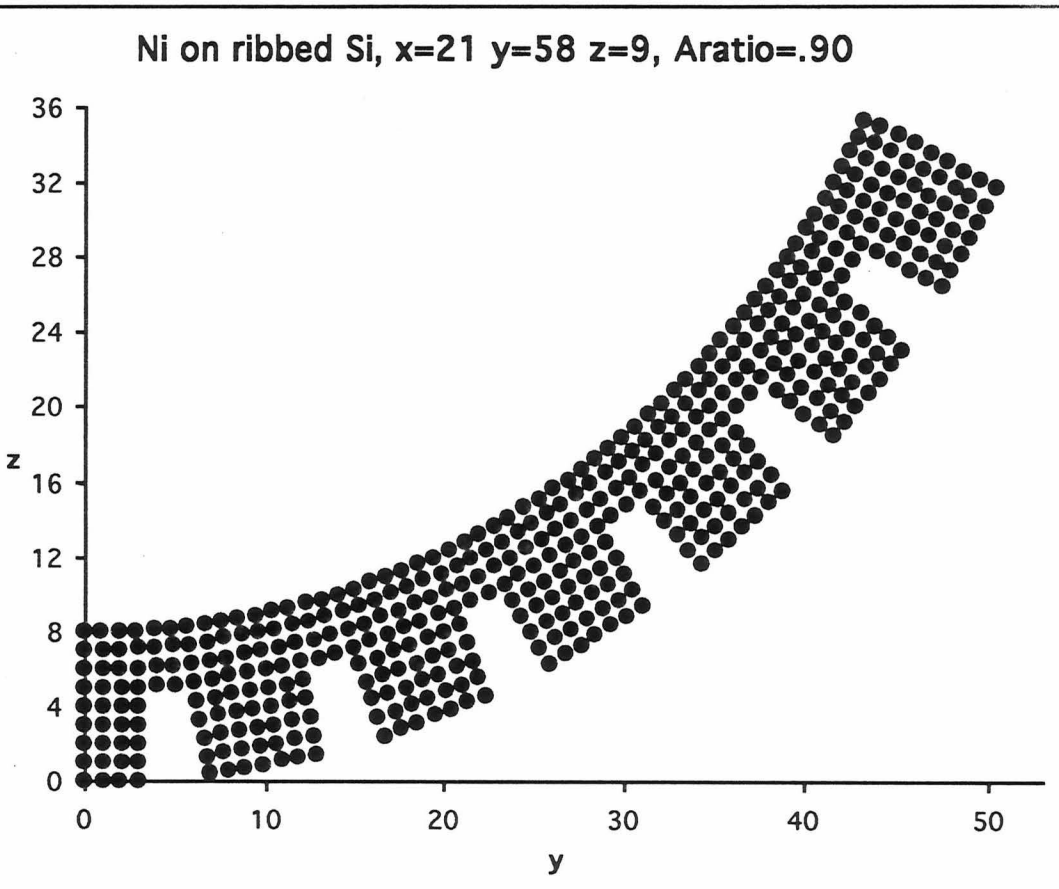

Figure 40—ribbed structure, perpendicular

The ribbed structure specified by x=21, z=9, zrib=6, zfilm=1, yrib=7, ypitch=9, yper=6. Curvature is 49 (3%).

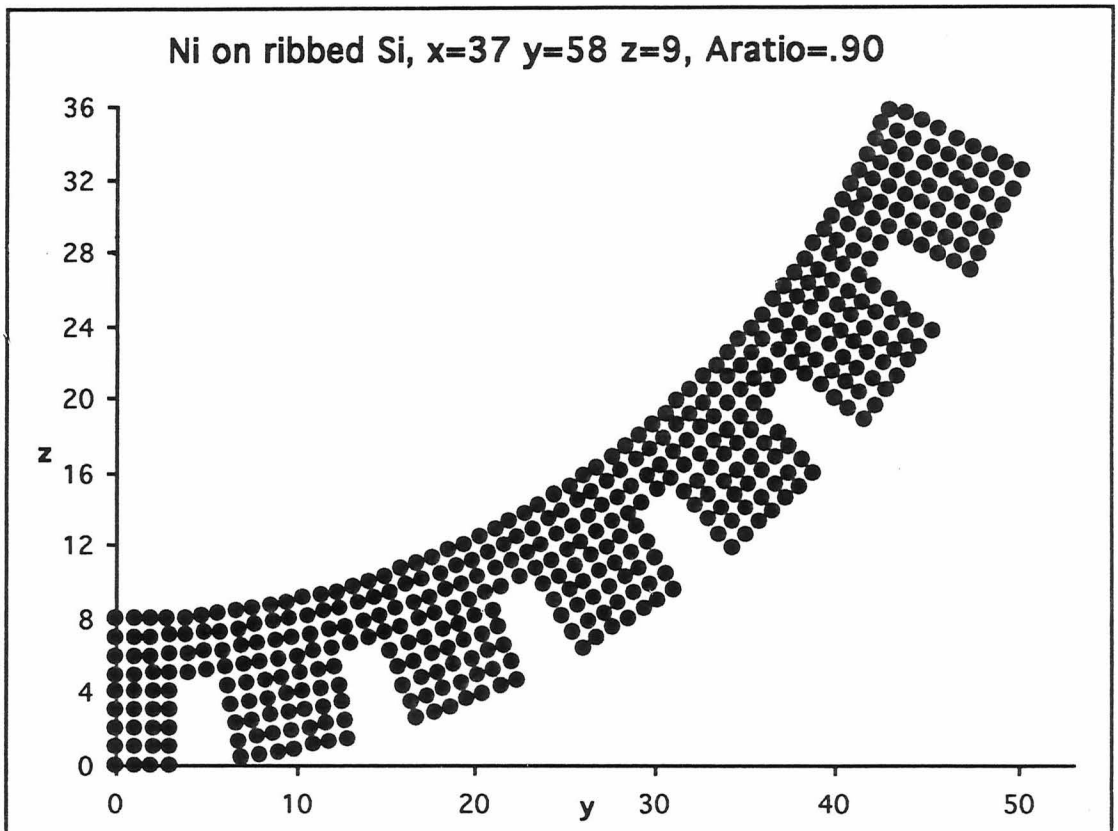

Figure 41—ribbed structure, perpendicular

The ribbed structure specified by x=37, z=9, zrib=6, zfilm=1, yrib=7, ypitch=9, yper=6. Curvature is 48 (3%).

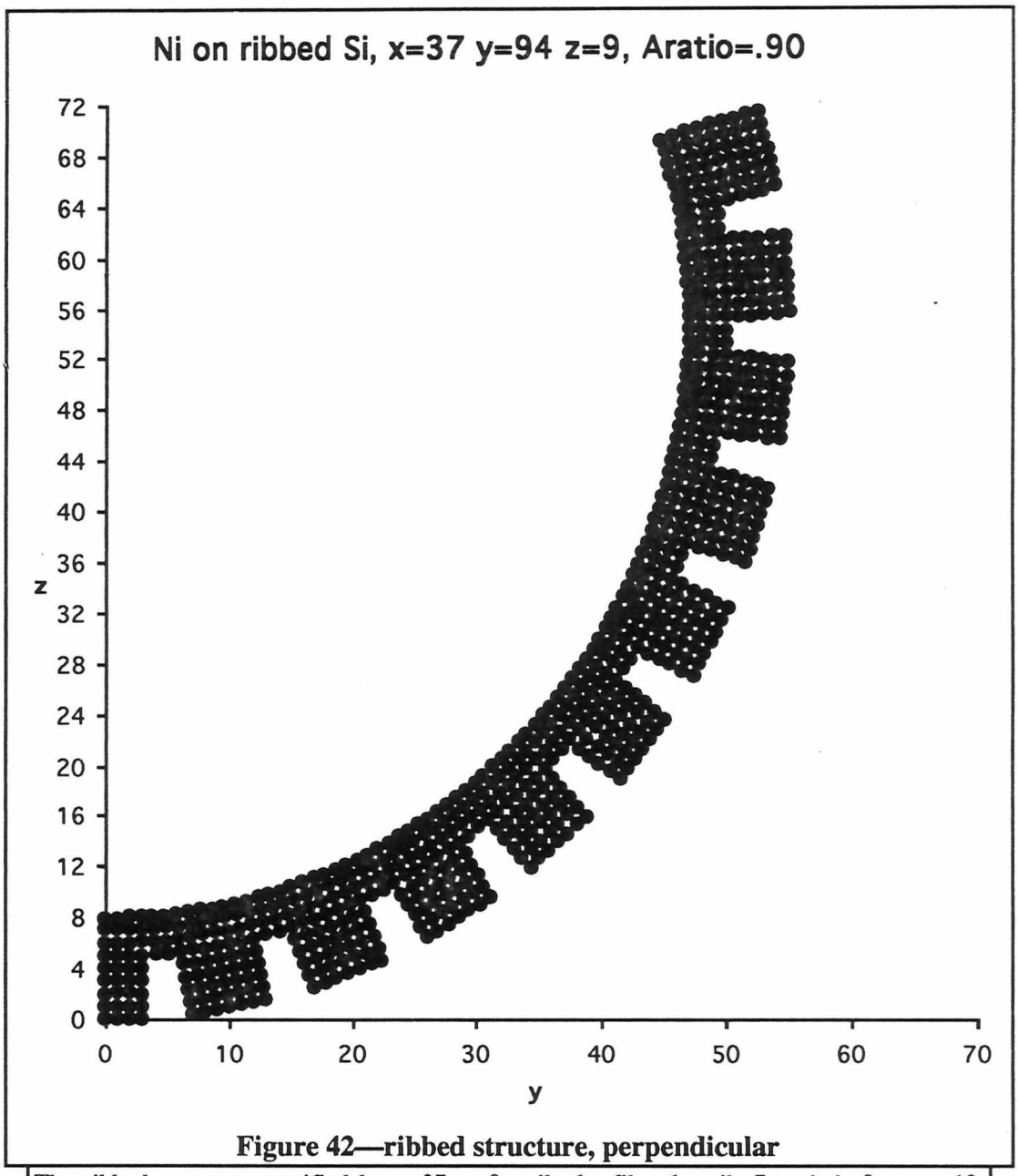

Figure 42—ribbed structure, perpendicular

The ribbed structure specified by x=37, z=9, zrib=6, zfilm=1, yrib=7, ypitch=9, yper=10. Curvature is 48 (2%).

X-Y-Z	zfilm	Aratio	parallel curvature	perpendicular curvature
z=11, zrib=5, zfilm=1				
21-57-11	1	0.90	296 (5%)	130 (1.5%)
37-57-11	1	0.90	275 (1.5%)	125 (0.3%)
37-93-11	1	0.90	274 (1.5%)	125 (0.6%)
z=9, zrib=7, zfilm=1				
21-58-9	1	0.90	225 (2%)	49 (3%)
37-58-9	1	0.90	233 (0.6%)	48 (3%)
37-94-9	1	0.90	233 (0.6%)	38 (2%)

Figure 43—summary, Ni on ribbed Si

Curvature near the center of the lines of the ribbed Si structures. Within each rib formation there is little difference in curvature between the different plate sizes.

The curves more closely resemble circles ($R = \frac{x^2 + z^2}{2z}$) than parabolas ($p = \frac{x^2}{2z}$). It appears the curvature of these ribbed structures is a function more of the rib configuration (width, depth, and pitch) and the film properties than of the ribs' extent in either the x- or y-directions. This suggests other curvatures could be construed by altering the film properties and the rib configuration, as well as possibly altering the periodicity of the ribs, that is, systematically changing rib width and spacing into patterns that would produce a desired surface shape.

V. Code—Key Points and User's Guide

The BEAML and PLATO codes are similar except for their method for inducing stress into the lattice. BEAML uses a weight placed at the end of a beam type structure, while PLATO uses a thin film that has different spring parameters from the bulk. This chapter presents some key points of the code and a basic user's guide.

A. Algorithm and Key Points

The equations of motion are integrated using the Verlet algorithm[22]. The mesoscopic code algorithm, which incorporates the Verlet algorithm, is outlined below.

ALGORITHM

0. Definitions:

   h is a time element, a specified fraction of a period
   k is the first neighbor spring constant
   i is the particle identification
   n is the iteration count
   beta is a frictional proportionality constant

1. Initialize the lattice, the table of particle neighbors, and other parameters

2. Update position and velocity

$$\vec{x}(i,n+1) = \vec{x}(i,n) + h\vec{v}(i,n) + \frac{h^2}{2m}\vec{f}(i,n)$$

$$h\vec{v}(i,n+1) = h\vec{v}(i,n) + \frac{h^2}{2m}\vec{f}(i,n)$$

3. Reset boundary points to proper conditions for position and velocity

4. Calculate potential energy and update the force

$$u(i,n+1) = \tfrac{1}{2}k\left|\vec{x}(i,n+1)\right|^2$$

$$\vec{f}(i,n+1) = \frac{du(i,n+1)}{dr} + mg(\text{at end}) = k\left|\vec{x}(i,n+1)\right| + mg(\text{at end})$$

A friction term may be included here to quench the motion, this one proportional to velocity

$$\frac{h^2}{2m}\vec{f}(i,n+1) = \frac{h^2}{2m}\vec{f}(i,n+1) - beta * h\vec{v}(i,n+1)$$

5. Update velocity and total kinetic energy

$$h\vec{v}(i,n+1) = h\vec{v}(i,n+1) + \frac{h^2}{2m}\vec{f}(i,n+1)$$

$$KE(n+1) = \tfrac{1}{2}m\sum_i \left|\vec{v}(i,n+1)\right|^2$$

Reset boundary as in step (3)

6. Quench the motion if total kinetic energy is decreasing and the particle velocity opposes the force

if $KE(n+1) < KE(n)$ and $v(i,n+1)f(i,n+1) < 0$

then $v(i,n+1) = 0$

7. Return to step (2) until (for a specified small number c, and particle i_o)

$$\left|\vec{x}(i_o,n+1) - \vec{x}(i_o,n)\right| < c$$

For the calculations performed here, *beta* = 0 and h = 0.25**period.* Other values of *beta* did not improve the time for convergence if also using the quench step (6); however, some experimentation with the value of h near unity did show some decrease in convergence time. It should be noted that if the dynamics of the motion are of interest rather than just the equilibrium configuration, there is more to consider than convergence time for choosing an appropriate value of h.

Notably missing from the parameters in the model is the lattice particle mass. The particle mass effects the dynamics of the motion, i.e., the particle speed and the period of

the motion, but not the amplitude nor the time increment which is stepped in fractions of a period. The time step is $\frac{h^2}{2m}$, and $h = .25\sqrt{\frac{m}{k}}$ so the mass cancels out of the resultant change in position. As with the parameter h, if the dynamics of the motion are of interest rather than just the equilibrium configuration, the lattice particle masses would need to be considered. The particle mass is accounted for in all the computations in the code, so changes to account for mass would be minimal.

B. User's guide

The two codes BEAML and PLATO are the codes that perform the mesoscopic model calculations. The additional codes BEAMTH and ECONSTANTS helped with supporting calculations. This section is a brief user's guide for these codes (the 'C' source code for each program is found in Appendix D). Each of the codes is executed in the standard method for the operating system used. Each will accept a command line argument following the program execution command that will be used as the output filename. If no command line argument is given then no output file is created. In that case if output is desired to be saved it will have to be done through the operating system (i.e. output redirection). Input is from the keyboard except as indicated, unless input redirection is used.

1. BEAML

Using the mesoscopic model, this program calculates the deflection of a rectangular beam fixed at one end with a mass placed at the free end. The usage is described below.

After a brief introduction the first menu is shown. The material parameters are entered from this menu.

(e) you will be prompted to enter the elastic constants for the material (10^{12} dynes/cm^2) and the length of the cell (10^{-8} cm), then a method for computing the spring constants (choose from the seven described in this thesis).

(s) you will be prompted to enter the spring constants directly—first, second, and third neighbors—(10^4 dynes/cm^2) and Young's modulus.

(#) a number represents a material with elastic constants pre-coded. You will be prompted to enter a method for computing the spring constants.

(q) quits the program.

The next prompt is for the run parameters.

F/B: 'F' to start the beam in a flat (or straight) position, 'B' to start with the beam already curved as predicted by beam theory.

Steps: the maximum number of iterations—the program automatically stops if the end condition is reached before this number, 'max steps', of iterations.

NPR: the number of particles to extend in the x, y, and z directions (x and z must be odd).

load: the load (*mg*) to be evenly distributed over the face at the free end of the beam. This is what deforms the beam.

The final prompt is for lattice parameters.

lattice particle mass: the mass of each lattice site. This turns out to make no difference in the calculations. The default is unity.

first neighbor distance: the distance between first neighbor lattice points. The default is unity.

The program then calculates the deflection until the motion reaches the end condition (a particle at the end of the beam changes its position less than 10^{-5} units), or until 'max steps' is reached.

The output gives some header information, then every 'max steps'/20 iteration position of the particle being followed for the end condition check. Finally the output

gives the position of the center line of the deformed beam and the center line that beam theory predicts.

2. PLATO

Using the mesoscopic model, this program calculates the deflection of a plate with a film on one surface, and the opposite surface may (or not) be etched making a deep grooved structure. The stress is caused by the difference in equilibrium positions between the bulk and the film. The usage is described below.

After a brief introduction the first menu is shown. The material parameters are entered from this menu.

(e) you will be prompted to enter the elastic constants for the material (10^{12} dynes/cm^2) and the length of the cell (10^{-8} cm), then a method for computing the spring constants (choose from the seven described in this thesis).

(s) you will be prompted to enter the spring constants directly—first, second, and third neighbors—(10^4 dynes/cm^2) and Young's modulus.

(#) a number represents a material with elastic constants pre-coded. You will be prompted to enter a method for computing the spring constants.

(q) quits the program.

This menu is repeated for the film parameters.

The next prompt is for the run parameters.

Steps: the maximum number of iterations—the program automatically stops if the end condition is reached before this number, 'max steps', of iterations.

NPRx: x = the number of lattice points to extend in the x direction (must be odd).

NPRy: *ypitch* = the number of lattice points in the y-direction that make up a single rib and space. *yrib* = the number of points in the y-direction making up a single rib. *yper* = the number of periods of ypitch to extend in the y-direction. The code automatically adds a half rib at the

beginning of the ribs so the structure is symmetric when reflected through the xz-plane, so *yrib* must be odd.

NPRz: *z* = the number of lattice points in the z-direction (must be odd). *zrib* = the number of points in the z-direction making up the rib. *zfilm* = the number of points in the z-direction making up the film.

The final prompt is for lattice parameters.

first neighbor distance: the equilibrium distance between first neighbor lattice points. The default is unity.

first neighbor distance in the film, Aratio: the equilibrium distance between first neighbor lattice points in the film. The distance between materials at the interface is averaged for the two materials.

The program then calculates the deflection of the plate until the motion reaches the end condition (a particle at the end of the beam changes its position less than 10^{-5} units), or until 'max steps' is reached.

The output gives some header information, then every 'max steps'/20 iteration position of the particle being followed for the end condition check. Finally the output gives the particle numbers and positions of various lines through the curved plate: three lines along the x-direction (wall, middle, end), three lines along the y-direction (front, center, back), and all the points at the wall plane in the x-direction (swall) and at the center plane in the y-direction (scenter).

3. BEAMTH

This program calculates the results of a rectangular beam as predicted by the beam theory equation. It calculates deflection at the end of the beam for a range of input values of Young's modulus. The purpose of this program is to help find the *effective* Young's modulus for a mesoscopic model structure. The usage is described below.

BEAMTH allows two parameters at the command line, the first the input filename, the second the output filename. Using 'none' for the input filename will direct the program to prompt for lattice size and load. If there are no parameters at the command line the program will prompt for the input filename and the output filename. It then asks for the minimum and maximum Young's modulus, E_{min} and E_{max}, and the number of points between (inclusive of endpoints).

The input filename must be either 'none' or the filename of an output file from BEAML. If the input filename is 'none' the program prompts for the lattice parameters x, y, z, and load (as described in BEAML above NPRx, etc.). If the input filename is an output file from BEAML the program locates the file and reads in the lattice information.

Output is the deflection of the endpoint for the values of Young's modulus input.

4. ECONSTANTS

This program calculates the mesoscopic spring constants from the material elastic constants and cell length. It uses the seven methods described in this thesis. It prompts for a material name (used only for identification in the output), then the four material parameters c_{11}, c_{12}, c_{14}, and a.

Output is the mesoscopic spring constants for the seven methods described in this thesis.

VI. Conclusions and Further Research

This dissertation has presented a model for simulation of structural mechanics that is simple in its approach, and easy to implement and use even with moderate computer hardware. The computations are simple to program, and run in reasonable time even on moderate speed computers. The model, even in its simplest form used here, has shown to be comparable to beam theory and to finite element computations of plates and ribbed plates with a thin film stressing one surface. The ability to complicate the model with neighbor-pair potentials that are not necessarily harmonic and create a lattice more complex than the simple cubic used here make it potentially attractive for modeling complicated structures and non-linear mechanics.

This mesoscopic code, because of the moderate computer requirements as compared to finite element codes, has allowed the modeling of plates and ribbed structures in their full three dimensional form rather than the cross sectional overlays performed by Mr. Liu using the finite element method. While the overlay modeling appeared to work well for these structures, the three dimensional approach more may prove advantageous for more complex geometries.

Another advantage of this model is its flexibility. With proper care in scaling mass and force terms, and removal of the quenching routines in the code, the oscillation dynamics can be studied. The addition of an appropriate friction term to the force allows investigation of damped motion.

A couple of conclusions relating to this study of beams, plates, and ribbed structures are worthy of note: 1) The ribs appear to provide some control over the final curvature of the substrate. This can be taken advantage of for making substrates for multilayer mirrors. How these ribs perform if etched nonuniformly is a good topic for further experiments. Using more lattice points, possibly more concentrated in certain areas or randomly varying some lattice positions, may be a good starting point. 2) The plate structures reach their new equilibrium condition much faster (fewer iterations) than do the beams. The plates typically contain many more particles than the beams, yet converge several times faster even for similar displacements. Apparently the more evenly distributed force in the plate creates less work for the iterative algorithm.

There are a number of things that could be pursued to make this a more powerful tool. A few such items are addressed here.

The integration scheme used in these programs, the Verlet algorithm, was chosen for its apparent advantages in accurately conserving energy. However, no other methods were tried. Some experimentation with other methods such as Runge-Kutta, Houbolt[23], Wilson θ-method[24], Gear[25], and Beeman[26] may find more efficient or otherwise more advantageous schemes than the one used here. The damping method should be further investigated as it has a direct effect on the speed of convergence. Also, as mentioned earlier in the body of the thesis, the size of the time integration steps affects the convergence and should be further investigated.

The lattice used for these calculations is a simple cubic. While one attempt of a model such as this is to simplify the atomic structure into something more manageable, the simple cubic lattice may limit the accuracy of this model in many cases. Creating a more complex lattice structure adds difficulty in setting up the lattice particles and their neighbor-pair potentials, but beyond that all calculations are the same. This may prove to

more accurately predict response of many materials with complex crystal structures or anisotropic properties.

Another method that may improve modeling of anisotropic media that is easier than creating a complex lattice is allowing the neighbor-pair potentials to be directionally as well as positionally determined. That is, first neighbors parallel to the xy-plane may be different from those parallel to the yz-plane, making the different directions respond differently. Second and third neighbors may also be similarly altered. This may be a fairly simple method to begin modeling materials with different properties in the different orientations.

The code creates a table of lattice particles, each particle's neighbors, and each particle-neighbor pair potential information (spring constant and equilibrium distance). With this structure it is a simple matter to include random (or ordered) dislocations in specific lattice sites, including position and pair potential changes or missing sites. In cases where this may be useful, such as imperfect crystal structures, localized deformations, etc., it is a simple extension of the existing code. It may also be useful in more easily modeling and calibrating cases like, for example, the thin film thickness in the structures in this thesis by creating the thin film equilibrium distances on a different scale than the bulk film or more tightly packing the lattice points.

Another added flexibility that is a simple change to existing code is the combination and generalization of BEAML and PLATO, allowing the two methods for stressing the structure—adding forces at specified points, and different thermal expansion coefficients for different materials—to be used together if desired. This could model a variety of different physical configurations of structures.

The final improvement addressed here was suggested at the outset of this thesis, that is, to create neighbor-pair potentials that go beyond Hooke's law forces to include

anharmonic terms or other more general potential interactions. The computation of these types of problems may require different algorithms than those used here, but the result may be a more generally applicable code that could solve a wider variety of problems, including non-linear systems that are not so easily treated by more conventional finite element schemes.

In conclusion, while much could be done to make the code more generally applicable, this thesis has shown the mesoscopic model to be useful in the realm that we have studied, and potentially more valuable as work is done to improve it.

VII. Acknowledgment

This work could not have been completed without the continued support of the Department of Physics and Astronomy at Brigham Young University, and, in particular, the support and direction of my advisor Dr. Manuel Berrondo and my advisory committee, whose names appear elsewhere in this paper. I thank you for your contributions. I thank my family, parents, brothers, sisters, and others who have offered endless words of encouragement. I cannot say enough to properly acknowledge my dear wife and children, without whose patience, love, and support this would not have been possible. And finally, as with most works of this nature which span many years and many situations, there are many who go unacknowledged by name, whose impact remains unknown or goes unseen, but whose influence is, nevertheless, surely present. I thank you for your contribution and your willingness to do so, and continue to do so, unacknowledged.

VIII. Appendices

A. Discrete to Continuous

Consider a lattice consisting of repeating cells of quasiparticles. We write the quasiparticle coordinates in terms of a vector, $\vec{x}(l)$, from the coordinate origin to each cell origin (labeled l), and a vector, $\vec{x}(k)$, from the cell origin to the particle k in the cell.

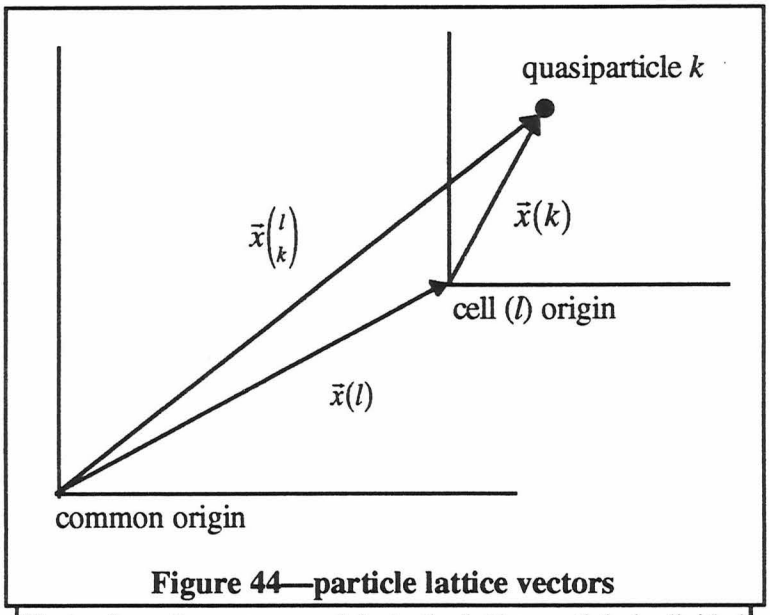

Figure 44—particle lattice vectors

Vector form the common origin to the lattice particle is divided into a vector from the common origin to the lattice cell origin plus a vector from the lattice cell origin to the particle.

1. Notation

Latin letters are used as lattice labels, while Greek letters will denote vector components. It is convenient to separate the vectors from the common origin to the quasiparticle into components, as shown in Figure 44,

$$\vec{x}\binom{l}{k} \equiv \vec{x}(l) + \vec{x}(k) \quad . \tag{35}$$

The label l identifies the lattice cell, and k the particle location within the cell. Because the particle positions within a cell are the same for each cell, the vector $\vec{x}(k)$ does not carry a lattice label l.

The actual particle positions are written in lower case ($\vec{x}$). Upper case letters ($\vec{X}$) denote the equilibrium position. The displacement from equilibrium is then written

$$\vec{u}\begin{pmatrix} l \\ k \end{pmatrix} = \vec{x}\begin{pmatrix} l \\ k \end{pmatrix} - \vec{X}\begin{pmatrix} l \\ k \end{pmatrix} \quad . \tag{36}$$

The potential (interaction) energy, V, is a function of the actual positions:

$$V = V\left(\ldots, \vec{x}\begin{pmatrix} l \\ k \end{pmatrix}, \ldots\right) = V\left(\ldots, \vec{X}\begin{pmatrix} l \\ k \end{pmatrix} + \vec{u}\begin{pmatrix} l \\ k \end{pmatrix}, \ldots\right) \quad . \tag{37}$$

2. Taylor Series Expansion

A Taylor series expansion is justified with the assumption

$$\left|\vec{u}\begin{pmatrix} l \\ k \end{pmatrix}\right| << \left|\vec{X}\begin{pmatrix} l \\ k \end{pmatrix}\right| \quad . \tag{38}$$

The general form of the Taylor series is

$$f(\vec{r} + \vec{a}) = \sum_{n=0}^{\infty} \frac{1}{n!} (\vec{a} \cdot \nabla)^n f(\vec{r}) \quad . \tag{39}$$

This general form can also be used with vectors of dimension m = (dimension of basis—3) x (number of particles in the lattice) = $\sum_{l,k,\alpha} 1$. The m-dimensional vectors will be labeled with a two sided arrow above the symbol—$\vec{\vec{x}}, \vec{\vec{X}}, \vec{\vec{u}}, \vec{\vec{\nabla}}$—while standard vector notation—$\vec{x}, \vec{X}, \vec{u}, \nabla$—denotes vectors in the basis. With this notation, V is expanded:

$$V\left(\ldots, \vec{X}\binom{l}{k}+\vec{u}\binom{l}{k}, \ldots\right)=V\left(\vec{X}+\vec{u}\right)=V\left(\vec{X}\right)+\vec{u}\cdot\vec{\nabla}V\left(\vec{X}\right)+\frac{1}{2}\left(\vec{u}\cdot\vec{\nabla}\right)^2 V\left(\vec{X}\right)+\cdots \quad . \tag{40}$$

Write $\vec{u}\cdot\vec{\nabla}$ and $\left(\vec{u}\cdot\vec{\nabla}\right)^2$ explicitly:

$$\vec{u}\cdot\vec{\nabla}=\sum_{l,k}\vec{u}\binom{l}{k}\cdot\nabla=\sum_{l,k}\sum_{\alpha}u_\alpha\binom{l}{k}\frac{\partial}{\partial x_\alpha\binom{l}{k}} \quad , \tag{41}$$

$$\begin{aligned}\left(\vec{u}\cdot\vec{\nabla}\right)^2&=\left[\sum_{l,k}\vec{u}\binom{l}{k}\cdot\nabla\right]^2=\sum_{l,k}\sum_{l',k'}\left[\vec{u}\binom{l}{k}\cdot\nabla\right]\left[\vec{u}\binom{l'}{k'}\cdot\nabla'\right]\\&=\sum_{l,k,l',k'}\sum_{\alpha,\beta}u_\alpha\binom{l}{k}u_\beta\binom{l'}{k'}\frac{\partial^2}{\partial x_\alpha\binom{l}{k}\partial x_\beta\binom{l'}{k'}} \quad ,\end{aligned} \tag{42}$$

and rewrite V,

$$V=V^o+\sum_{l,k}\sum_{\alpha}u_\alpha\binom{l}{k}V_\alpha\binom{l}{k}+\frac{1}{2}\sum_{l,k,l',k'}\sum_{\alpha,\beta}u_\alpha\binom{l}{k}u_\beta\binom{l'}{k'}V_{\alpha\beta}\binom{l\quad l'}{k\quad k'}+\cdots \quad , \tag{43}$$

where

$$\begin{aligned}V^o&=V(\vec{x})\big|_{\vec{X}}\\V_\alpha\binom{l}{k}&=\left.\frac{\partial V(\vec{x})}{\partial x_\alpha\binom{l}{k}}\right|_{\vec{X}}\\V_{\alpha\beta}\binom{l\quad l'}{k\quad k'}&=\left.\frac{\partial^2 V(\vec{x})}{\partial x_\alpha\binom{l}{k}\partial x_\beta\binom{l'}{k'}}\right|_{\vec{X}} \quad .\end{aligned} \tag{44}$$

V^o represents the potential at the equilibrium configuration, which is a reference energy.

$V_\alpha\binom{l}{k}$ is the α-component of the external force on the particle $\binom{l}{k}$ in the equilibrium configuration. This term is zero since there is no net force on any particle in equilibrium. The equilibrium position is defined by $V_\alpha\binom{l}{k}=0$.

$V_{\alpha\beta}\binom{l\ \ l'}{k\ \ k'}$ is the first non-trivial term, and represents the deformation energy. It takes the form of a spring constant in a three-dimensional harmonic oscillator, that is (in one dimension), k in $F=-kx$ and $V=\frac{1}{2}kx^2$. $V_{\alpha\beta}$ allows coupling of energy in the α and β directions. No assumption is made about the form of $V_{\alpha\beta}$. Although it carries indices for the positions l,k and l',k', it is dependent on the whole set of coordinates.

The potential energy is now approximated by

$$U=V-V^o\cong\frac{1}{2}\sum_{l,k,l',k'}\sum_{\alpha,\beta}u_\alpha\binom{l}{k}u_\beta\binom{l'}{k'}V_{\alpha\beta}\binom{l\ \ l'}{k\ \ k'}\quad . \tag{45}$$

The kinetic energy is simply the sum of each particle's kinetic energy,

$$T=\frac{1}{2}\sum_{l,k}\sum_{\alpha}m_k\left[\dot{u}_\alpha\binom{l}{k}\right]^2\quad , \tag{46}$$

where

$$\dot{u}_\alpha\binom{l}{k}\equiv\frac{\partial u_\alpha\binom{l}{k}}{\partial t}\quad . \tag{47}$$

This form for the kinetic energy allows for different particle masses within a cell.

The Lagrangian, $L=T-U$, is written

$$L=\frac{1}{2}\sum_{l,k}\sum_{\alpha}\left\{m_k\left[\dot{u}_\alpha\begin{pmatrix}l\\k\end{pmatrix}\right]^2-\sum_{l',k'}\sum_{\beta}u_\alpha\begin{pmatrix}l\\k\end{pmatrix}u_\beta\begin{pmatrix}l'\\k'\end{pmatrix}V_{\alpha\beta}\begin{pmatrix}l & l'\\k & k'\end{pmatrix}\right\} \quad . \tag{48}$$

The equations of motion are obtained from the Lagrangian:

$$\frac{d}{dt}\frac{\partial L}{\partial \dot{x}_\alpha}=\frac{\partial L}{\partial x_\alpha} \quad . \tag{49}$$

Carrying out the differentiation yields

$$\sum_{l,k}\sum_{\alpha}m_k\ddot{u}_\alpha\begin{pmatrix}l\\k\end{pmatrix}=\sum_{l,k,l',k'}\sum_{\alpha,\beta}u_\beta\begin{pmatrix}l'\\k'\end{pmatrix}V_{\alpha\beta}\begin{pmatrix}l & l'\\k & k'\end{pmatrix} \quad . \tag{50}$$

With $u_\alpha\begin{pmatrix}l\\k\end{pmatrix}$ arbitrary, the summation over l, k, and α must be equivalent term by term. This result gives the equations of motion we will continue to work with

$$m_k\ddot{u}_\alpha\begin{pmatrix}l\\k\end{pmatrix}=\sum_{l',k'}\sum_{\beta}V_{\alpha\beta}\begin{pmatrix}l & l'\\k & k'\end{pmatrix}u_\beta\begin{pmatrix}l'\\k'\end{pmatrix} \quad . \tag{51}$$

3. Invariance Requirements

The form for the potential V in equation (45) can now be simplified by means of several invariance requirements that arise from the form of the potential. Until this point, $V_{\alpha\beta}$ has been an arbitrary function. By exploiting some of the invariance requirements—arbitrariness in numbering the cells, rigid body motions, etc.—we will impose some structure to the form of $V_{\alpha\beta}$.

a› Changing the starting cell—invariance to counting origin. This is expressed by invariance in the energy when changing the index $l\rightarrow l+p$ and $l'\rightarrow l'+p$. (We don't change the index k. Recall $\vec{x}(k)$ is relative to the cell origin, so is already shifted with l.)

$$\frac{1}{2}\sum_{l,k,l',k'}\sum_{\alpha,\beta}u_\alpha\begin{pmatrix}l+p\\k\end{pmatrix}u_\beta\begin{pmatrix}l'+p\\k'\end{pmatrix}V_{\alpha\beta}\begin{pmatrix}l+p & l'+p\\k & k'\end{pmatrix}=\frac{1}{2}\sum_{l,k,l',k'}\sum_{\alpha,\beta}u_\alpha\begin{pmatrix}l\\k\end{pmatrix}u_\beta\begin{pmatrix}l'\\k'\end{pmatrix}V_{\alpha\beta}\begin{pmatrix}l & l'\\k & k'\end{pmatrix} \quad , \tag{52}$$

which implies

$$V_{\alpha\beta}\begin{pmatrix}l+p & l'+p\\k & k'\end{pmatrix}=V_{\alpha\beta}\begin{pmatrix}l & l'\\k & k'\end{pmatrix} \quad . \tag{53}$$

This can be satisfied for arbitrary l, l', and p only if l and l' appear through their difference. Then

$$V_{\alpha\beta}=V_{\alpha\beta}\begin{pmatrix}l-l'\\k & k'\end{pmatrix} \quad . \tag{54}$$

b› Changing the direction of counting—invariance to particle interchange. This is expressed by $l\rightarrow -l$ and $l'\rightarrow -l'$. (Again, k is not changed. It changes implicitly with the cell index l.) Then

$$V_{\alpha\beta}\begin{pmatrix}l-l'\\k & k'\end{pmatrix}=V_{\alpha\beta}\begin{pmatrix}l'-l\\k & k'\end{pmatrix} \quad . \tag{55}$$

which can be satisfied for arbitrary l and l' only if l-l' = l'-l, or

$$V_{\alpha\beta}=V_{\alpha\beta}\begin{pmatrix}|l-l'|\\k & k'\end{pmatrix} \quad . \tag{56}$$

c› Invariance to rigid translation of the lattice. This is expressed as $\vec{x}\begin{pmatrix}l\\k\end{pmatrix}=\vec{X}\begin{pmatrix}l\\k\end{pmatrix}+\vec{b}$, or $\vec{u}\begin{pmatrix}l\\k\end{pmatrix}=\vec{b}$, for all l,k. Under this condition, invariance in the energy requires the deformation energy to vanish

$$\frac{1}{2}\sum_{\alpha,\beta}\left[\sum_{l,k,l',k'}V_{\alpha\beta}\begin{pmatrix}l-l'\\k & k'\end{pmatrix}\right]b_\alpha b_\beta=0 \quad . \tag{57}$$

For $\vec{b}$ arbitrary, the inner sum must vanish. In addition, because all lattice cells are equivalent, the sum over l,k,l',k' can be reduced to a sum over l',k' only, giving

$$\sum_{l',k'} V_{\alpha\beta}\begin{pmatrix} l-l' \\ k \quad k' \end{pmatrix} = 0 \quad . \tag{58}$$

This suggests that not only the total energy of the system is conserved with the translation, but also the energy of each particle. It is convenient to write the above equation isolating the term $l',k' \neq l,k$

$$\bar{\sum_{l',k'}} V_{\alpha\beta}\begin{pmatrix} l-l' \\ k \quad k' \end{pmatrix} = -V_{\alpha\beta}\begin{pmatrix} 0 \\ k \quad k \end{pmatrix} \quad , \tag{59}$$

where the bar on the summation indicates the exclusion of the term $l',k' \neq l,k$.

d› Invariance to rigid rotation of the lattice. A general rotation can be written in matrix form as $\bar{x} = \hat{R}\bar{X}$, where $\hat{R}$ is an antisymmetric, orthonormal matrix with elements defined

$$\begin{aligned} r_{\alpha\beta} &= \delta_{\alpha\beta} + \omega_{\alpha\beta} \\ \omega_{\beta\alpha} &= -\omega_{\alpha\beta} \\ \delta_{\alpha\beta} &= \begin{cases} 0 & \alpha \neq \beta \\ 1 & \alpha = \beta \end{cases} \quad . \end{aligned} \tag{60}$$

The components of $\vec{x}\begin{pmatrix} l \\ k \end{pmatrix}$, and the displacements $\vec{u}\begin{pmatrix} l \\ k \end{pmatrix}$, can be written

$$\begin{aligned} x_\alpha\begin{pmatrix} l \\ k \end{pmatrix} &= \sum_\beta \left(\delta_{\alpha\beta} + \omega_{\alpha\beta}\right) X_\beta\begin{pmatrix} l \\ k \end{pmatrix} \\ u_\alpha\begin{pmatrix} l \\ k \end{pmatrix} &= \sum_\beta \omega_{\alpha\beta} X_\beta\begin{pmatrix} l \\ k \end{pmatrix} \quad . \end{aligned} \tag{61}$$

Again, the deformation energy must vanish, written

$$\frac{1}{2}\sum_{\alpha,\beta}\sum_{\gamma,\delta}\sum_{l,k,l',k'} V_{\alpha\beta}\begin{pmatrix} l-l' \\ k \quad k' \end{pmatrix}\omega_{\alpha\gamma}X_{\gamma}\begin{pmatrix} l \\ k \end{pmatrix}\omega_{\beta\delta}X_{\delta}\begin{pmatrix} l' \\ k' \end{pmatrix} = 0 \quad . \tag{62}$$

For an arbitrary rotation the coefficients must vanish, yielding

$$\sum_{\alpha,\delta}\sum_{l',k'} V_{\alpha\beta}\begin{pmatrix} l-l' \\ k \quad k' \end{pmatrix}\omega_{\alpha\delta}X_{\delta}\begin{pmatrix} l' \\ k' \end{pmatrix} = 0 \quad . \tag{63}$$

We first isolate the $l',k'=l,k$ term, then substitute equation (46) from the rigid lattice translation to rewrite the above equation in a more favorable form,

$$\begin{aligned} \sum_{\alpha,\delta}\bar{\sum_{l',k'}} V_{\alpha\beta}\begin{pmatrix} l-l' \\ k \quad k' \end{pmatrix}\omega_{\alpha\delta}X_{\delta}\begin{pmatrix} l' \\ k' \end{pmatrix} &= -\sum_{\alpha,\delta} V_{\alpha\beta}\begin{pmatrix} 0 \\ k \quad k \end{pmatrix}\omega_{\alpha\delta}X_{\delta}\begin{pmatrix} l \\ k \end{pmatrix} \\ &= \sum_{\alpha,\delta}\left[\bar{\sum_{l',k'}} V_{\alpha\beta}\begin{pmatrix} l-l' \\ k \quad k' \end{pmatrix}\right]\omega_{\alpha\delta}X_{\delta}\begin{pmatrix} l \\ k \end{pmatrix} \quad . \end{aligned} \tag{64}$$

Rearranging terms inside the same summation yields

$$\sum_{\alpha,\delta}\sum_{l',k'} V_{\alpha\beta}\begin{pmatrix} l-l' \\ k \quad k' \end{pmatrix}\omega_{\alpha\delta}\left[X_{\delta}\begin{pmatrix} l' \\ k' \end{pmatrix} - X_{\delta}\begin{pmatrix} l \\ k \end{pmatrix}\right] = 0 \quad . \tag{65}$$

The bar is removed from the summation since the $l',k'=l,k$ term equals zero.

e› Invariance arising from the definition of $V_{\alpha\beta}$. Recall

$$V_{\alpha\beta}\begin{pmatrix} l \quad l' \\ k \quad k' \end{pmatrix} \equiv \left.\frac{\partial^2 V(\vec{x})}{\partial x_{\alpha}\begin{pmatrix} l \\ k \end{pmatrix}\partial x_{\beta}\begin{pmatrix} l' \\ k' \end{pmatrix}}\right|_{\vec{X}} \quad . \tag{66}$$

Symmetry in the order of differentiation yields

$$V_{\alpha\beta}\begin{pmatrix} l & l' \\ k & k' \end{pmatrix} = V_{\beta\alpha}\begin{pmatrix} l' & l \\ k' & k \end{pmatrix} = V_{\alpha\beta}\begin{pmatrix} l' & l \\ k' & k \end{pmatrix} \quad . \tag{67}$$

The last equality arises from equation (56).

4. Equations of Motion

Now, having simplified the form for the potential, we concentrate on the equations of motion. First, rewrite equation (51) isolating the $l',k'=l,k$ term,

$$\begin{aligned} m_k \ddot{u}_\alpha\begin{pmatrix} l \\ k \end{pmatrix} &= \sum_{l',k'} \sum_{\beta} V_{\alpha\beta}\begin{pmatrix} l & l' \\ k & k' \end{pmatrix} u_\beta\begin{pmatrix} l' \\ k' \end{pmatrix} \\ &= \bar{\sum_{l',k'}} \sum_{\beta} V_{\alpha\beta}\begin{pmatrix} l-l' \\ k & k' \end{pmatrix} u_\beta\begin{pmatrix} l' \\ k' \end{pmatrix} + \sum_{\beta} V_{\alpha\beta}\begin{pmatrix} 0 \\ k & k \end{pmatrix} u_\beta\begin{pmatrix} l \\ k \end{pmatrix} \quad . \end{aligned} \tag{68}$$

Substitute equation (59) and combine into a single summation to obtain

$$\begin{aligned} m_k \ddot{u}_\alpha\begin{pmatrix} l \\ k \end{pmatrix} &= \bar{\sum_{l',k'}} \sum_{\beta} V_{\alpha\beta}\begin{pmatrix} l-l' \\ k & k' \end{pmatrix} u_\beta\begin{pmatrix} l' \\ k' \end{pmatrix} - \bar{\sum_{l',k'}} \sum_{\beta} V_{\alpha\beta}\begin{pmatrix} l-l' \\ k & k' \end{pmatrix} u_\beta\begin{pmatrix} l \\ k \end{pmatrix} \\ &= \sum_{l',k'} \sum_{\beta} V_{\alpha\beta}\begin{pmatrix} l-l' \\ k & k' \end{pmatrix} \left[u_\beta\begin{pmatrix} l' \\ k' \end{pmatrix} - u_\beta\begin{pmatrix} l \\ k \end{pmatrix} \right] \quad . \end{aligned} \tag{69}$$

Again, the bar is removed from the summation since the $l',k'=l,k$ term is zero.

It is convenient to rewrite the above equation in terms of $l-l'=p$, that is, let $l' \rightarrow l-p$, then change to a summation over p,

$$\sum_{l',k'} \sum_{\beta} V_{\alpha\beta}\begin{pmatrix} l-l' \\ k & k' \end{pmatrix} \left[u_\beta\begin{pmatrix} l' \\ k' \end{pmatrix} - u_\beta\begin{pmatrix} l \\ k \end{pmatrix} \right] = \sum_{p,k'} \sum_{\beta} V_{\alpha\beta}\begin{pmatrix} p \\ k & k' \end{pmatrix} \left[u_\beta\begin{pmatrix} l-p \\ k' \end{pmatrix} - u_\beta\begin{pmatrix} l \\ k \end{pmatrix} \right] \quad . \tag{70}$$

A more symmetric form is obtained by making use of equation (55), $V_{\alpha\beta}\begin{pmatrix} p \\ k & k' \end{pmatrix} = V_{\alpha\beta}\begin{pmatrix} -p \\ k & k' \end{pmatrix}$, (the $p=0$ term vanishes),

$$m_k \ddot{u}_\alpha \binom{l}{k} = \sum_{p>0,k'} \sum_{\beta} V_{\alpha\beta}\left(k\ {}^{p}_{}\ k'\right)\left[u_\beta\binom{l-p}{k'} - u_\beta\binom{l}{k}\right] + \sum_{p<0,k'} \sum_{\beta} V_{\alpha\beta}\left(k\ {}^{p}_{}\ k'\right)\left[u_\beta\binom{l-p}{k'} - u_\beta\binom{l}{k}\right]$$
$$= \sum_{p>0,k'} \sum_{\beta} V_{\alpha\beta}\left(k\ {}^{p}_{}\ k'\right)\left[u_\beta\binom{l-p}{k'} - 2u_\beta\binom{l}{k} + u_\beta\binom{l+p}{k'}\right] \quad . \tag{71}$$

This has the more familiar form of a three-dimensional harmonic oscillator with spring constant $V_{\alpha\beta}\left(k\ {}^{p}_{}\ k'\right)$ between elements k and k' in cells separated by the distance represented by $p = |l - l'|$.

Finally, by similar techniques, we rewrite the potential U given in equation (45),

$$U = \frac{1}{2} \sum_{l,k,p,k'} \sum_{\alpha,\beta} V_{\alpha\beta}\left(k\ {}^{p}_{}\ k'\right)\left[u_\alpha\binom{l+p}{k'} - u_\alpha\binom{l}{k}\right]\left[u_\beta\binom{l+p}{k'} - u_\beta\binom{l}{k}\right] \quad . \tag{72}$$

5. Continuum Limit

For the continuum limit, consider the equations of motion as described by equation (71). Define $\vec{u}\binom{l}{k} \equiv \vec{u}\left(\vec{x}\binom{l}{k}, t\right)$ and expand $u_\beta\binom{l\pm p}{k'}$ in a Taylor series. Using the form in equation (39), let

$$\begin{aligned} \vec{r} &\Rightarrow x_\beta\binom{l}{k} \\ f(\vec{r}) &\Rightarrow u_\beta\binom{l}{k} \\ \vec{a} &\Rightarrow x_\beta\binom{l}{k} - x_\beta\binom{l'}{k'} \equiv x_\beta\left(k\ {}^{p}_{}\ k'\right) \quad , \end{aligned} \tag{73}$$

then

$$u_\beta\binom{l\pm p}{k'} = u_\alpha\binom{l}{k} + \sum_\gamma X_\gamma\left(k\ {}^{\pm p}_{}\ k'\right)\frac{\partial}{\partial x_\gamma} u_\beta\binom{l}{k} + \frac{1}{2}\sum_{\gamma,\delta}\left[X_\gamma\left(k\ {}^{\pm p}_{}\ k'\right)X_\delta\left(k\ {}^{\pm p}_{}\ k'\right)\frac{\partial^2}{\partial x_\gamma \partial x_\delta}\right] u_\beta\binom{l}{k} + \cdots \tag{74}$$

Noting $u_\gamma\begin{pmatrix}-p\\k'\end{pmatrix} = -u_\gamma\begin{pmatrix}p\\k'\end{pmatrix}$, the equations of motion can now be written

$$m_k \ddot{u}_\alpha\begin{pmatrix}l\\k\end{pmatrix} = \sum_{p>0,k'}\sum_{\beta} V_{\alpha\beta}\begin{pmatrix}p\\k\ k'\end{pmatrix}\sum_{\gamma,\delta} X_\gamma\begin{pmatrix}p\\k\ k'\end{pmatrix}X_\delta\begin{pmatrix}p\\k\ k'\end{pmatrix}\frac{\partial^2}{\partial x_\gamma \partial x_\delta}u_\beta\begin{pmatrix}l\\k\end{pmatrix} \quad . \tag{75}$$

For the energy, start with equation (72), again using a Taylor expansion and keeping only the first non-zero term,

$$U = \frac{1}{2}\sum_{l,k,p,k'}\sum_{\alpha,\beta} V_{\alpha\beta}\begin{pmatrix}p\\k\ k'\end{pmatrix}\left[\sum_{\gamma} X_\gamma\begin{pmatrix}p\\k\ k'\end{pmatrix}\frac{\partial}{\partial x_\gamma}u_\alpha\begin{pmatrix}l\\k\end{pmatrix}\right]\left[\sum_{\delta} X_\delta\begin{pmatrix}p\\k\ k'\end{pmatrix}\frac{\partial}{\partial x_\delta}u_\beta\begin{pmatrix}l\\k\end{pmatrix}\right] \quad . \tag{76}$$

Some simplification is possible here by introducing the following symmetric and antisymmetric functions, given by

$$\frac{\partial u_\beta}{\partial x_\gamma} = \frac{1}{2}\left(\frac{\partial u_\beta}{\partial x_\gamma} + \frac{\partial u_\gamma}{\partial x_\beta}\right) + \frac{1}{2}\left(\frac{\partial u_\beta}{\partial x_\gamma} - \frac{\partial u_\gamma}{\partial x_\beta}\right) \equiv \varepsilon_{\beta\gamma} + \xi_{\beta\gamma} \quad . \tag{77}$$

By rotational invariance earlier given by equation (65), the $\xi_{\beta\gamma}$ term vanishes in both the equations of motion and the energy.

Finally, equation (75) is averaged over the cell by summing over k, then dividing by the volume of the cell, *v*. Use is made of the following substitutions:

$$\begin{aligned} \rho &= \frac{1}{v}\sum_{k} m_k \\ c_{\alpha\gamma\beta\delta} &= \frac{1}{v}\sum_{k,p>0,k'} V_{\alpha\beta}\begin{pmatrix}p\\k\ k'\end{pmatrix}X_\gamma\begin{pmatrix}p\\k\ k'\end{pmatrix}X_\delta\begin{pmatrix}p\\k\ k'\end{pmatrix} \quad , \end{aligned} \tag{78}$$

giving

$$\rho \frac{\partial^2 u_\alpha}{\partial t^2} = \sum_{\beta\gamma\delta} \frac{\partial}{\partial x_\gamma} \left(c_{\alpha\gamma\beta\delta} \varepsilon_{\beta\delta} \right) \quad . \tag{79}$$

Similar techniques can be used for the energy, equation (76). In addition, the summation over l is replaced by an integral over the volume, V, and dividing by the cell volume v, to obtain

$$U = \frac{1}{2} \int dV \, c_{\alpha\gamma\beta\delta} \varepsilon_{\alpha\gamma} \varepsilon_{\beta\delta} \quad . \tag{80}$$

B. Different methods for computing $k_l(c_{ij})$

The equations relating the elastic constants, c_{ij}, to the spring constants, k_l, are

$$c_{11} = \frac{2}{a}\left(k_1 + 2k_2 + \tfrac{4}{3}k_3\right), \quad c_{12} = c_{44} = \frac{2}{a}\left(k_2 + \tfrac{4}{3}k_3\right) \quad .$$

Because there are three unknowns and only two equations, a third constraint must be used to solve the equations. The constraints considered here is as follows:

$$1)\ \ k_3 = 0, \qquad 2)\ \ k_3 = rk_2, \qquad 3)\ \ k_3 = rk_1 \quad .$$

Some possible choices for r are:

$$a)\ \ r = \frac{c_{44}}{c_{12}}, \qquad b)\ \ r = \frac{c_{44}}{c_{11}}, \qquad c)\ \ r = \gamma^{-1} \quad ,$$

where γ is the anisotropy factor defined by $\gamma \equiv \dfrac{2c_{44}}{c_{11} - c_{12}}$.

There are seven meaningful combinations of the above conditions. They are summarized, with results for the $k_l(c_{ij})$, below. NaCl was chosen for the comparison material because it exhibits ionic bonding where the pairwise approximation is valid for the microscopic lattice.

Conditions	k_l	k_l for NaCl
1	$k_1 = \frac{a}{2}(c_{11} - 2c_{12})$ $k_2 = \frac{a}{2}c_{12}$ $k_3 = 0$	$k_1 = 0.2018$ $k_2 = 0.1105$ $k_3 = 0$

Conditions	k_i	k_i for NaCl
2a	$k_1 = \frac{a}{2}\left[c_{11} - \frac{2c_{12} + \frac{4}{3}c_{44}}{c_{12} + \frac{4}{3}c_{44}} c_{12}\right]$	$k_1 = 0.2652$
	$k_2 = \frac{a}{2}\left[\frac{c_{12}^2}{c_{12} + \frac{4}{3}c_{44}}\right]$	$k_2 = 0.0471$
	$k_3 = \frac{a}{2}\left[\frac{c_{12}c_{44}}{c_{12} + \frac{4}{3}c_{44}}\right]$	$k_3 = 0.0475$
2b	$k_1 = \frac{a}{2}\left[c_{11} - \frac{2c_{11} + \frac{4}{3}c_{12}}{c_{11} + \frac{4}{3}c_{44}} c_{12}\right]$	$k_1 = 0.2306$
	$k_2 = \frac{a}{2}\left[\frac{c_{11}c_{12}}{c_{11} + \frac{4}{3}c_{44}}\right]$	$k_2 = 0.0818$
	$k_3 = \frac{a}{2}\left[\frac{c_{12}c_{44}}{c_{11} + \frac{4}{3}c_{44}}\right]$	$k_3 = 0.0215$
2c	$k_1 = \frac{a}{2}\left[c_{11} - \frac{4c_{44} + \frac{4}{3}(c_{11} - c_{12})}{2c_{44} + \frac{4}{3}(c_{11} - c_{12})} c_{12}\right]$	$k_1 = 0.2738$
	$k_2 = \frac{a}{2}\left[\frac{2c_{12}c_{44}}{2c_{44} + \frac{4}{3}(c_{11} - c_{12})}\right]$	$k_2 = 0.0385$
	$k_3 = \frac{a}{2}\left[\frac{c_{12}(c_{11} - c_{12})}{2c_{44} + \frac{4}{3}(c1_1 - c_{12})}\right]$	$k_3 = 0.0540$
3a	$k_1 = \frac{a}{2}\left[\frac{c_{44}(c_{11} - 2c_{12})}{c_{12} - \frac{4}{3}c_{44}}\right]$	$k_1 = -0.5870$
	$k_2 = \frac{a}{2}\left[\frac{c_{12}^2 - \frac{4}{3}c_{44}(c_{11} - c_{12})}{c_{12} - \frac{4}{3}c_{44}}\right]$	$k_2 = 0.8994$
	$k_3 = \frac{a}{2}\left[\frac{c_{12}(c_{11} - 2c_{12})}{c_{12} - \frac{4}{3}c_{44}}\right]$	$k_3 = -0.5917$

Conditions	k_1	k_1 for NaCl
3b	$k_1 = \frac{a}{2}\left[\frac{c_{11}(c_{11}-2c_{12})}{c_{11}-\frac{4}{3}c_{44}}\right]$	$k_1 = 0.3110$
	$k_2 = \frac{a}{2}\left[\frac{c_{11}c_{12}-\frac{4}{3}c_{44}(c_{11}-c_{12})}{c_{11}-\frac{4}{3}c_{44}}\right]$	$k_2 = 0.0012$
	$k_3 = \frac{a}{2}\left[\frac{c_{44}(c_{11}-2c_{12})}{c_{11}-\frac{4}{3}c_{44}}\right]$	$k_3 = 0.0819$
3c	$k_1 = \frac{a}{2}\left[\frac{2c_{44}(c_{11}-2c_{12})}{2c_{44}-\frac{4}{3}(c_{11}-c_{12})}\right]$	$k_1 = -0.2321$
	$k_2 = \frac{a}{2}\left[\frac{2c_{12}c_{44}-\frac{4}{3}(c_{11}-c_{12})^2}{2c_{44}-\frac{4}{3}(c_{11}-c_{12})}\right]$	$k_2 = 0.5444$
	$k_3 = \frac{a}{2}\left[\frac{(c_{11}-c_{12})(c_{11}-2c_{12})}{2c_{44}-\frac{4}{3}(c_{11}-c_{12})}\right]$	$k_3 = -0.3254$

Elastic constants and bond length used for NaCl are[27] (c_{ij} in units of 10^{12} dynes/cm^2, a in units of 10^{-8}cm): $c_{11} = .486$, $c_{12} = .127$, $c_{44} = .128$, $a = 1.74$.

As can be noted above, a few of the conditions result in negative values for some k_1. For most materials it was found that conditions 1 and 2c gave positive values for all k_1.

To show the differences between the different methods, three were plotted using the mesoscopic code for two different load values and beam lengths. The results show little difference in the method used as compared to differences in Young's modulus. The results are shown below. The calculated value of Young's modulus used here is that for a cubic crystal in the <100> direction, as follows:

$$E' = \frac{(c_{11}+2c_{12})(c_{11}-c_{12})}{c_{11}+c_{12}} \quad .$$

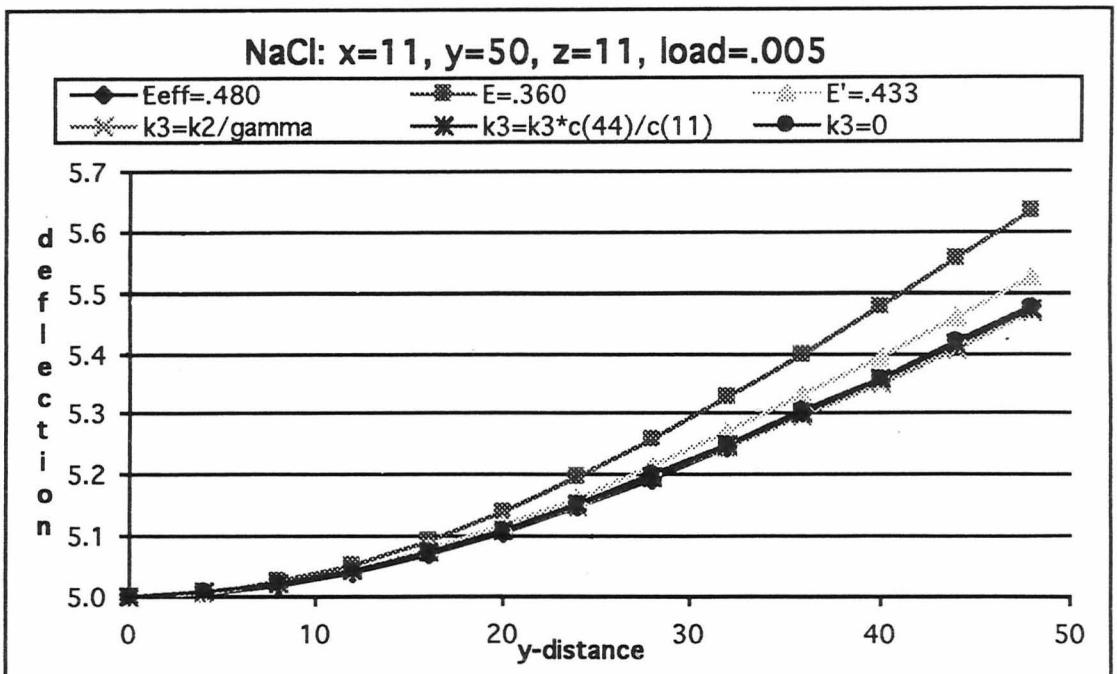

Figure 45—deflection vs. y, y=50, load = .005

Deflection of beam for different methods of calculating k_b and comparing to Young's modulus

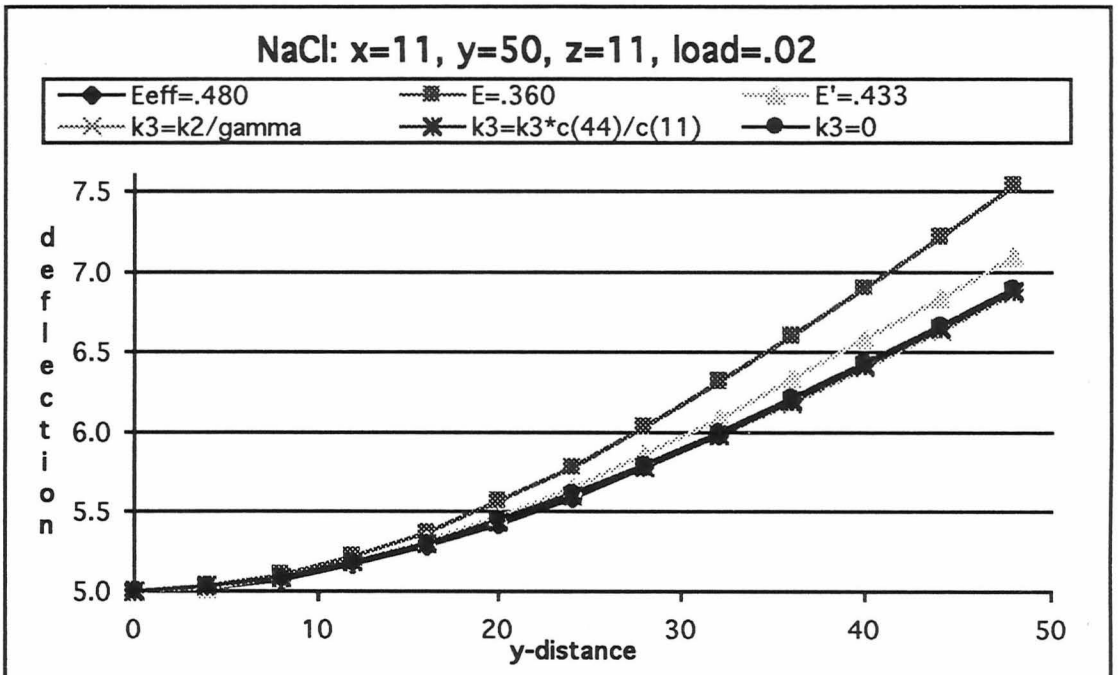

Figure 46—deflection vs. y, y=50, load = .02

Deflection of beam for different methods of calculating k_b and comparing to Young's modulus

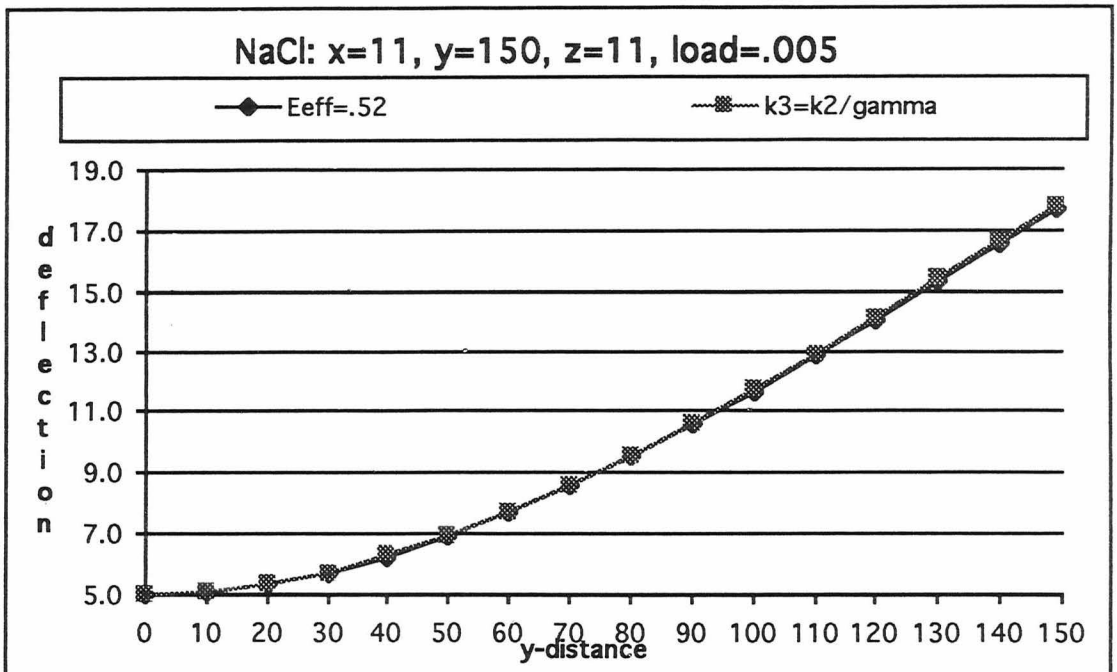

Figure 47—deflection vs. y, y=150, load = .005

Deflection of beam for different methods of calculating k_p and comparing to Young's modulus

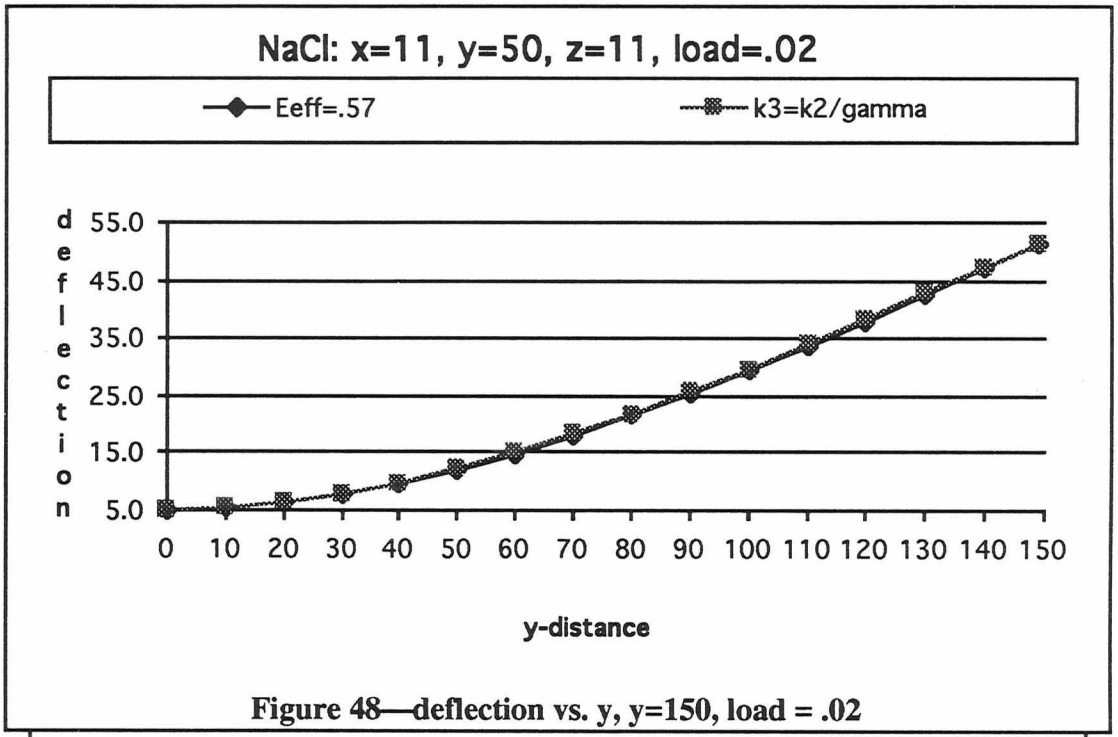

Figure 48—deflection vs. y, y=150, load = .02

Deflection of beam for different methods of calculating k_p and comparing to Young's modulus

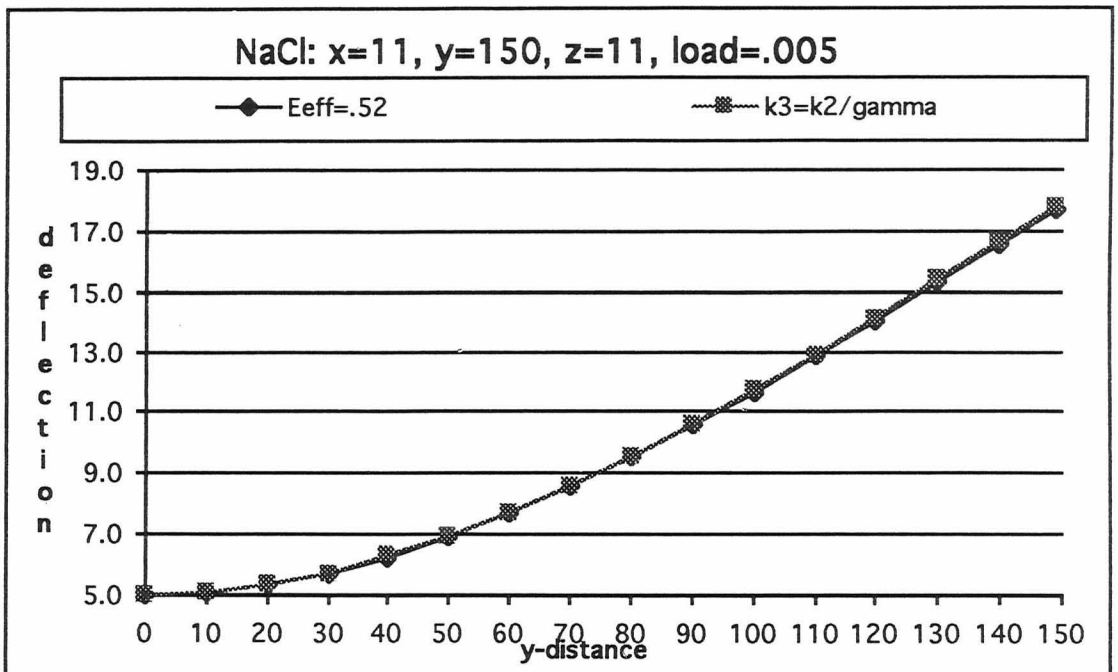

Figure 47—deflection vs. y, y=150, load = .005

Deflection of beam for different methods of calculating k_p and comparing to Young's modulus

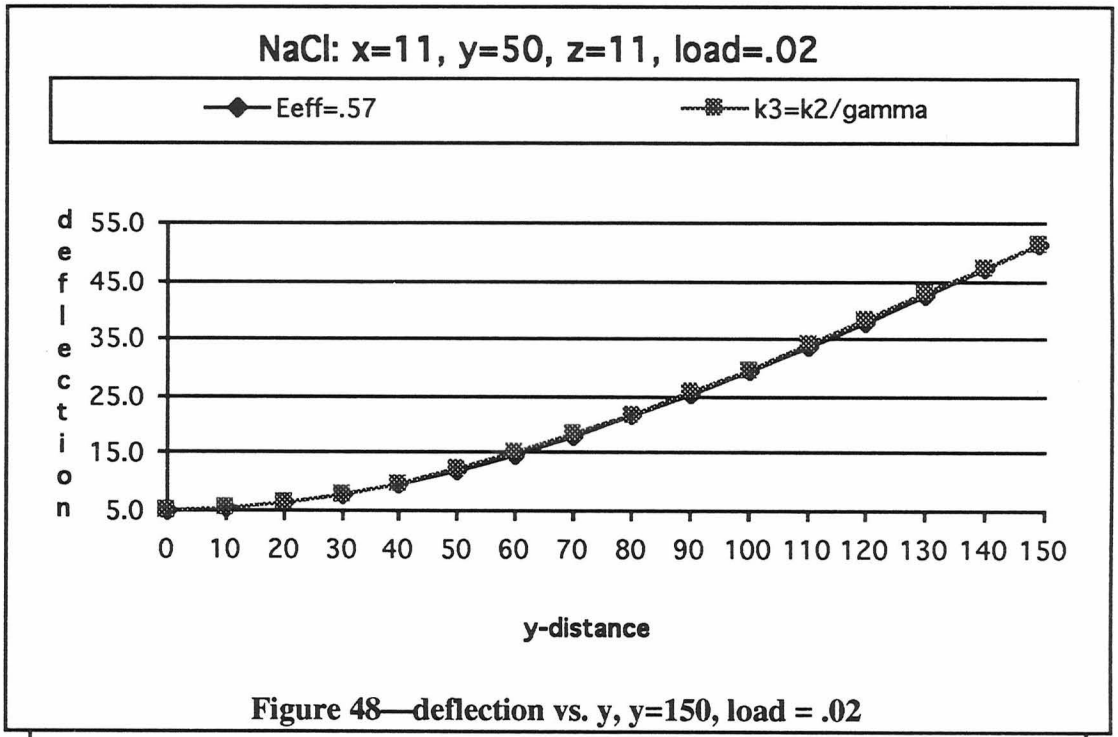

Figure 48—deflection vs. y, y=150, load = .02

Deflection of beam for different methods of calculating k_p and comparing to Young's modulus

C. Young's Modulus and Elastic Constants of Various Materials

Material constants for various materials. The table gives the experimental values E, ν, c_{11}, c_{12}, c_{44}, then the calculated values $\gamma \equiv \frac{2c_{44}}{c_{11}-c_{12}}$, and $E_{<100>}$ and $E_{<111>}$ from the equation for Young's modulus using the formula for a cubic crystal:

$$E^{-1} = \frac{c_{11}+c_{12}}{(c_{11}+2c_{12})(c_{11}-c_{12})} + \left(\frac{1}{c_{44}} - \frac{2}{c_{11}-c_{12}}\right)\left(n_x^2 n_y^2 + n_x^2 n_z^2 + n_y^2 n_z^2\right) \quad .$$

E is in units of N/m^2. The c_{ij} are in units of 10^{12} dynes/cm^2.

Material	E	ν	c_{11}	c_{12}	c_{44}	γ	$E_{<100>}$	$E_{<111>}$
NaCl	.360	.25	.486	.127	.128	.71	.433	.327
Si	1.10	-	1.66	.639	.796	1.6	1.30	1.88
Ni	2.14	.31	2.45	1.40	1.25	2.4	1.43	3.03
V	1.31	-	2.29	1.19	.43	.78	1.48	1.18
Cu	1.17	.36	1.68	1.21	.75	3.2	.667	1.90
Ag	.724	.37	1.24	.93	.46	3.0	.443	1.20
Pb	.138	.40-.45	.46	.39	.144	4.1	.102	.387
Ta	1.86	.35	2.67	1.61	.82	1.5	1.46	2.16
Fe	1.97	-	2.34	1.36	1.18	2.4	1.34	2.87
K	.045	.29	.041	.033	.026	6.5	.012	.063
Nb	1.03	-	2.47	1.35	.287	.51	1.52	0.82

D. Mesoscopic codes

The source code (written in C by the author) for the programs used in this dissertation are included in a pouch on the inside back cover. The files are in ASCII format on a DOS formatted disk. The programs were written using Think C on an Apple Macintosh computer.

Disk Contents:

BEAML.C: calculates deflection of a square beam fixed at one end and a mass placed at the other.

BEAMTH.C: calculates deflection of a beam using beam theory and Young's modulus. Uses the output from BEAML as a comparison.

ECONSTANTS.C: calculates the spring constant from input elastic constants and cell side length. Uses the seven methods described in this thesis.

PLATO.C: calculates deformation of a plate deformed by a thin film on one surface. The plate may have ribs etched into the back surface.

IX. References

[1] H. D. Hibbit, *Some Issues in Numerical Simulation of Nonlinear Structural Response*, NASA Conference Publication **3034**, 7 (1989).

[2] N. W. Ashcroft and N. D. Mermin, *Solid State Physics*, (Saunders College, Philadelphia, 1976), p. 443.

[3] M. Berrondo, *Computer Simulation of Linear and Nonlinear Structural Mechanics. A New Model.*, unpublished, (1993).

[4] R. C. Woodbury, H. Fan, L. V. Knight, and J. M. Thorne, *Curved Silicon Substrates for Multilayer Structures*, Proc. SPIE, **691**, 69 (1986).

[5] R. D. Cook, *Concepts and Applications of Finite Element Analysis*, (Wiley, New York, 1981).

[6] R. C. Woodbury et. al., ibid.

[7] M. A. Newcomb, *Predicting the Curvature of Etched Silicon Wafers Subjected to Thin Film Residual Stress*, Master thesis, Brigham Young University, Provo, UT (1989).

[8] J. Liu, *Design of Soft X-Ray Focusing Reflector Based on Etched Film/Substrate Structure*, Ph.D. thesis, Brigham Young University, Provo, UT (1994).

[9] N. W. Ashcroft and N. D. Mermin, ibid.

[10] J. J. Tuma, *Structural Analysis*, Schaum's Outline Series, (McGraw-Hill, 1969), p. 1, 107.

---

[11] A. Askar, *Lattice Dynamical Foundations of Continuum Theories*, (World Scientific, Singapore, 1985) p. 66-75.

[12] A. Askar, ibid., p. 61.

[13] A. B. Bhatia and R. N. Singh, M*echanics of Deformable Media*, (Bristol, 1986), p. 94.

[14] *Handbook of Chemistry and Physics*, 25th ed., edited by C. D. Hodgman, (Chemical Rubber Publishing Co., Cleveland, 1941) p. 2177.

[15] L. D. Landau and E. M. Lifshitz, *Theory of Elasticity - A Course of Theoretical Physics*, 3rd ed. (Pergamon Press, London, 1959), p. 37.

[16] L. D. Landau and E. M. Lifshitz, ibid.

[17] P. G. Ciarlet, *Lectures on Three Dimensional Elasticity*, (Springer-Verlag, New York, 1983), p. 44.

[18] A. B. Bhatia and R. N. Singh, ibid., p. 55-58.

[19] Y. Shi, *Development and Modeling of Cylindrical Shaped Multilayer X-Ray Reflectors*, Ph.D. thesis, Brigham Young University, Provo, UT (1991).

[20] R. Perkins, (private communication).

[21] J. Liu, ibid.

[22] A. L. Garcia, *Numerical Methods for Physics*, (Prentice Hall, New Jersey, 1994) p. 44-50.

[23] J. C. Houbolt, *A Recurrence Matrix Solution for the Dynamic Response of Elastic Aircraft*, J. Aero. S. **17**, 540 (1950).

---

[24] E. L. Wilson, I. Farhoomand, and K. J. Bathe, *Nonlinear Dynamic Analysis of Complex Structures*, Earthq. En. Str. Dyn. **1**, 241 (1973).

[25] C. W. Gear, *Numerical Initial Value Problems in Ordinary Differential Equations*, (Prentice-Hall, Englewood Cliffs, NJ, 1971).

[26] D. Beeman, *Some Multistep Methods for Use in Molecular Dynamics Calculations*, J. Comput. Phys. **20**, 136 (1976).

[27] A. Askar, ibid., p. 83.

A Computer Simulation of Structural Mechanics

— *A Mesoscopic Model* —

Eric W. Gardner

Department of Physics and Astronomy

Ph.D. Degree, December 1995

ABSTRACT

A method is introduced for computational analysis and simulation of structures that is intermediate between the atomistic view and the continuum limit. This method, labeled here the mesoscopic model, consists of a large number of mass points representing the shape of the material, each interacting with their neighbors through Hooke's law forces (springs). The arising dynamical equations are then solved by direct integration. This same method may be extended to use anharmonic interactions rather than the more simple Hooke's law forces in order to model nonlinear phenomena. The model is tested by comparing to beam theory for a rectangular bar fixed at one end, a load placed at the other. The results are linear in all spatial dimensions as predicted by beam theory, and linear in load for light to intermediate loads (slight negative curvature for heavier loads). Finally, a different method for material deformation is presented, i.e., a thin film on top of the bulk material that has different elastic and thermal properties from the bulk. With this method, structures with ribs etched in the back to control the deformation are modeled.

COMMITTEE APPROVAL:

Manuel Berrondo, Committee Chair

Larry V. Knight, Committee Member

David D. Allred, Committee Member

H. Mark Nelson, Committee Member

Chair Bruce Jay Collings, Statistics Minor

Jean Francois VanHuele, Graduate Coordinator